The Hydrology of a Sandur-Wetland in a Volcanic Environment, Southeast Iceland

Harold-Alexis Scheffel

A THESIS SUBMITTED TO

THE FACULTY OF GRADUATE STUDIES

IN PARTIAL FULFILLMENT OF THE REQUIREMENTS

FOR THE DEGREE OF

MASTER OF SCIENCE

GRADUATE PROGRAM IN GEOGRAPHY

YORK UNIVERSITY

TORONTO, ONTARIO

February 2018

ABSTRACT

Iceland is a geothermally active island with sharp contrasts in climate and geography. A 2.5 km stretch of a proglacial river neighboring an inhabited wetland was monitored between September 2015 to September 2016. Water wells along transects coupled with pressure transducers monitored the water table response across this sandur-wetland landscape. Additional geomorphic and climatic data were also collected at this site in order to better understand the sandur's response to both seasonal and episodic weather events. UAV derived DEMs coupled with hydrological data, allowed for the mapping of flooding extents during the study period. Through a combination of climatological, hydrological and remote sensing means, this study attempts to provide spatial and temporal information of flooding levels in response to rainfall and episodic floods and seeks to better understand how variable/extreme events can generate significant hydrological and geomorphic changes within this dynamic sandur-wetland landscape.

DEDICATION

Dedicated to my grandmother Hélène Dunand

ACKNOWLEDGMENTS

I would like to thank my supervisor Dr. Kathy L. Young for her generous help, support and council given consistently throughout the length of my B.Sc. and M.Sc. programs at York University. The training and acquisition of new sets of skills and knowledge that she has passed along to me will prepare me for a professional career in physical geography. I would also like to thank Dr. Tarmo Remmel, MSc committee member for his wise counsel and training. Dr. Remmel has helped me immensely in acquiring a new set of geomatic skills, which have improved my thesis and will help me in my future career goals.

During my time in Iceland, I am particularly grateful for the outstanding logistical support and friendship from Kristinn Guðjónsson, his wife Helga Þorsteindóttir and their son Guðjón. I would also like to thank Étienne Boucher, Rehanna Ali and my parents, John and Dominique Scheffel for their logistical support and assistance in the field during the 2016 field season. My mom, dad, sister and friends have been a great source of moral support and I could not have finished this thesis without their love, understanding and continuing financial contributions.

This research was supported primarily through research funds to Dr. Kathy L. Young, York University Field Research Cost Fund and the Government of Canada Northern Student Scientific Training Program. An international scholarship also assisted me in spending a term in France at the Université Savoie Mont Blanc through the Ontario-Rhone Alpes exchange program to improve my geographical skills which were helpful for this thesis.

TABLE OF CONTENTS

LIST OF TABLES

LIST OF FIGURES

CHAPTER ONE: INTRODUCTION

1.1 Introduction

Sandur (plur. Sandar), an Icelandic word signifying “sand” or “sand plain”, defines alluvial glacial outwash plains formed by braided rivers carrying meltwater from glacier fronts (Church, 1972). Studies on sandur development first started in Iceland by Thorarinsson (1939) who initially studied glacial outburst floods and later coined the phenomenon with the term “jökulhlaup”, yet a complete report on sandur processes and development was not completed until Church (1972)’s work on sandar located on Baffin Island in the Canadian High Arctic.

Skeiðarársandur (63.94 N, 17.23 W) the world’s largest sandur with an area of 1300 km^2, is located in southeastern Iceland between Vatnajökull, Iceland’s largest glacier and the North Atlantic Ocean. This outwash plain largely formed by glacial retreat (Magilligan et al., 2002) sees its long term development depending on the extent and amplitude of jökulhlaups (Maizels, 1991, 1997). These outburst floods are often the product of subglacial geothermal activity, heavy rainfall events or periods of extreme ice melt (Roberts, 2005). Volcanic activity in the last 20 years has led to several of these jökulhlaups which have caused significant damage to property, such as the Grímsvötn jökulhlaup in 1996 (Haraldsson, 1997; Björnsson, 2003) and the Eyjafjallajökull jökulhlaup in 2010 (Þorkelsson, 2012; Magnússon et al., 2012).

This sandur is near an active volcanic plate boundary where eruptions have and often occur, usually spewing large amounts of tephra over the area including adjacent lavafields, farmlands and coastal wetlands. Additionally, during volcanic eruptions, large quantities of ash can travel and remain in nearby catchments, eventually precipitating down to lower reaches of the rivers that cross over the landscape. Some of these coastal wetlands are inhabited and serve as grazing

grounds for sheep and cattle, while some fields are used to grow hay and other crops. Large water inputs prevail in these coastal wetlands and the water table is usually near the surface allowing for abundant vegetation growth, mostly consisting of grasses and mosses. This contrasts to the adjacent barren sandur landscape that is mainly composed of black sand, ash and alluvial deposits. The ponds and lush vegetation of these wetlands have attracted many local and migratory arctic birds and other wildlife that use these areas as resting and breeding grounds (Gunnarsson, 2006). Yet these vegetated ecosystems have been observed to be steadily replaced by sandy deserts, with low fertility and water-holding capacity (Arnalds, 2000; Arnalds et al., 2001).

Water and sediment contributions from the many rivers and streams found in the surrounding environment, help nourish this sandur-wetland landscape. Seasonal floods and jökulhlaups in Skeiðarársandur contribute to both high water levels and elevation increases in the stream bed, with additions of much water, ash and sediments. Flood events can also enhance erosion of the stream channels and adjacent wetlands, even those protected by man-made berms.

Furthermore, sustained high wind speeds often strike these barren landscapes, suspending dust particles from the glacial outwash plains and transporting them both locally and to greater distances (100's of kms – Arnalds, 2016). These sand storms can reach velocities over 25 m/s, often burying the surrounding vegetation altering infiltration and evaporation processes (Arnalds, 2008, 2010). Moreover, ash and sand deposits on seasonal snowcovers, perennial snowbanks and glaciers, can decrease surface albedo, enhancing ablation and therefore generating higher glacial runoff (Wittmann et al., 2017).

In this study, two sites adjacent to an inhabited wetland and along the Brunná River at the north-western corner of Skeiðarársandur were selected in order to better understand the flooding patterns across the sandur and its interactions with an adjacent inhabited wetland. The study

investigated the response of the sandur-wetland landscape to seasonal climatic conditions (rainfall, snowmelt) and episodic events (e.g., glacial outburst floods). A suite of climatic, hydrological and geomorphological parameters were monitored in order to assess processes and interactions within this complex landscape. Moreover, acquisition of high spatial resolution photographs (<1m per pixel) demonstrated both historical (since 1979) and recent depositional and erosional patterns here.

Given the large amount of sediment in this landscape as either brought in by glacial streams, deposited by winds or volcanic eruptions, this study also explores the sediment exhaustion model of a paraglagial environment, a term first coined by Church and Ryder (1972). They examined how landscapes, especially their fluvial and sediment supply transform after glaciation. However they never sought to consider the role and impact of episodic events such as jökulhlaup and volcanic eruptions. Ballantyne (2002) and Knight and Harrison (2014) enhanced current understanding of exhaustion models by including episodic events such landslides in their schemes, as they result in a temporary increase in sediment supply, but they like Church and Ryder (1972) did not consider volcanic eruptions and dust storms. In Iceland, there is still a particular need to better understand how episodic events (volcanic eruptions, dust storms) are reshaping this unique paraglacial landscape.

Additionally, similar to other low arctic environments experiencing deglaciation in response to climate warming, this study area is in proximity of the Vatnajökull glacier, which has experienced rapid retreat since the 1930's, and more considerably, since the early 2000's. This has resulted in a shift in the reworking of the surrounding pro-glacial landscape, increases in glacial stream discharge and an increase in sediment transport (Bjornsson et al., 2008). Improved understanding of the hydrology, flow regime and sediment pattern of a growing sandur and its

relationship with a nearby wetland will help to better determine the shifts which might occur in this unique paraglacial environment, as the climate warms. This is especially critical for farmers and local residents who live within this dynamic and quickly shifting landscape, as reliable plans to adapt to these rapid changes are paramount.

This study therefore seeks to understand the influence of the local seasonal climate and episodic events such as severe weather, sand storms and jökulhlaups, on a sandur's hydrological regime and its relationship with a nearby low-lying inhabited wetland. This investigation thereby involves understanding linkages between climate, hydrology and sediment delivery. Furthermore this study aims to expand the paraglacial theoretical concept by investigating the role of volcanic tephra/ash and severe rainfall on the sandur landscape.

CHAPTER TWO: LITERATURE REVIEW

2.1 Seismic and Volcanic Activity in Iceland

Iceland is located in the middle of the North Atlantic Ocean, on a tectonic ridge separating the Eurasian and North American continental plates. It has around 30 active volcanic systems with many of these active volcanoes and thermal hotspots overtopped by temperate glaciers. The island is mainly composed of volcanic rocks, primarily of basaltic composition with some basaltic sediments and andesitic intrusions (Johannesson and Saemundsson, 1989). Volcanic eruptions occur in Iceland every 3–5 years (Thordarson and Höskuldsson, 2008) with many active volcanoes located under these ice caps enhancing the production of volcanic ash during "wet explosive eruptions" (Arnalds et al., 2016).

In April 2010, Eyjafjallajökull, a volcano covered by a small glacier of the same name, erupted, spewing large quantities of fine ash into the upper atmosphere, closing most of the European airspace, triggering enormous disruptions to air travel across western and northern Europe over a period of six days. In Iceland, fine ash blanketed glaciers as well as surrounding farmlands and floodplains. Additionally, during this eruption, neighbouring roads were also closed due to damage from sub-glacial outburst floods. The Eyjafjallajökull eruption is not unusual in Iceland. Similar wet ash eruptions occurred in 2004 and 2011 under the Vatnajökull glacier at the Grímsvötn crater. In 2004, the eruption here sent over a meter of ash into surrounding areas. In March 2011 Grímsvötn erupted again, and thick coarse ash once again blanketed coastal areas and parts of the interior upland. Massive mudflows triggered by the eruption blocked stream channels and raised water levels by ca. 2 m (Per. Comm. Haness, Aug 2011). Enhanced seismic activity suggests that the Katla volcano (Mýrdalsjökull glacier) may erupt soon, and its impact will be 10

to 100x greater than Eyjafjallajökull (Dawson et al., 2010). Locally, it will cause wide-spread flooding, road closures, coastline expansion and globally it will lead to atmospheric cooling and water quality issues (Dawson et al., 2010).

As described above, wet explosive volcanic eruptions often cause large scale deposition of volcanic ash. The thicknesses of tephra (ash and dust) can range from a few mm to more than 100 cm. Finer sediments can also be carried over a great distance from the volcanic source by wind (Arnalds, 2016). Volcanic ash in Iceland is cohesively weak, and subjected to intense aeolian redistribution, as demonstrated after the 2010 Eyjafjallajökull eruption (Thorsteinsson et al., 2012; Arnalds, 2013; Arnalds et al., 2013), and the 2011 Grímsvötn eruption (Liu et al., 2014). Even now, southern and interior areas of Iceland continue to be inundated by these tephra deposits, especially during extreme wind events. Tephra is often redistributed on snow, within both glacial and non-glacial catchments (Figure 2.1.a.), often forming linear rills of sediment on late-lying snowbeds (Figure 2.1.b.). Upper stream catchments located near Eyjafjallajökull still store substantial quantities of ash, both on snowpacks and glacial ice. Moreover, sediment deposited on bare ground after the seasonal snowpack had melted out still shows considerable thicknesses, even several years after the eruption (Figure 2.1.c.).

Dust storms are quite frequent in Iceland, which experiences between 34 to 135 days with dust storms annually (Arnalds, 2016). Most of these dust events develop in the sandy floodplains located in the south, such as Skeiðarársandur and can mix with the snow found in the environment, even during the winter seasons (Arnalds, 2016). This Icelandic dust is made of dark basaltic to andesitic poorly crystallized glass particles and comes from dust plume areas which are mostly located near glaciers and glacial river beds (Peltoniemi et al., 2015). Previous research has shown

the effect of these dark particulates on the acceleration of snowmelt (Conway et al., 1996; Painter et al., 2012; Steenburgh et al., 2012; Meinander et al., 2014; Peltoniemi et al., 2015).

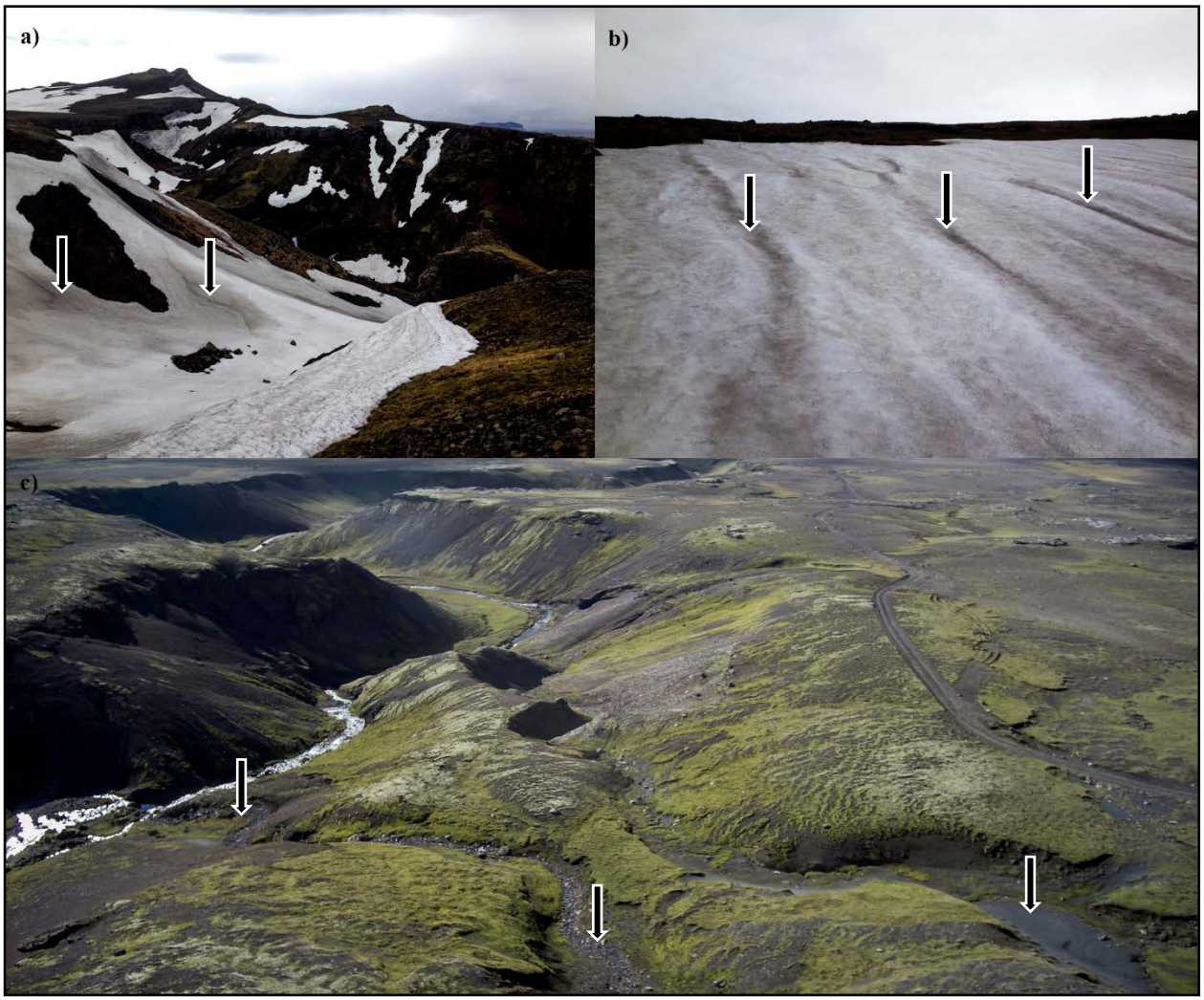

Figure 2.1 Photographs taken in spring 2015 of a hillslope catchment located near Fimmvörðuháls just east of Eyjafjallajökull, 516 m a.s.l. (a) Ash on snow at upper and lower regions of catchment. Arrows indicate areas of ash deposition on snow. (b) Rills of ash over a south-facing late-lying snowbed. (c) Looking south, two sub-catchments. The arrows indicate deposition of ash on dried streambeds.

In Iceland, aeolian processes and dust storms are part of the geomorphic landscape playing an important role in the surrounding ecosystems – both on land and glaciers (Arnalds, 2016). The frequency of the dust storms is much higher than other arctic areas, with storms occurring throughout the year, owing to the mild oceanic climate in winter. Additionally, the amplitude and

the frequency of jökulhlaups, which create and recharge these active aeolian regions are unique in Iceland (Arnalds, 2016). Cold desert areas can be found in other parts of the world such as in Alaska (Crusius et al., 2011), Greenland (Bullard, 2013) and Patagonia (Gassó et al., 2010), but Iceland has been identified as being the largest and most active high-latitude dust source area (Arnalds, 2016). Dust deposition is estimated to influence an area of >500,000 km^2 (Arnalds et al., 2013, 2014; Dagsson-Waldhauserova et al., 2013, 2014) and has also been shown to influence the mass balance of glaciers in Iceland by generating significant quantities of snowmelt (Wittmann et al., 2017).

2.2 Flooding Regimes in Iceland

Icelandic rivers were initially classified by Kjartansson (1945) and then later revised by Gardarsson (1979). They are glacial-fed rivers and non-glacial rivers, such as spring-fed or direct run-off rivers (snowmelt/rainfall). Glacier-fed rivers in Iceland exhibit large annual and diurnal fluctuations in discharge and temperature, and usually are low in pH and conductivity (Olafsson, 2002). Glacial rivers can be found in most parts of Iceland but mainly flow in South Iceland, in the vicinity of glacial margins. Here a substantial amount of meltwater and sediment, including ash and silt is transported year round (Gardarsson, 1979).

Jökulhlaups, which were first studied in Iceland by Thorarinsson (1939) are a feature of glacial retreat, and during the last ice age many of them occurred on a large scale (Bjornssonn, 2003). These massive floods are commonly associated with subglacial volcanic eruptions or geothermal activity, and often occur when meltwater collecting on a glacier or ice cap, usually associated with a failing ice dam, or due to the initiation of a new or old sub-glacial tunnel causes a brief yet significant flood event (Björnssonn, 1992; Étienne et al., 2008). Jökulhlaups can also

be the product of heavy rainfall events or periods of intense snow and ice melt. Jökulhlaups triggered by heavy rainfall generally occur during the summer months when they coincide with intense glacier ablation and meltwater production (Roberts, 2005).

Jökulhlaups can cause sandur aggradation due to the high discharge of sediments into the barren floodplain, but these delivered sediments can subsequently be eroded within a few years after the passage of other extreme events (Smith et al, 2006; Roussel, 2008). Presently, glacial retreat is considered the main driver for the accumulation of sediment on Skeiðarársandur, and over time, multiple regions of differing channel patterns distribute sediment across the plain (Magilligan et al., 2002). Seasonal meltwater does contribute to some sediment transport but it is really jökulhlaups which exert dominant control on the long-term development of Skeiðarársandur (Maizels, 1991, 1997).

The 1996 jökulhlaup event was unprecedented in South-east Iceland, with discharges exceeding some of the largest jökulhlaups across Skeiðarársandur during the past 100 years (Rist, 1957; Nummedal et al., 1987; Tweed and Russell, 1999). Magilligan et al. (2002) report that during the 1996 Grímsvötn eruption, a peak discharge of ca. 53,000 m^3/s occurred at the Skeiðará stream which drains part of the Vatnajökull ice cap. Repeat airborne laser altimeter measurements revealed net elevation gains of +29 and +24 cm in braided channels of the Gígjukvísl and Skeiðará rivers respectively (see Figure 3.1), although nearly half of these gains were eroded in four years (Magilligan et al., 2002).

On the West side of Vatnajökull is found a snout where much water drains from subglacial lakes, referred to as the Skaftá cauldrons, which are located near the Grímsvötn volcano. They initially formed in response to the underlying geothermal activity beneath Vatnajökull. They often release large quantities of meltwater into the Skaftá River, though if the interval between floods is

shorter (ca. 2 years), floods are usually smaller (IMO, 2017). Jökulhlaups emerging from here tend to travel down the Skaftá River until reaching the lowlands and the sandur. Jökuhlaups have also occurred along the Hverfisfljót and Brunná River in 1994 and 1995 (Einarsson, 2009).

Despite their short lengths (ranging between 10-50 km), the southern glacial streams draining Vatnajökull can cause substantial damage to existing infrastructure such as berms, roads and bridges. Floods in southern Iceland have washed out the N1 road (Þjóðvegur 1), the only road that connects the capital with the rest of the country. High sediment yields from these turbid glacial streams can fill up harbors with sediment, which then have to be dredged out (Donley, 1961).

Some of these glacial streams neighbour wetlands, which in Iceland, cover about 19.4% of the total landmass (Arnalds, 2016b). Iceland has lost over 90% of its wetlands since the mid-20th century, primarily in the southern and western parts of the country (Oskarsson, 1998; Thorhallsdottir et al., 1998). Much of this loss has resulted from extensive drainage, with the conversion of wetlands to agricultural lands (Gunnarson et al., 2006). About 47% of inland wetlands are impacted by this drainage (Arnalds, 2016b), yet they remain key habitat sanctuaries for certain breeding birds found both here, and elsewhere (Gunnarsson, 2006). They also provide crops for sheep, pigs and cattle which are important food sources for Icelandic rural communities. These wetlands have unique soil characteristics formed from a mixture of volcanic and organic soils (Arnalds, 2016b). A favorable pH maintained by nutrient release caused by the weathering of the basaltic glass found in the volcanic rocks, ash enhances wetland fertility (Gíslason, 2008; Arnalds, 2008, 2010).

The wetlands found in Iceland are strongly influenced by the volcanic nature of the island and by the intense aeolian redistribution which occurs here, distinguishing them from the rest of the world (Arnalds, 2016). The wetland of interest in this thesis is located in the south-eastern part

of the country, and has been experiencing shrinkage for several years as the surrounding sandur expands. The rate of sandur expansion into wetland/coastal areas is of real concern to the Icelandic farming community, and studies such as this one may help them to better understand how to protect their lands.

2.3 Climate Change in Iceland

Temperatures in the Arctic have been increasing faster than anywhere else over the last few decades (IPCC, 2007). This unprecedented warming has led to earlier spring melt events and lengthening of the thaw season in Alaska (Stone et al., 2002); in Greenland (Stroeve et al., 2006; Box et al., 2006), and also throughout Iceland (Bjornsson et al., 2008). Extreme warming events have led to mid-winter snowmelt events (ESE) in Kobbefjörd, southwest Greenland (Pedersen et al., 2015), and recent tundra wildfires near Sisimiut in southern Greenland (Cartier, 2017).

In 2008, the Ministry for the Environment of Iceland published a full report on the expected impacts of climate change in Iceland (Bjornsson et al., 2008). Some of the expected trends include a temperature increase of 0.2°C per decade with winter temperatures increasing more than summer temperatures. A rise in precipitation by about 0.4% to 0.8% per decade is expected, and a complete retreat of Icelandic glaciers in the next 150-200 years. Moreover, expectations are for a 10% increase in volcanic eruptions due to isostatic rebound from a retreating glacial mass (Bjornsson et al., 2008; Compton et al. 2016). The main consequences of these environmental changes include increases in meltwater floods and occurrence of glacial river floods in the winter season (Bjornsson et al., 2008; Jonsdottir, 2008). Discharge from Icelandic rivers near glacial margins is projected to increase by approximately 30% by 2030 and by about 50% by the end of this century (Bjornsson et al., 2008). A recent report published in 2017 by the Icelandic Meteorological Office (IMO)

(Gosseling, 2017) expects a considerable warming of 1.8 to 3.1ºC in the 21st century, with an increase in warm summer days. The report also found that there will likely be an increase in precipitation throughout most of the country, correlating with increasing temperatures, and a greater probability of high precipitation events (10 mm/day or more).

Increases in glacial runoff are considered to be the most important hydrological impact of climate change in Iceland (Bjornsson, 2008). Improved understanding of these impacts on the landscape in response to both recent and future warming is generally warranted. Therefore, in this thesis, a framework is proposed to study shifts in the hydrological regime of an Icelandic sandur-wetland complex in response to seasonal and episodic hydro-climatological events.

2.4 Paraglacial Theory

Paraglacial theory was first formalised by Church and Ryder (1972), and is defined as non-glacial processes that are directly conditioned by glaciation across a period of time. The concept was initially coined earlier by Ryder (1971) to describe alluvial fans in British Columbia following the Late Wisconsin deglaciation. Their shape was mainly controlled by processes transitioning from glacial to post-glacial conditions, at a time when abundant glacial debris and sediments were available. The term “paraglacial” is therefore synonymous with unstable conditions caused by processes which result in transformed geomorphic patterns following glacial intervals. Rates of landscape change and sediment output are typically elevated during paraglacial episodes (Church, 1972).

Hence, the paraglacial theory highlights a period where deglaciated landscapes adjust to non-glacial conditions with the paraglacial period ending once sediment yield drops to rates typical of unglaciated catchments (Figure 2.2 a). Ballantyne (2002) suggested that the paraglacial period typically lasts as long as sources and storages of paraglacial sediment are not depleted. The gradual decline in sediment yield characteristically follows a curve of exponential law, correlated to the volume of available sediments (Figure 2.2 b).

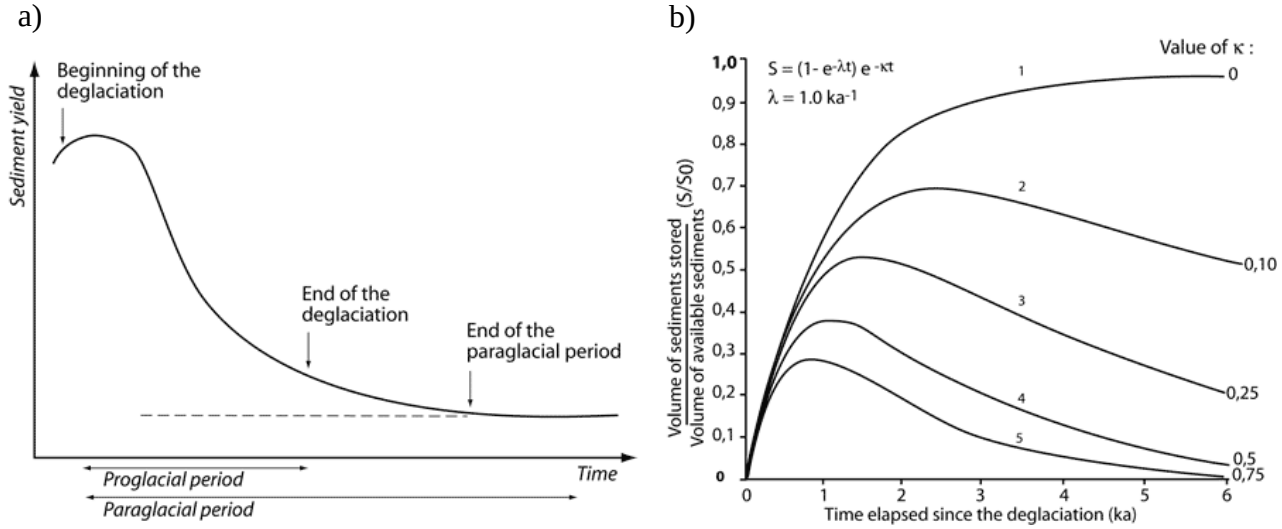

Figure 2.2 The paraglacial period as defined by Church and Ryder (1972) (a); application of the exhaustion model to assess the evolution of the volume of sediments within a paraglacial store (Ballantyne, 2003) (b). Source: Mercier, 2008.

Ballantyne (2002) initially augmented and refined the definition lengthening the use of the term paraglacial from a descriptor of processes, to a descriptor of consequential landforms, sediments patterns and landscapes. He identified six paraglacial landsystems: rock slopes, drift-mantled slopes, glacier forelands, and alluvial, lacustrine and coastal systems. Skeiðarársandur was classified in the study as an active paraglacial coastal system with the unconfined sandur meeting the sea in exposed locations. The resulting configuration of the coast and sedimentology reflects the transport of glacially derived sediment, as well as sediment re-worked from sandur

surfaces by the proglacial braided rivers and the re-working of these sediments by waves, tidal currents and longshore drift (Ballantyne, 2002). Similar processes have been documented in North-west Spitsbergen (Hequette and Ruz, 1990) and the Gulf of Alaska (Forbes and Taylor, 1994).

Since Church and Ryder's initial thoughts, understanding of paraglacial processes now comprise an array of geomorphological processes (see Knight and Harrison 2009, 2014). Knight and Harrison (2014) in particular related the effects of global warming such as episodic landslides, erosion and rainstorm events to the model in releasing stored quantities of sediment (Figure 2.3).

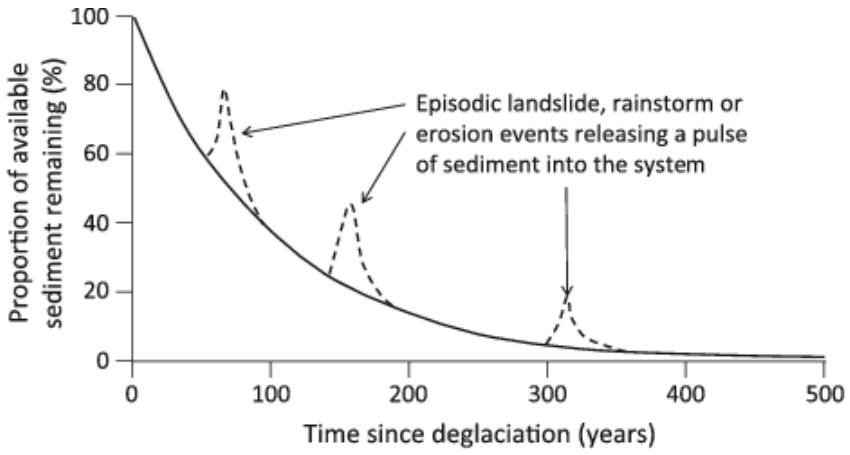

Figure 2.3 Schematic graph showing decline in sediment yield over time during the period of paraglacial readjustment, and the role of episodic high-magnitude events such as landslides, rainstorms or periods of enhanced erosion in temporarily increasing the sediment yield (after Church and Ryder 1972; Ballantyne 2002). Source: Knight and Harrison (2012).

The life expectancy of the paraglacial land system is limited but has the potential to be prolonged for centuries or millenniums in areas with large sediment storage (Cossart and Fort, 2008). Climate change can also lead to paraglacial geomorphological re-adjustments, yet in southern Iceland, frequent volcanic eruptions can rapidly re-adjust the surrounding geomorphology by re-stocking sediment deposits in both upper and lower parts of a drainage basin, thereby generating a continuous refilling pattern of sediment within the drainage system – creating a “one of a kind” paraglacial environment.

2.5 Aims of Study

Recent field observations suggest increasing erosion along the banks of the Brunná River and an expansion of the sandur into the adjacent wetland, especially after large flooding events. This thesis therefore seeks to understand how tephra and glacial material coupled with the local climate and episodic events influences a sandur's expansion and hydrological regime. This first involves analyzing the hydrological regime of a glacial river –the Brunná River draining from Vatnajökull, identifying periods of melt, jökulhlaups and episodic events, and linking these hydrological patterns to sediment transportation regimes. Then an estimation and visualization of these erosional and depositional patterns is attempted using remote sensing means and an unmanned aerial vehicle (UAV) in order to scan the topography and undertake a DoD (DEM of Difference) analysis of the sandur-wetland. Hydrological interactions between the sandur and adjacent wetland site are also examined. Specifically, this research attempts to:

1. understand the general hydrological regime of this sandur-wetland and it's linkages with climate variability and extreme events which are unique to this environment;
2. asses the degree of hydrological interactions between the sandur and nearby wetland by describing and quantifying the amount of water being transferred between the two landscapes;
3. expand on the paraglacial theoretical concept here by investigating the role of volcanic tephra/ash on the sediment exhaustion regime of this sandur landscape.

2.6 Theory-Hydrology and Water Balance

This study documents the effects of tephra fallout on the hydrology of a sandur-wetland landscape and monitors a suite of flooding regimes generated by both seasonal and severe meteorological conditions. Employing a water balance framework to assess inputs and outputs of water and sediment sheds light on the processes driving the hydro-geomorphic dynamics of this sandur-wetland system.

The water balance approach is a useful tool serving to assess overall inputs, outputs and changes in storage within this sandur-wetland environment (Thornthwaite, 1955). The water balance equation is shown below:

$$P(Sn + R) - E + Q_{in} - Q_{out} = \pm\Delta S + \zeta \quad (1)$$

where P is precipitation, Sn = Snowfall (or Melt), R = Rainfall, E is evaporation (including transpiration), Q_{in} is inflow (surface/subsurface flow) and Q_{out} is surface/subsurface outflow out of the sandur (surface + subsurface flow). ΔS is the change in storage and ζ is the error term. The storage (ΔS) and error component (ζ) are often not measured directly, and often are combined into one term (ΔS) (Kane and Hinzman, 1988; Young and Woo, 2004).

Monitoring the individual components of the water balance equation of a sandur and an adjacent wetland zone is an ideal approach, allowing for a comprehensive analysis of two contrasting land types. This also allows one to discern the shifts in processes that might occur

within the hydrological regime of the wetland during sandur expansion. Oftentimes, in such remote studies, only a few of the variables in Equation 1 are studied as is the case here.

Understanding the hydrologic regime of an Icelandic sandur in response to moderate hydro-climatic cycles and extreme events that can occur within this unique paraglacial environment requires information on the local climate as well as evidence of sediment transport and erosional patterns. The hydro-geomophological approach of this study is outlined in Figure 2.4. It is a conceptual diagram signifying the influence of tephra or volcanic ash on the hydrological regime of a sandur, especially in terms of its flooding pattern and resultant geomorphologic signature.

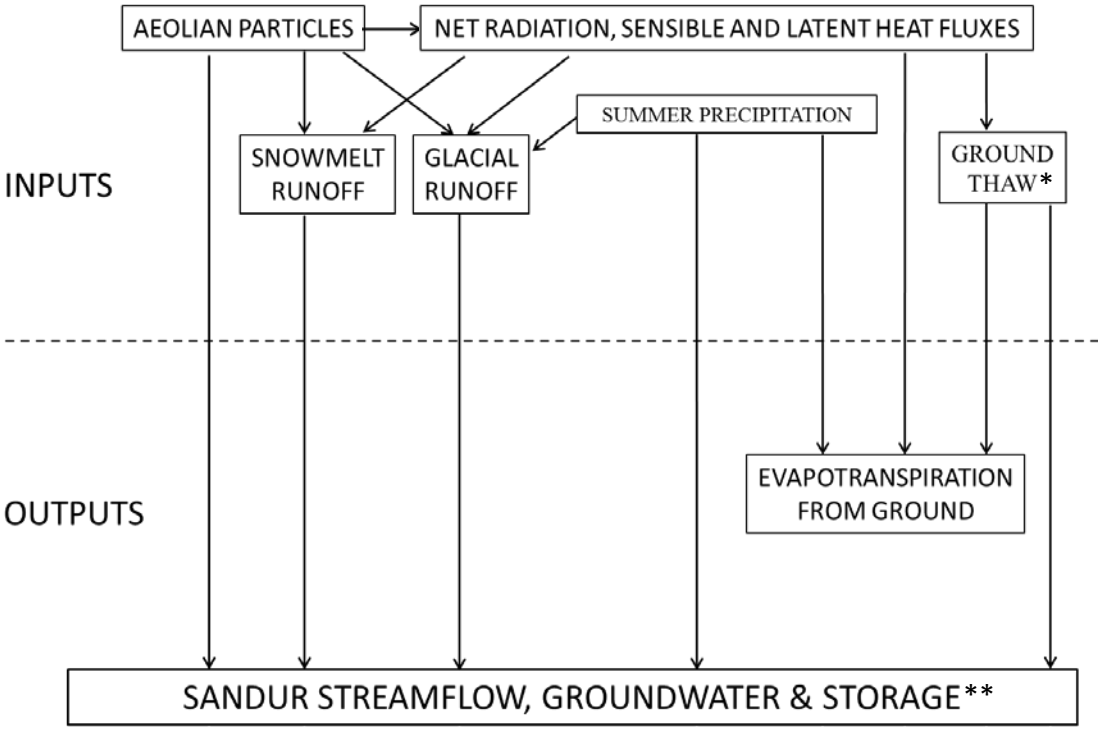

Figure 2.4 Influence of aeolian particles (specifically ash and tephra fallouts) on net radiation, sensible and latent heat fluxes, which consecutively influence rates of melt, runoff and evapotranspiration from the ground. These hydrological processes in turn influence streamflow, groundwater and storage. Climatological variables such as temperature, precipitation and wind can also influence these same hydrological processes and therefore the hydrological regime of the sandur. *Some locations may include ground thaw. **Storage can include soil moisture, and water level fluctuations in temporary water pools. Diagram adapted after Lewkowicz (1977).

CHAPTER THREE: STUDY AREA

3.1 General Climate and Hydrology of Iceland

Iceland's weather pattern is governed by the influence of many geographical and meteorological processes. At this latitude, there is a considerable deficit in total radiation, yet significant heat transfers from lower latitudes are carried here through both atmospheric and oceanic circulations (Einarsson, 1984). In coastal areas, the maritime winter climate yields numerous free-thaw cycles and a thin and fluctuating snow cover (Einarsson, 1984). Most of the Icelandic climate is characterized by frequent intense precipitation, strong winds, and mild winters (Olafsson et al., 2007). Its climate is also influenced by warm and cold ocean currents. The North Atlantic Drift, and one of its branches, the Irminger current passes the southern coast of the country on a north-eastward direction while the cold East Greeland current flows southerly along the east coast (Einarsson, 1984). Arctic and mid-latitudinal atmospheric cyclones also often occur here, bringing precipitation, strong winds and rapid changes in weather (Einarsson, 1984; Bjornsson et al., 2013). Since 2014, severe rainfall events triggered by these cyclones have resulted in mudslides and rapid flooding at lower elevations (IMO, 2014, 2015, 2016).

Atmospheric circulation and sea surface temperatures tend to influence seasonal and annual precipitation in Iceland, (Jónsdóttir and Uvo, 2009). In general, mean precipitation varies from 1000 mm in coastal areas to less than 45 mm in the interior polar deserts where most falls as snow (Einarsson, 1984). Most of the overlying seasonal snow melts from April to June but in mountainous areas, the melt season can extend well into July and August (Jónsson, 2002). Precipitation is highest on glaciers and mountains along the southern coast (Eyþórsson and Sigtryggsson, 1971).

About 11% of Iceland's territory is covered with glaciers (Sigurðsson et al., 2007) with roughly 85 streams draining 71% of the entire country (Donley, 1961). Glacier-fed rivers in Iceland exhibit large annual and diurnal fluctuations in discharge and temperature, and usually have low pH and conductivity values (Olafsson, 2002). Glacial rivers can be found in most parts of Iceland though they are common in south Iceland in the vicinity of glacial margins (Gardarsson 1979).

Iceland's climate is unique as it is more temperate than would be expected for its latitude just south of the Arctic Circle yet atmospheric mixing, high wind speeds and severe rainfall events typify Iceland's climate to be extremely variable.

3.2 Study Site

In front of Skeiðarárjökull, the flood plains of the river Skeiðará form Skeiðarársandur, an outwash plain made of black sand and ash, intersected by small glacial streams (Figure 3.1). It covers the whole area between the Vatnajökull ice cap and the Atlantic Ocean located 20 km away.

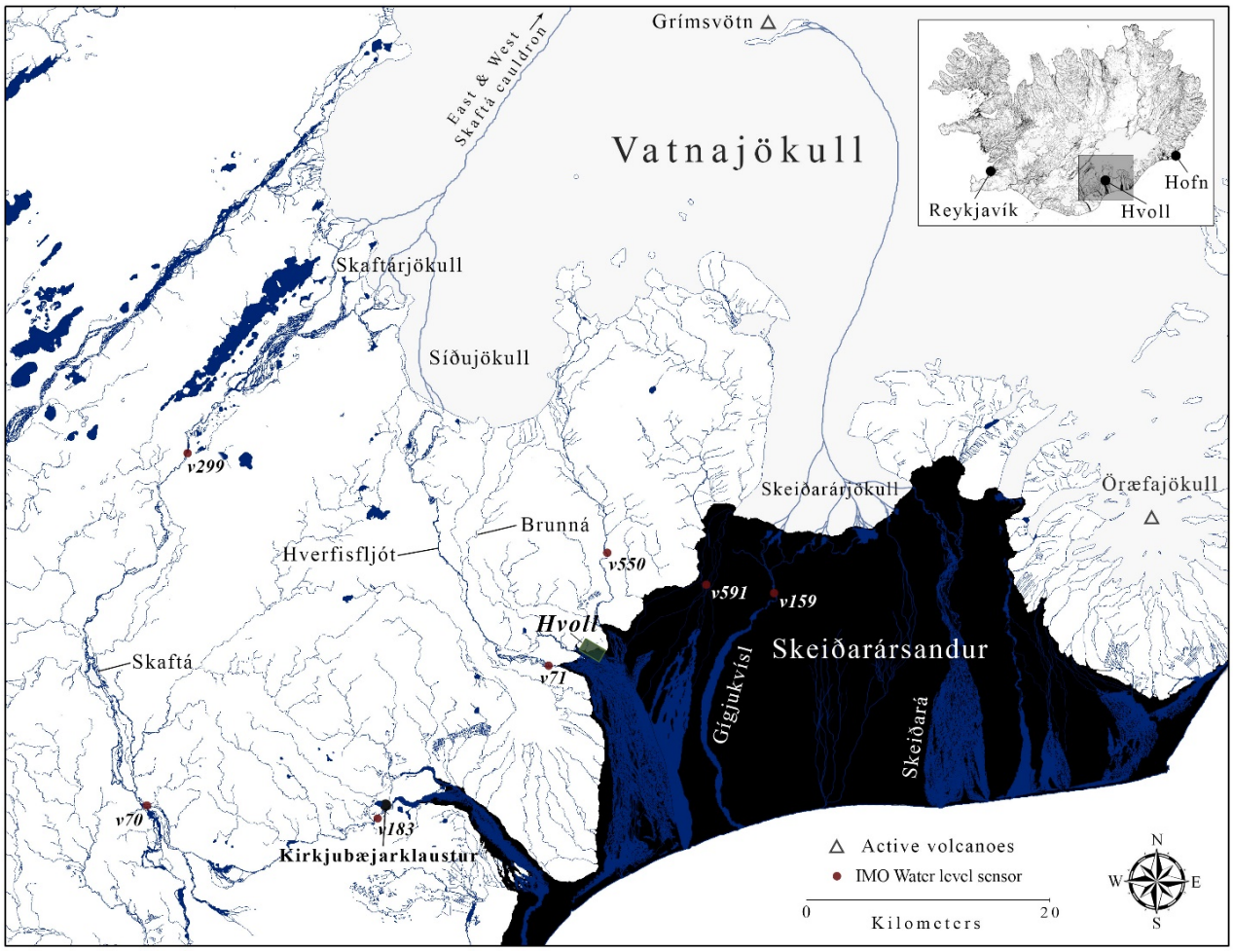

Figure 3.1 Map of Skeiðarársandur marked with the location of the Hvoll study site. The Skaftá, Hverfisfljót and Brunná rivers carry meltwater from the Skaftárjökull and Síðujökull glaciers, smaller glaciers located west of Vatnajökull. The Gígjukvísl and Skeiðará rivers originate from the Skeiðarárjökull glacier. Subglacial lakes are located near the active Grímsvötn volcano which often releases large quantities of meltwater into these rivers in the form of jökulhlaups. Locations of Icelandic Meteorological office water level sensors are marked with red circles with their respective identification number. River data is sourced from the National Land Survey of Iceland (NLSI).

The research site (Hvoll Farm) is set on the shores of the Brunná River in South-east Iceland (63.90 N, 17.68 W) and is located in the north-west corner of Skeiðarársandur. The multiple glacial streams that form a network across the landscape, outflow into smaller sandurs that make up the whole of Skeiðarársandur. The study site is located at the junction where the river shifts from a channel to a braided pattern, typifying the start of the sandur. Before the sandur, the river flows through a steep mountainous landscape before entering into the Laki lava field which borders the low gradient Skeiðarársandur to the south (Figure 3.2). This area is of special interest as it borders a wetland and a working farm that has been under threat from flooding, both from the Brunná and Hverfisfljót Rivers.

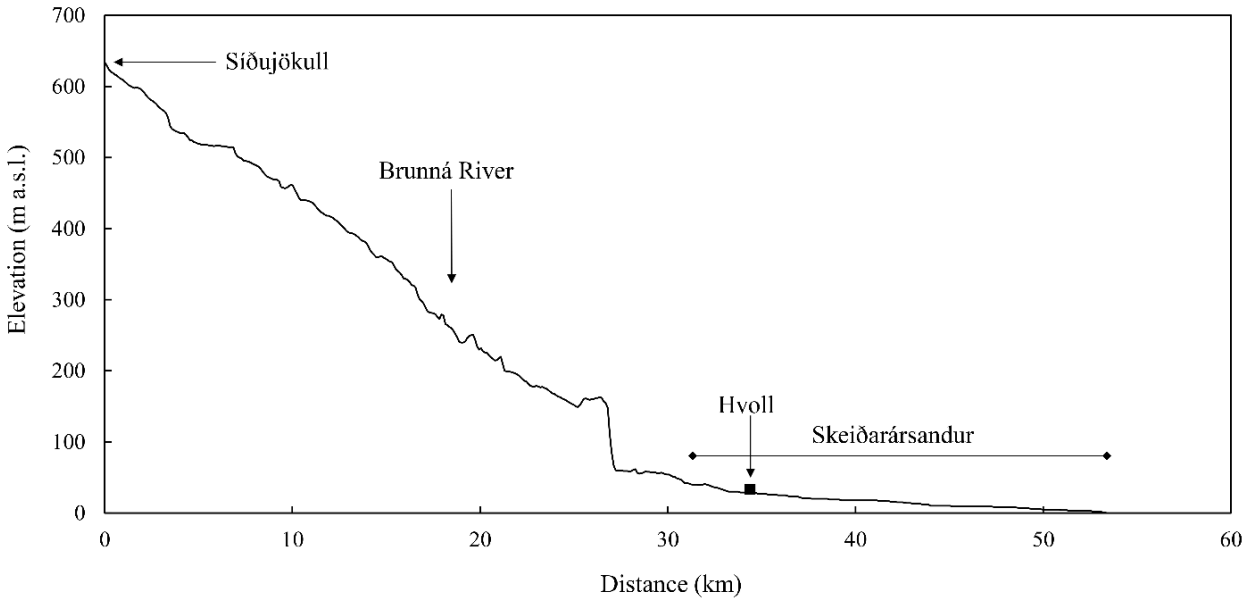

Figure 3.2 Elevation profile of the Brunná River, starting from the tongue of Síðujökull, a smaller glacier to the west of Vatnajökull. It passes through the Hvoll study site where the elevation levels off, until it empties into the Atlantic Ocean. The DEM from which the flow path was traced originates from the NLSI.

The region of southern Iceland has a low arctic maritime climate characterized by cool summers and mild winters. Mean January and July temperatures near the study site at Kirkjubaejarklustur, are about 0.8ºC and 11.2ºC respectively. Annual precipitation in the form of rain and snow here amounts to 1,538 mm (IMO, 2016). Relative humidity is high (86 - 100%), largely due to the nearness of the Atlantic Ocean. This region is often marked by frequent changes in weather due to mild Atlantic air interacting with colder Arctic air. Most of the precipitation in Iceland falls in the south on the surrounding mountains, ice caps and along the coast.

Three glacial streams; Hverfisfljót, Brunná and Djupá originating from the Vatnajökull ice cap neighbour the study site (Figure 3.3). These glacial streams continuously transport sediment from the nearby glaciers into Skeiðarársandur creating a desert landscape predominantly made up of black alluvial materials such as ash and sand (Arnalds, 2008). The many streams of Skeiðarársandur exhibit a highly braided landscape predominantly composed of gravelly, coarse deposits with a downstream decrease in particle size (Magillian et al., 2002). Fluctuations in meltwater discharge coupled with re-occurring outburst floods yields continuously changing erosional and depositional patterns in the landscape.

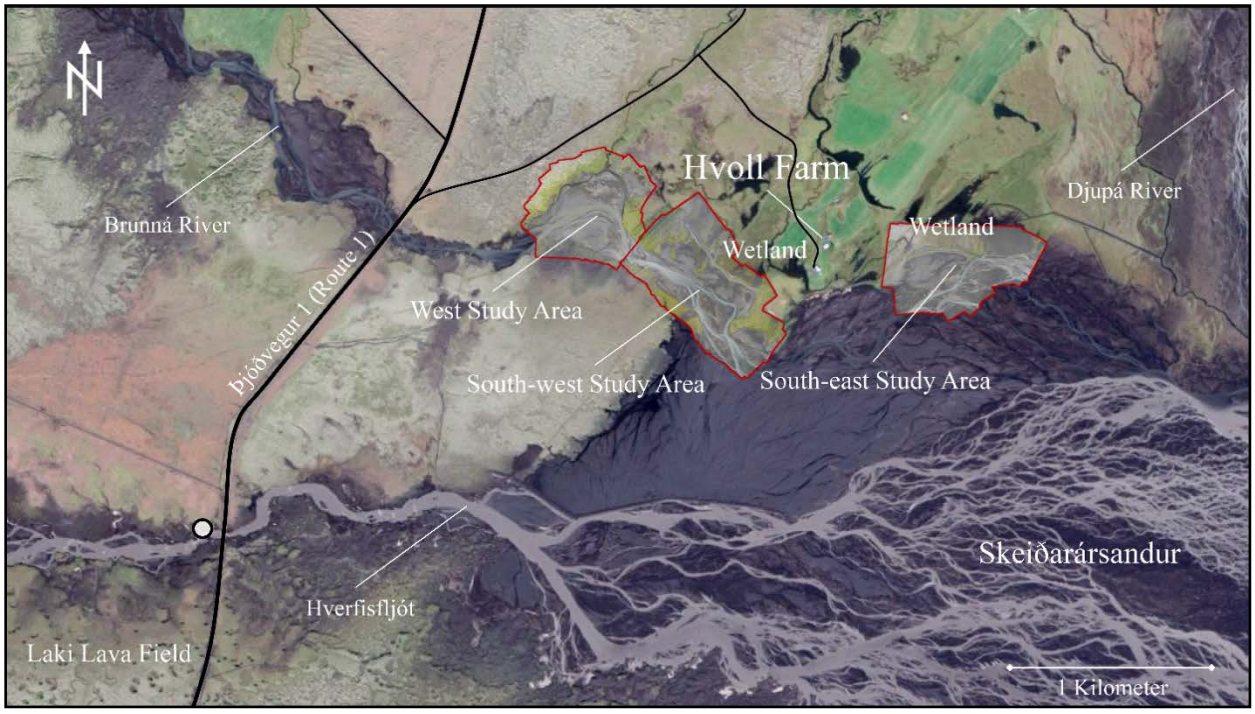

Figure 3.3 Location of the three study sites (West, South-west and South-east) in relation to the Hverfisfljót, Brunná and Djupa Rivers. Location of IMO water level and conductivity sensor at Hverfisfljót (v71) indicated by a white circle. Base image sourced from Google Earth.

The landscape surrounding the Hvoll farm is diverse as it borders the ancient Laki lava field to the West and the inhabited wetland to the east with an area ca 1.19 km^2. At the South-east study site (area = 0.124 km^2), the wetland is lower in elevation by ca. 1 m in comparison to the adjacent sandur. This elevation difference is attributed to the presence of a berm that was initially built to stop water and sediment from the Brunná and Hverfisfljót rivers, entering into the wetland. Over the years, an accumulation of ash fall from Grímsvötn eruptions (usually every 10 years) and sediment inputs from the Brunná River has built up the sandur streambed, explaining the current elevation difference here. Hay bales are routinely placed throughout the sandur near the sandur-wetland boundary to trigger dune formation, another line of defense used by the farmer to prevent floodwaters from entering into the wetland. On the South-west site (area = 0.238 km^2) the wetland

is at about the same elevation as the sandur. A berm was built here in late 2011 to protect the farm from floods also originating from the Brunná and Hverfisfljót rivers. Figure 3.4 illustrates the elevation and general topography of the land surrounding the farm including the location of the wetland ponds, streams and the path of the Brunná River.

The wetland is predominantly comprised of smaller channelized springs, ponds and small streams providing habitat for many Arctic bird species. The shifting course of the Brunná River on the sandur side has been observed to cause bank erosion along stretches of the river which will be investigated later in this thesis. These sandur-wetland zones were chosen to qualify and quantify the seasonal water fluctuations and groundwater fluxes from the sandur into the wetland in response to various climatological and episodic events.

The South-west site berm that was built in late 2011 diverted water from a suite of small springs that discharged into the Brunna River. Ponds have now emerged with overland flow moving through man-made channels to the south of the wetland, essentially diverting water further south into the sandur. These ponds and streams provide shelter for migratory and local birds. Additionally, the water table is usually near or above the ground surface in this sandur-wetland area (Figure 3.5).

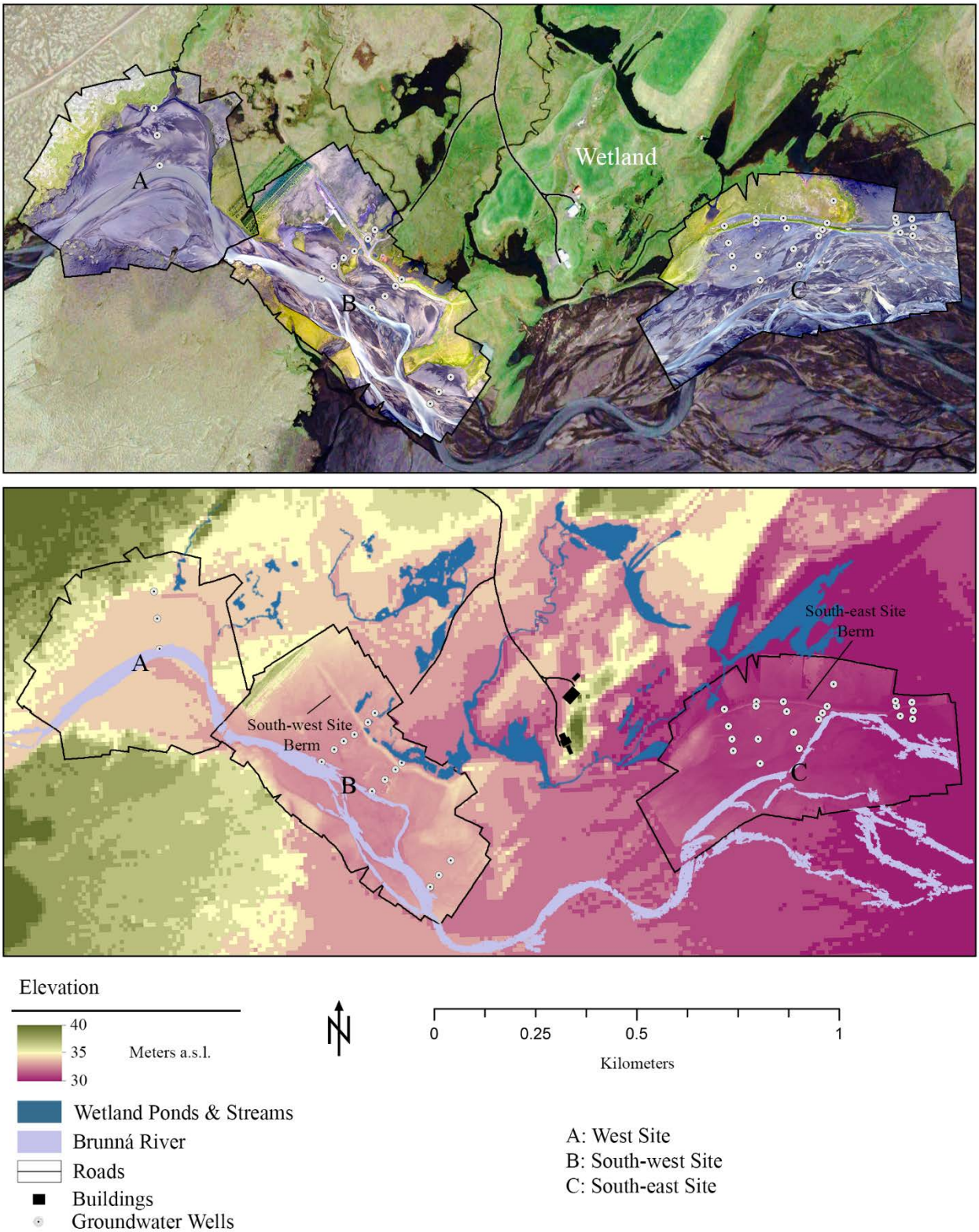

Figure 3.4 Digital elevation model around the inhabited Hvoll farm. Site A, B and C represent the West, South-west and South-east study zones. Top diagram illustrates the study area around the Hvoll farm in true colour. A color gradient is applied to respective elevation values of the mosaicked NLSI and UAV derived DEMs in the bottom diagram.

Figure 3.5 Aerial photo looking south towards the Atlantic Ocean with the distant white caps of Vatnajökull located to the east. The boundaries of the West, South-west, South-east sites are shown. The water table here in this sandur-wetland landscape is usually found near the surface.

3.2.1 Site Surface Materials

Sandur soil grading of the area ranges from gravel to sand-sized material with layers of fine ash compacted within the soil stratigraphy. Bulk density and porosity values of samples collected throughout the study area are listed in Table 3.1. Bulk density values ranged from 1.25 g/cm^3 to 2.09 g/cm^3 with glacial flour and fine ash, having lower values compared to coarser stream gravels. The spatial pattern of sediments in the sandur (gravels to fine) ash can be observed from UAV imagery (Figure 3.6). Gravels were found closer to the river banks where fine particles would be washed away. Yet finer particles were also found near these same river banks after floods when the stream water level receded. In sandar landscapes, gravels generally keep stream banks stable as finer particles are often washed away (Church, 1972). Sands were found throughout the sandur, mainly localized in the middle between the river banks and berms. Finer ash and glacial flour was located in localized sites where floodwaters inundated the sandur. Falling water levels after a flood event would allow fine particles to settle over the underlying soil, drying up until the

next flooding event. This process of sediment distribution is examined in the Discussion section of this thesis but is visually clear from Figure 3.6.

Porosity which is the percentage of voids in a volume of soil, were highest for fine ash and glacial flour, which is able to hold ca. 38-40% of water. Layers of this fine ash were also found down in the soil profile and exhibited similar porosity values (Figure 3.7).

Table 3.1 Bulk Density, Porosity and Particle density values collected throughout the study area during spring and summer 2016. * indicates fine sediments that clogged the first well along transect 3 (T3W1-See Section 4.2.3) during the August 15th 2016 rainfall event.

Transect - Particle sizes	Bulk Density (g/cm^3)	Porosity	Particle Density (g/cm^3)
T2W1 - Gravels	2.09	0.29	2.95
T2W2 - Sand	1.52	0.32	2.25
T2W3 - Silt, Sand	1.33	0.33	1.98
T3W1 - Silt*	1.47	0.35	2.27
T3W3 -Silt, Sand	1.34	0.37	2.13
T5W3 - Silt	1.38	0.39	2.28
T6W1 - Sand, Gravels	1.70	0.30	2.44
T6W2 - Silt	1.35	0.38	2.19
T6W2-3 - Silt	1.36	0.38	2.19
T6W3 - Sand	1.34	0.36	2.09
T7W3 - Silt	1.25	0.40	2.07
T7W3 - Sand	1.27	0.33	1.89

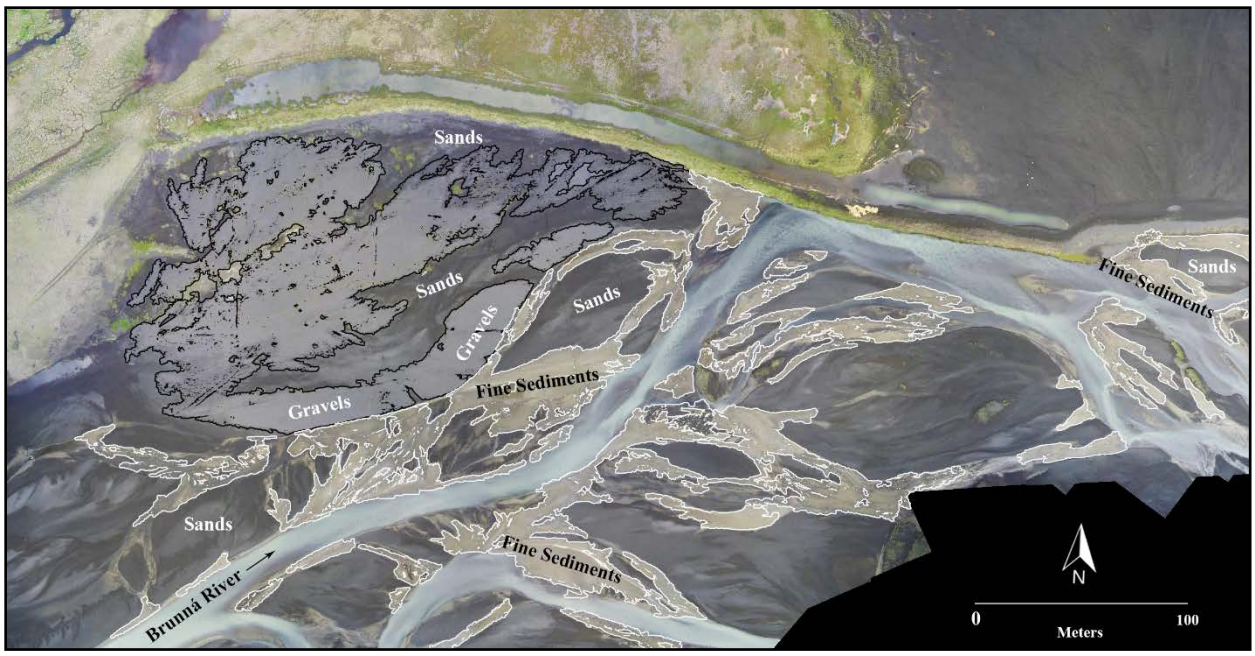

Figure 3.6 Aerial photo taken on June 17th of the Brunná River at the South-east site during low water levels. Notice deposition of finer sediment (mud) along flood tracks. Gravel areas are lighter in colour than dark sand (basalts).

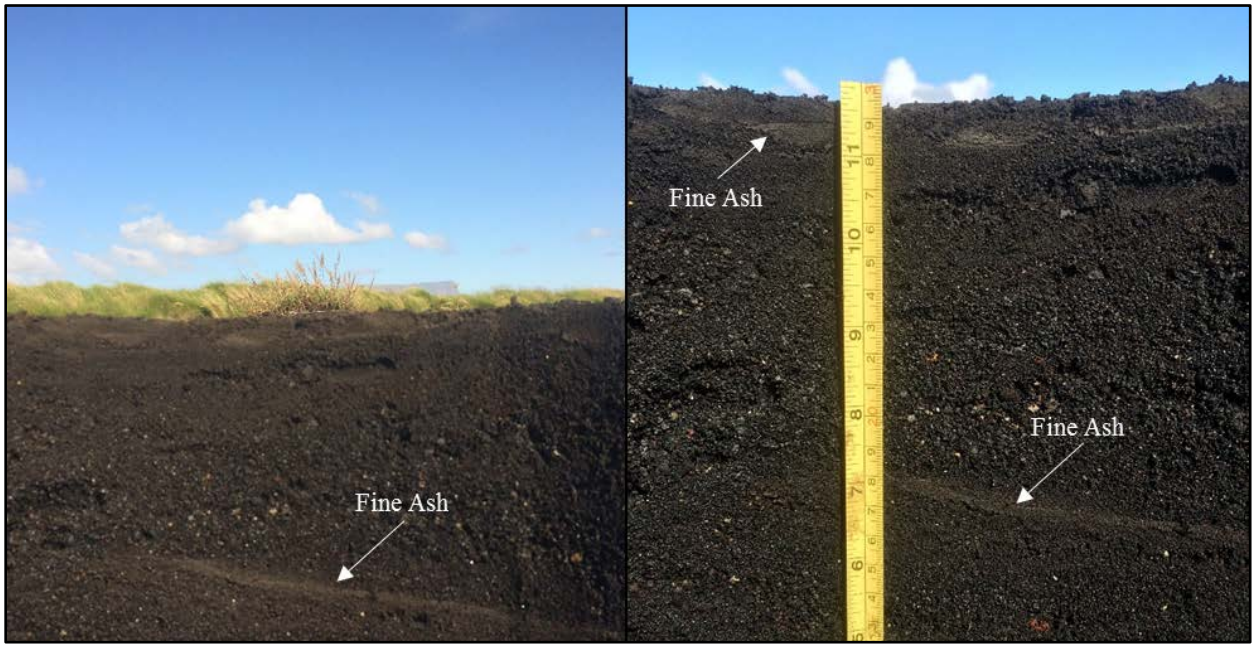

Figure 3.7 Photographs of shallow soil pits taken at the South-east study sandur site illustrates layers of finer ash compacted between coarser sediment (coarse sand).

3.2.2 Vegetation

At this sandur-wetland site, sharp contrasts between the two surface types were observed. The sandur is generally devoid of vegetation with the exception of areas where piles of hay were spread by the farmer to promote vegetation growth. Some vegetation can be found on the wetland side, mainly grasses and thufurs, a type of small vegetated hummock that mainly develops in volcanic loess on drained basaltic rocks (Van-Vliet-Lanoe, 2000). Although it has been demonstrated that some vegetation (usually small grasses) manage to take hold in Skeiðarársandur between flooding events (Shoopala, 2008), much of the sediment in this environment is loose and easily transported by wind (Arnalds, 2008). Some anthropogenic activities such as improper land-usage and sheep grazing has contributed to sandur expansion (Raynolds et al., 2015) though; it is still the large input of sediments brought in by the glacial streams and deposited throughout the landscape which nourish the sand fronts that expand into vegetated areas (Arnalds, 2008, 2010). These fronts have been observed to abrade and bury the vegetation with sand (Figure 3.8). Actions have been undertaken to prevent further erosion and stabilize eroded areas through revegetation and ecosystem restoration (Arnalds et al., 2000). For example, local farmers have built berms and planted trees in order to stabilize barren areas and initiate a vegetation cover.

Figure 3.8 Photograph taken on June 21st 2016 after a sandstorm event showing the burial of plants.

CHAPTER FOUR: METHODOLOGY

This chapter details the various climate and hydrological methods and equipment used to collect field data for this thesis. Site data collection was carried out in both the springs and summers of 2015 and 2016 but the main study period was between 1 June and 1 September 2016. This section also describes the process of collecting photogrammetric data for the purpose of creating a digital elevation model, and the steps undertaken to perform a three dimensional change detection analysis between flooding events. This was carried out in an attempt to detect patterns of erosion and deposition across the sandur.

In addition to field data, water level records from neighboring streams were sourced from the IMO. Data was obtained for the Skaftá River located 21 km west of Hvoll, and the Hverfisfljót River, a neighboring river located just 1.2 km west of Hvoll. The IMO is a public institution under the umbrella of the Icelandic Ministry for the Environment and Natural Resources and has the responsibility of monitoring natural hazards and conducting research in related fields. The IMO's monitoring system consists of a network of 170 hydrological gauges installed in rivers throughout the Icelandic territory. The data is accessible to the public and is utilized here to support some of the study's general findings. Hydrological data: conductivity, water level and temperature as well as meteorological data (wind speed, temperature, rainfall) were useful in validating results. Two IMO water level gauges: Hverfisfljót (v71) and Skaftá við Sveinstind (v299) augmented site water well data and were useful in hydrologic analysis (see Figure 3.1. for location of IMO sensors).

4.1 Climatology

A small automated weather station (AWS) was installed on site to monitor climatic conditions. Climate in this region directly affects many hydrological processes, including glacial melt, snowmelt and evaporation losses (including transpiration). Barometric pressure maps and wind data from the Icelandic meteorological office (IMO) at Hofn located 128 km from the site were used to assess wind direction and storm intensity. Daily spot wind speeds (m/s) and direction, including severe wind events were measured on site using a hand-held Kestrel.

4.1.1 Air Temperature

Air Temperature (T_{air} °C) data was logged throughout the site with four ONSET HOBO Temperature/Light 64K Data Loggers (± 0.53°C from 0° to 50°C) at a height of 1 m above the ground. T_{air} data was collected on a 30 minute interval yielding mean daily temperature records from August 30th 2015 to September 3rd 2016. This time period spanned both freeze-back and melt. Air temperature estimates were regularly checked against a hand-held Kestrel (± 0.5°C) during the June 19th 2016 jökulhlaup and August 15th 2016 severe rainfall event.

4.1.2 Relative Humidity

Relative humidity was logged on a 30 minute interval using an ONSET HOBO U23 Pro v2 Temperature/Relative Humidity (RH%) Data Logger (± 2.5%) installed at 1 m above the ground, on the West site near T2W5 (Transect 2, Well 5 – See Section 4.2.3). The sensor was installed on August 24th 2015 and logged until September 2nd 2016 yielding continuous RH% throughout the study period.

4.1.3 Surface Energy Balance

Many hydrological activities are modified by the surface energy budget which accounts of all exchanges of energy:

$$Q^* = K^* + L^* = Q_H + Q_E + Q_G \quad (2)$$

here net radiation (Q^*) consists of radiative fluxes (both net shortwave (K^*) and net longwave (L^*), the turbulent fluxes are sensible (Q_H) and latent heat (Q_E), and Q_G is the ground heat flux. These fluxes contribute to energy and water exchanges at the surface: latent heat flux (Q_E), represents the portion of energy used in the evaporative process (condensation is the reverse), Q_H is the sensible heat flux, and accounts for the warmth of the air (air temperature), and Q_G moves heat into/out of the ground across the surface/atmospheric interface.

Net radiation (Q^* - W/m^2) was measured using two Kipp & Zonen NR-LITE2 net radiometers that were connected to a Campbell Scientific CR10X datalogger. One net radiometer was installed in the sandur at the South-west site, and the other ca. 8 m away in the adjacent wetland. Both net radiometers were calibrated to ± 3% and data collection extended from June 5th to August 31st 2016. These data were averaged on a 30 min interval. Ground heat flux (Q_G - W/m^2) was measured in the sandur and wetland between June 5th and August 31st 2016 using four Campbell Scientific CN3 heat flux plates with two plates installed in each surface type. The plates were installed 5 cm below the ground surface. Q_E (W/m^2) was calculated using the Priestley-Taylor equation following Woo and Guan (2006) and averaged over 30 minutes (Jun. 5 - Sept. 3, 2016). Daily totals allowed mass estimates of evapotranspiration (mm/d) to be made for each surface (see evaporation in section 4.2. Owing to only spot estimates of wind speed, Q_H (W/m^2) was determined as the residual in the equation for each surface.

4.1.4 Albedo

Surface albedo (α), the ratio of incident radiation reflected upon a surface K* = K↑/K↓, was measured using a LI-COR LI-200R pyranometer, 1.0 m above the ground. It was connected to an EXTECH MN62 digital voltmeter. Sandur, berm and wetland surface types were sampled four times each at the time of sampling (mid-day) and then averaged to a single value for that day. Albedo measurements were taken several times over the season to track the seasonal pattern of α.

4.1.5 Soil Temperature

Near surface soil temperature (-1 cm) is a valuable indicator in determining contrasting patterns in energy receipt between the wetland and the adjacent sandur. Therefore four copper–constantan thermocouples (±0.1°C) hooked up to a Campbell Scientific CR10X datalogger collected soil temperature data at the barren sandur (n = 2) and adjacent vegetated wetland (n = 2). Data from both surficial types was collected on a 30 min interval from June 5th to August 31st 2016 and averaged to provide daily averages.

4.2 Hydrology

4.2.1 Precipitation

Three ONSET HOBO RG3-M tipping bucket rain gauges (±0.25 mm/tip) summed rainfall receipt (mm) on a 30 minute interval, providing daily totals (mm) from June 5th 2016 to August 2nd 2016. Two rain gauges were installed in the South-west site, with one on the east and the other on the West side of the Brunná River. One rain gauge was installed in the South-east site at the highest point on the berm. Location of the tipping bucket rain gauges are shown on Figure 4.1. Daily rainfall data from the weather station at Hofn was also collected and compared with site amounts.

4.2.2 Evaporation

In order to estimate atmospheric water losses in the sandur and wetland, daily evaporation losses (*E*) (mm/d) were estimated using the Priestley-Taylor (1972) approach (Equation 3). Here

$$E = \frac{\alpha \frac{S}{S+\gamma}(Q^* - Q_g)}{L_v \times \rho_w} \quad (3)$$

where α is the Priestley-Taylor coefficient, *S* is the slope of saturation vapor pressure-temperature curve (Pa K^{-1}), γ is the psychrometric constant, Q^* is net radiation (MJ/d), Q_g is the ground heat flux (MJ/d), *Lv* is the latent heat of vaporization ($\lambda_v = 2.501 \cdot 10^6 - (2370 \cdot T)$ J/kg) and ρ_w is the density of water (1000 kg/m^3). *T* is air temperature (°C).

The calculation of the slope of the temperature-saturated vapour pressure curve and the psychrometric constant (γ) is achieved using the following equations, respectively:

$$\Delta = \frac{4098 \times e_{as}}{(237.3+T)^2} \quad (4)$$

and

$$\gamma = \frac{C_p \times P_A}{0.622 \times \lambda_v} \quad (5)$$

where e_{as} is the saturated vapour pressure at air temperature T in °C, and can be computed using the following equation (after Reid 2004):

$$e_{as} = 611^{\frac{17.27 \times T}{237.3+T}} \quad (6)$$

The specific heat of air C_p is 1006 J/kg·°C and air pressure, P_A, is 101.3 x 10^3 Pa.

Studies indicate that the α term can vary from 1.08 to more than 1.60 depending on the advectivity of the surrounding environment (Villalobos et al., 2002). Marsh et al. (1981) were able to calculate an α value as a function of soil moisture at a site predominantly made of gravel and loamy soil in the High Arctic. This α value can be expressed as:

$$\alpha = \frac{1.26}{[\exp(a+bS_m)+1]} \quad (7)$$

where a = 5.24, b = -21.56 and S_m is volumetric soil moisture content. Subsequently, α values were determined in this study as a function of soil moisture. They ranged from 1.25 to 1.26 for the wetland, and 0.678-1.25 for the sandur.

4.2.3 Water Table and Water Levels

Water table and pond water level information is required to examine storage changes in the sandur and wetland, specifically periods of flooding and inundation versus drought conditions. Continuous water table and water level records were obtained starting from August 28th 2015 to September 3rd 2016 using a series of water wells installed along transects crossing from the sandur to the wetland. This study initially started with two transects of water wells (Transect 2 at the South-west site and Transect 5 at South-east site). Here the water table and water level measurements began on August 28th 2015. By June 5th 2016, these two transects were complemented with eight more transects (10 in total) with an average of four wells per transects. There were five transects on the South-east side of the wetland-sandur border (Transect 5 to Transect 10), 4 on the South-west side (Transect 2 to Transect 4). One transect (Transect 1) was installed on the West site. It spanned from the Brunná River to a smaller stream fed by macropores running adjacent to the lava field. They were observed to supplement water inputs into the sandur in 2016.

The wells were constructed of ABS tubing: 31 at 3.17 cm in diameter and at 7 at 2.1 cm. They were slotted every 10 cm and screened throughout their entire length in order to prevent the accumulation of fine sediments. ONSET HOBO U20 water level pressure transducers (±0.075% per 0.3 cm of water) were placed within the pipes to continuously collect water levels on a 30 minute interval. One atmospheric pressure transducer (1 m above the ground) allowed water levels to be determined based on pressure differences. A Velleman MK108 water level beeper was also used to manually estimate water levels (± 5 mm) (Hodgson and Young, 2001). This also served to verify the HOBO U20 water level sensors.

Well elevations were surveyed with a Leica TPS 800 Total Survey Station (± 1.5 mm) to estimate distances and absolute water levels. Water levels and pond data yielded 3-dimensional spatio-temporal information on the dynamics of the water table and level features over 0.238 km^2 (South-west site) and 0.124 km^2 (South-east site). On days when water table or water level information was not collected, or was missing, values were estimated graphically. Placement of wells and their respective transects are shown in Figure 4.1.

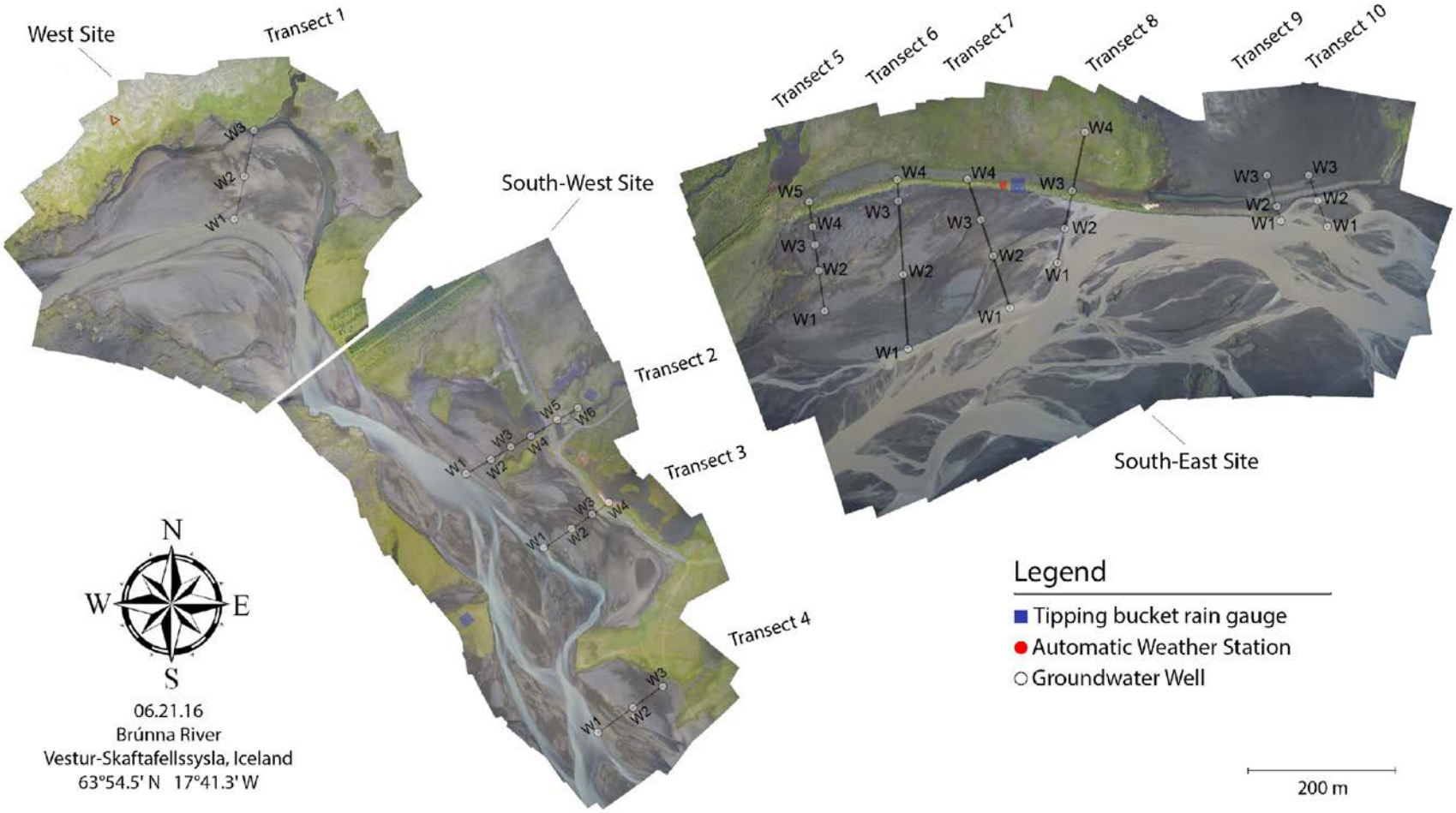

Figure 4.1 Map of West, South-west and South-east sites. Transect 1 is the only transect of water wells found on the West site. On the South-west site, transects ranged from 2 to 4 with wells starting in the sandur and finishing in the wetland. At the south-west site, there were 6 transects ranging from transect 5 to 10.

4.2.4 Groundwater

One of the research objectives involved qualifying and quantifying groundwater seeping from the elevated sandur into the adjacent wetland. Here, groundwater flow estimates can be determined according to Darcy's approach using the following equation (Young et al., 2017):

$$Q_w = k \bullet w \bullet ds \bullet \frac{\Delta h}{\Delta l} \quad (8)$$

where Q is the rate of water flow (m^3/d^{-1}), k is hydraulic conductivity (m/d), w is the width of the subsurface flow zone (m), d_s is the thickness of the saturated zone (m), here being the elevation difference between the bottom of the water wells (m) and the ground surface, since no frost table nor bedrock (impermeable barrier) could be determined, $\Delta h/\Delta l$ is the hydraulic gradient – the difference in water table (m) over distance (m). Groundwater flux (sandur-wetland) was obtained by measuring the change in water elevations between pairs of water wells at three different locations (T2W4-T2W5, T5W4-T5W5, T8W2-T8W3; see Figure 4.1). Hydraulic conductivity k estimates were determined using pumping tests with the rate of rise technique employed by Luthin (1966). Three hydraulic conductivity estimates were sampled at a borehole between T5W4 and T5W5. Three at a borehole between T9W1 and T9W2 and three between wells T2W4 and T2W5. Samples were taken on June 24th 2016 and August 24th 2016. Flow path widths were estimated at 130 m in the South-west site and 306 m in the South-east.

4.3 Additional Environmental Measurements

4.3.1 Water Conductivity

Water electrical conductivity (μS/cm) is a measure of electrical current flow through a solution. It is often used to assess the quality of water and can signal when there is a change in the water source (e.g., surface water to groundwater inflow – Hiscock et al., 1996; Dingman, 2002, p. 614). Water conductivity of Icelandic rivers typically yield low values but frequent conductivity measurements can signal the initiation of jökulhlaups (IMO, 2008). Specifically, in Iceland, increasing turbid water and rising water conductivity readings are often used as an indicator of an approaching jökulhlaup (IMO, 2008). Here at the Hvoll farm by the Brunná River, a YSI 30 conductivity meter was used to monitor water conductivity on a daily basis. The conductivity regime of the river during jökulhlaups, severe rainfall and drought events was examined in order to try and determine its origins. Additional water conductivity estimates were collected from the IMO Hverfisfljót River sensor (v71), which was installed in 2008.

4.3.2 Infiltration

Water infiltration tests were used as an indicator for assessing the rate of water movement down into the soil profile. This provided an indication of surface flooding and drainage characteristics here. Six infiltration tests were carried out at the south study site: 3 in the sandur, and 3 in wet meadow zone. Infiltration tests were determined using a double ring infiltrometer following after Burgy and Luthin (1956). Surface soil types where infiltration tests were initiated were photographed for future reference. Field observations indicated that after flooding, fine ash

material settled throughout areas of the sandur. They would later harden and impact infiltration rates.

4.3.3 Soil Moisture

Soil moisture is a key variable in controlling the exchange of water and heat energy between the land surface and the atmosphere through evaporation and plant transpiration. Volumetric soil moisture was collected manually with a Detla-T CL2x Theta Probe (± 0.1%) sampling the top 6 cm of soils on a regular basis next to the water wells. Abnizova and Young (2010) previously demonstrated the reliability of the CL2x Theta probe in comparison to standard gravimetric soil surface measurements ($R^2 = 0.86$, $p < 0.05$). Additionally, four CS-650 soil moisture sensors (two in the sandur, two in the wetland) collected volumetric soil moisture data (%) here, every 30 minutes. For each surface type, one CS-650 was installed perpendicular to the ground surface and the other at a 45º angle, recording soil moisture patterns within the top 30 cm and 15 cm of the soil profile respectively. These two sets of soil moisture measurements (one temporal, one spatial) provided valuable information on the spatial and temporal response of soil moisture to flooding, and periods of drought.

4.4 Soils

In total 30, soil samples (55 mm dia. · 35 mm) along transects and on freshly deposited surfaces across the sandur were collected and analyzed at the York University Geography soil laboratory for further analysis. GPS coordinates were recorded at all sampling locations. Three soil pits were dug within the sandur to evaluate its soil history – both erosion/deposition, and locate layers of ash from previous volcanic eruptions. Soil horizons were photographed and soil texture and type were determined based on field texturing. This "feel" approach (Brady 1984), consisted of rubbing a small soil sample between the thumb and fingers.

4.4.1 Bulk Density

Bulk density (ρ) is an indicator of the degree of soil compaction. The bulk density of samples was calculated using the following equation:

$$\rho \frac{Md}{V} \tag{9}$$

where: M_d is the mass of dried soil (g) and V is total volume of the soil sample (cm^3). Samples collected in the field and brought back to the laboratory for analysis were oven dried at 100ºC for 48 hours and later weighted on an ENTRIS 124 laboratory scale. The bulk density of most soil types varies within the range of 1.1-1.6 g/cm^3. In sandy soils, dry density can be as high as 1.6 g/cm^3 versus clayey soils and aggregated loams, which can be as low as 1.1 g/cm^3 (Hillel, 1980).

4.4.2 Soil Porosity

Porosity defines the volume of soil voids that can be filled by water and air, and can be calculated using the following equation:

$$\theta = \frac{v_v}{v_t} \tag{10}$$

where *Vv* is the volume of void space (such as fluids) and *Vt* is the total or bulk volume of material. It characterizes the soil particle density of a general mineral soil (Freeze and Cherry, 1979). Porosity varies depending on particle size and aggregation and provides an indication on how much water the underlying soil can retain. For example, porosity and water holding capacity tends to be greater in clayey and organic soils than in sandy soils, such as those found within the sandur.

4.5 Image and Photogrammetric Analyses

4.5.1 Imagery and Topographic data

This section provides the remote sensing, photogrammetric and modelling methods used to provide insight into the flooding and geomorphological changes in the study sandur.

To date, satellite remote sensing and aerial photography play critical roles in documenting temporal changes in river systems (Marcus and Fonstad, 2008). However, recently, close range photogrammetry from unmanned aircrafts, such has UAV's has become an additional tool in the generation of 3-dimensional topographic models (Remondino and El-Hakim, 2006; Matthews, 2008; Fraser and Cronk, 2009).

Following the approach by Long et al. (2016), aerial photographs and point cloud derived DEMs were used in an attempt to determine sandur planimetric and volumetric changes over time. The available SRTM v3 DEM with a rather coarse spatial resolution of approximately 30 m x 30 m and no temporal resolution inhibit much detailed topographical analysis upon the banks of Brunná River. The DEM of the Icelandic territory provided by the NLSI has a fine resolution of 5 meters per pixel but no temporal resolution. Nevertheless, a land classification of two pairs of multispectral satellite images at a 30 m x 30 m resolution provided valuable information on land cover changes that have occurred in the vicinity of the Hvoll farm between 1985 and 2016. The Landsat passive microwave satellites series have acquired data over this region since the 1980's.

Non-multispectral images from the Microsoft Bing map portal were also used as it provided RGB images collected by the DigitalGlobe satellite on September 30th 2011, when an important flooding event had occurred at the Hvoll study site. Historical panchromatic grayscale aerial photographs of the area used for administrative purposes were also collected from the National

Land Survey of Iceland (NLSI) and georeferenced using features and coordinates of the region. Images from Microsoft Bing were orthomosaicked using the Microsoft Image composite editor (ICE) and georeferenced in ArcMap. Non-UAV imagery and their respective sources are listed in Table 4.1 below.

Table 4.1 Details of the images acquired of the Hvoll site from 1979 to 2016 for land-use and land-cover comparisons.

Data Type	Data Source	Acquisition date	Spatial Resolution (m)	Bands
Administrative Aerial Photo	NLSI	1979-08-09	1 m	1
Administrative Aerial Photo	NLSI	1986-07-17	1 m	1
Landsat 8 (OLI-TIRS)	USGS	2015-09-25	30 m	11
Landsat 8 (OLI-TIRS)	USGS	2016-05-22	30 m	11
Landsat 5 (TM)	USGS	1985-06-09	30 m	7
Landsat 5 (TM)	USGS	1986-06-21	30 m	7

The process in creating high resolution three dimensional elevation models of the South-west and South-east sites, was organized in different steps and by applying a similar photogrammetric approach as Long et al., (2016) (Figure 4.2). The process involved having a camera housed on the underside of a DJI Phantom 2 UAV taking a series of pictures while in motion. The UAV flew at a constant altitude of 170 and 150 m a.s.l. during the first flight (June 22nd 2016) and second (September 2nd 2016) respectively. This allowed for the generation orthomosaics at a fine resolution of 4 cm per pixel for the June 22nd 2016 survey and 3 cm per pixel for the September 2nd 2016 survey. The camera used was a 10 megapixels f/2.8 Go Pro Hero 4 with an alternative lens manufactured by Peau Productions, replacing its original wide angle fish eye lens with a non-distorted 4.35 mm or 35 mm film equivalent rectilinear one. The images were mosaicked in Agisoft Photoscan which aligns the images and computes a triangulated irregular

network (TIN) used for the generation of a surface. The model was then referenced to ground control points (GCP) surveyed with a LEICA TPS 800 total station.

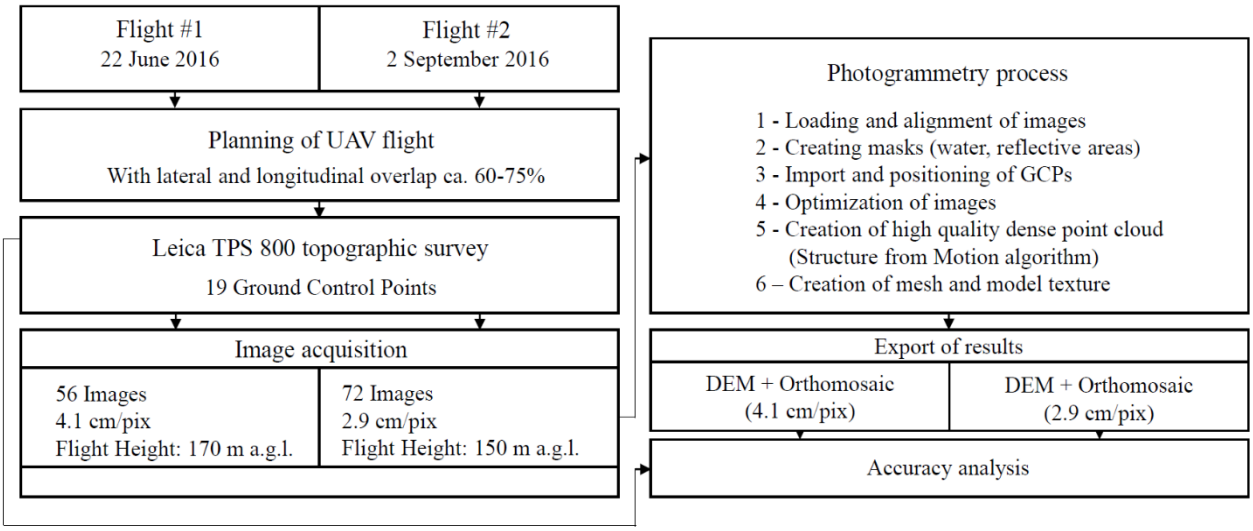

Figure 4.2 Conceptual diagram illustrating the general overview of the DEM acquisition method, the planning of UAV flights, the generation of DEMs and the verification of orthomosaic accuracy with total station data (after Long et al., 2016).

The use of structure from motion (SfM) photogrammetry (Westoby et al., 2012) provided high resolution digital elevation models (DEM) (<1 m resolution) of the sandur-wetland landscape. GCPs were mandatory for the geo-referencing and calibration of the DEMs therefore artificial targets were deployed on the ground next to selected water wells and their coordinates were surveyed with the total station. The DEMs and the orthomosaics were analyzed within a geographical information system (GIS) based on the ArcGIS software 10.4. The GCPs were imported in Photoscan, then correctly assigned on each image.

The dense point cloud model was generated using the “Ultra high quality” and an “aggressive” depth filtering options of Photoscan which increases processing time when dealing with a large number of tie points; identical matching points in the batch images used to accurately mosaic the entire study area. Then, the mesh of the ground height was computed from the dense cloud without interpolation of the data, which avoids filling in areas where data are lacking (Long

et al., 2016). In certain reflective sandy and water areas, the generation of the DEM was difficult because the model did not find a sufficient number of tie points. In these cases, wet surfaces were masked out.

The pixel based subtraction DEM of Difference (DoD) method can determine areas where change in height between two datasets has occurred. For the purpose of this study, this also allows for a spatial representation of the areas where river bank erosion or accretion has occurred. In order to perform a consistent comparison between both DEMs, a mask was produced to only keep surfaces that were scanned by the UAV on both dates. Areas found beyond the network of ground control points were clipped out of the datasets. Changes in the volume of the bars located to the south of the study area were eventually quantified in Photoscan and Arc GIS. This spatial analysis was performed at a modest scale (0.124 km^2 South-east site) in order to identify morphological changes. This finer scale analysis highlights small 3D morphological features and changes, which are difficult to identify from satellite images or from other coarser spatial resolution imagery.

4.5.2 Flood and Sediment Accretion Maps

Topography and elevation maps of Iceland at a rather fine (10 meter or less) resolution per pixel is made available to the public by the National Land Survey of Iceland and was used here to determine low lying areas which are vulnerable to flooding. This DEM varies in spatial resolution as it is a mosaic made from various datasets ranging from LiDAR and topographic maps. In addition, DEMs from the UAV were overlaid to increase the spatial resolution of the DEM around the Hvoll farm, and more specifically at the South-west and South-east sites

ArcScene was then used to simulate flooding by entering pressure transducer water level records from floods that occurred between September 1st 2015 and September 1st 2016. The model

was mainly generated for the South-east site owing to the reliability of an accurate network of ground control points here. This method was also used in determining the “tipping point” where water levels would spill over into the adjacent wetland.

The DEMs generated by stereo photogrammetry were then used to perform the pixel differencing analysis. This method follows Long et al. (2016) which provides elevation changes. It was performed on these geospatial datasets in order to visualize elevation gains or losses, with gains interpreted as deposition of sediment and losses as erosion. Volume changes were estimated by multiplying elevation change with area.

Topographic elevation maps were generated to determine areas of depression, potential flood pathways as well as to visualize the extent of flooding during severe rainfall events and the 2015 jökulhlaup. In total 4 DEMs were generated and georeferenced, yet only the ones from the South-east site were used for DoD analysis as they were accurately surveyed with a total station. The remainders were georeferenced with the total station at wells along Transect 2 and 3, however the boundaries of the South-west site were surveyed with a handheld GARMIN GPSMAP 64 with large vertical and horizontal errors (1-4 m), hence they were only used to get an idea of the elevation of the West and South-west study sites and mosaicked with the NLSI DEM to check for accuracy along Transect 2 and 3. The accuracy of the two models used for the DoD analysis are listed in Table 4.2.

Table 4.2. Below are listed the DEMs acquired from structure from motion photogrammetry at the South-east site and their associated errors measured at GCPs (n = 20)

DEM	Easting Error (m)	Northing Error (m)	Altitude Error (m)	RMS Error (m)	Error (pix)
2/9/2016 - South-east Site	0.029	0.027	0.016	0.043	0.384
22/6/2016 - South-east Site	0.022	0.025	0.028	0.044	0.696

CHAPTER FIVE: RESULTS

5.1 Study Site Climate Conditions

This section outlines the September 1st 2015 to September 1st 2016 seasonal and extreme climatic conditions at the Hvoll farm study site relative to Höfn (located 128 km away), and where the nearest government weather station is located. It has been collecting local weather data since June 1965. Daily patterns of air temperature, wind speed and rainfall at Höfn are found in Figure 5.1 below.

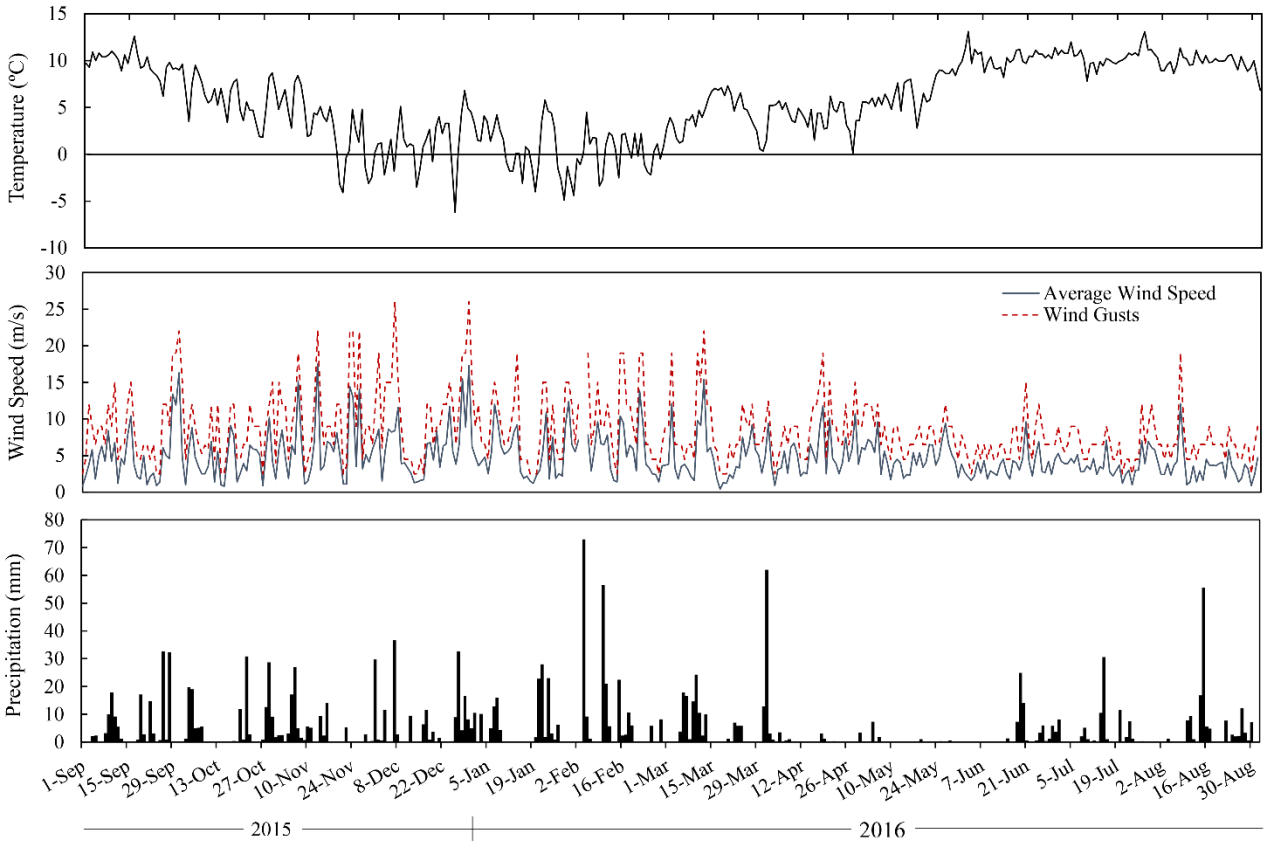

Figure 5.1 Daily pattern of air temperature, wind speed and precipitation from the Höfn weather station.

5.1.1 Air Temperature

Air temperature records collected at the Hvoll farm and the Höfn weather station helped establish the temperature regime of the area. Daily patterns of air temperature from September 1st 2015 to September 1st 2016 are plotted in Figure 5.1. At the Hvoll farm, the average temperature over the year (September 1st 2015 – September 1st 2016) was about 6.5°C. June and July were the warmest months with monthly averages of 12.6°C and 13.1°C while December and January were the coldest with monthly averages of -0.3°C and -0.9°C respectively (Table 5.1). June was exceptionally warm for southern Iceland with night temperatures averaging ca. 9°C and daily maximums reaching highs of 24°C. Temperature records from the study site indicate that the climate is comparable to that of Höfn's ($R^2 = 0.91$) with the exception of the month of February which, at Hvoll, was warmer by an average of 2°C. The average annual range in temperature readings between winter and summer at Hvoll was 14°C compared to 11.2ºC at Höfn.

Temperature data of this area reflects the subpolar oceanic climate of the region (southeast Iceland), which consists of cool summers and a cool but not freezing winter, with the exception of a few days (Einarsson, 1984). Monthly temperature averages from September 2015 to September 2016 year were compared to monthly temperature averages from the years 1967 up to 2017 (IMO, 2016). Nearly all months between September 2015 and September 2016 were warmer than the long-term normals (1967-2017), with the exception of February, which was colder by ca. 0.7ºC at Höfn. Typically, the coldest month in this region is January with an average temperature of 0ºC and July the warmest, with an average temperature of 10.2ºC.

Table 5.1 Average monthly air temperature (ºC) at Hvoll and Höfn. Climate data for Höfn including the 30 year mean data are from the Icelandic Meterological Office (IMO, 2016, 2017).

	2015					2016							
	Aug	Sep	Oct	Nov	Dec	Jan	Feb	Mar	Apr	May	Jun	Jul	Aug
Hvoll (*T*°C)	12.6	10.6	6.0	1.7	-0.3	-0.9	2.0	4.6	6.2	8.5	12.6	13.1	12.2
Hofn (*T*°C)	10.9	9.8	6	2.8	1.5	0.4	0.2	2.4	4.2	6.8	10.3	11.4	11.1
Hofn 30 yr. Mean (*T*°C)	9.9	7.7	4.7	1.7	0.4	0.1	0.9	1.4	3.4	5.9	8.6	10.2	9.9

5.1.2 Relative Humidity

Daily patterns of relative humidity (%) at the Hvoll farm are plotted with air temperature in Figure 5.2. Relative humidity was fairly high throughout the study period with an average of 87.5%. The highest readings were recorded in September and October 2015 with monthly averages of 92% and 93% respectively. Moreover, April and May had the lowest relative humidity with monthly averages of 81.5% and 76%. May 2016 in southern Iceland was fairly sunny and dry with little precipitation and low humidity, contrasting with initial field observations from May 2015, which were cold and wet. The relative humidity pattern collected throughout the study period is typical of Iceland with May, having on average, the lowest humidity, and August and October the highest (Einnarson, 1984).

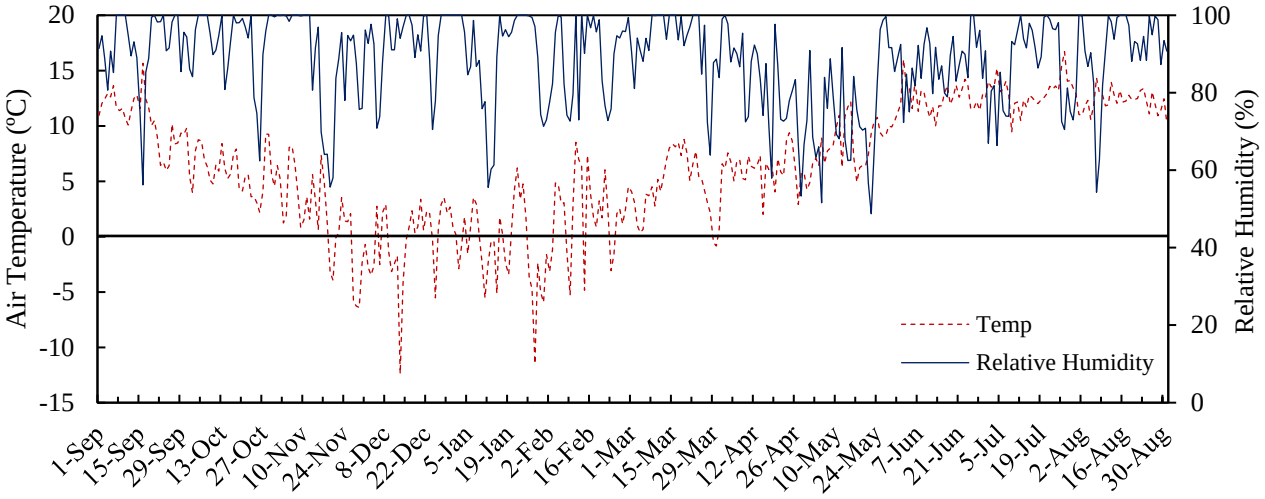

Figure 5.2 Daily average temperature (ºC) and relative humidity (%) measured at the Hvoll study site from September 1st 2015 to September 1st 2016.

5.1.3 Precipitation

Monthly sums of precipitation from the Hvoll farm (June 1st 2016 – September 1st 2016) and the Höfn weather station (September 1st 2015 – September 1st 2016) are listed in Table 5.2. Daily cumulative precipitation data collected at the sites around the Hvoll farm were compared with Höfn precipitation records (Figure 5.3). Typical of South Iceland's climate, frequent rain events were observed to occur throughout the September 2015 – September 2016 study period with 204 rain days (>1 mm). The rainiest seasons in South Iceland are typically winter and fall with the months of January and October receiving on average, the most in terms of precipitation (Einnarsson, 1984). February received the most rain (225 mm) over the 2015-2016 period, receiving 61% or 87.3 mm more rainfall in comparison to the long-term normal. Fall 2015 was particularly wet with some Icelandic weather stations receiving 20% more precipitation in comparison to long-term totals (IMO, 2016). On the other hand, early spring 2016 was unusually dry with the month of May receiving very little rain (15 mm) in comparison to other months.

Frequent rainfall events occurred throughout the study period with major precipitation events (>50 mm) occurring in the winter (see precipitation records plotted in Figure 5.1). The August 15th 2016 rain event was the sole intensive rainfall episode that occurred over the summer 2016, with ca. 55 mm of rain falling in a day. This represented about 42% of the total rainfall in August, 2016. Records from Höfn indicate that an additional 51.5 mm of rainfall had fallen for the month of August, 2016 compared to the long-term normals (IMO, 2016).

Table 5.2 Average monthly precipitation data (mm) from Hvoll and Höfn. Precipitation data for Höfn including the 30 year mean data is drawn from the Icelandic Meterological Office (IMO).

	2015					2016							
	Aug	Sep	Oct	Nov	Dec	Jan	Feb	Mar	Apr	May	Jun	Jul	Aug
Hvoll (mm)	N/A	N/A	N/A	N/A	N/A	N/A	N/A	N/A	N/A	N/A	27.6	64.2	129.6
Hofn (mm)	104.2	156.2	174.6	105.4	186.8	152.1	225.0	120.8	88.5	15.0	65.7	85.4	139.7
Hofn 30 yr. Mean (*mm*)	88.2	166.7	183.0	163.5	159.9	186.1	137.7	146.7	89.7	61.8	41.9	91.1	88.2

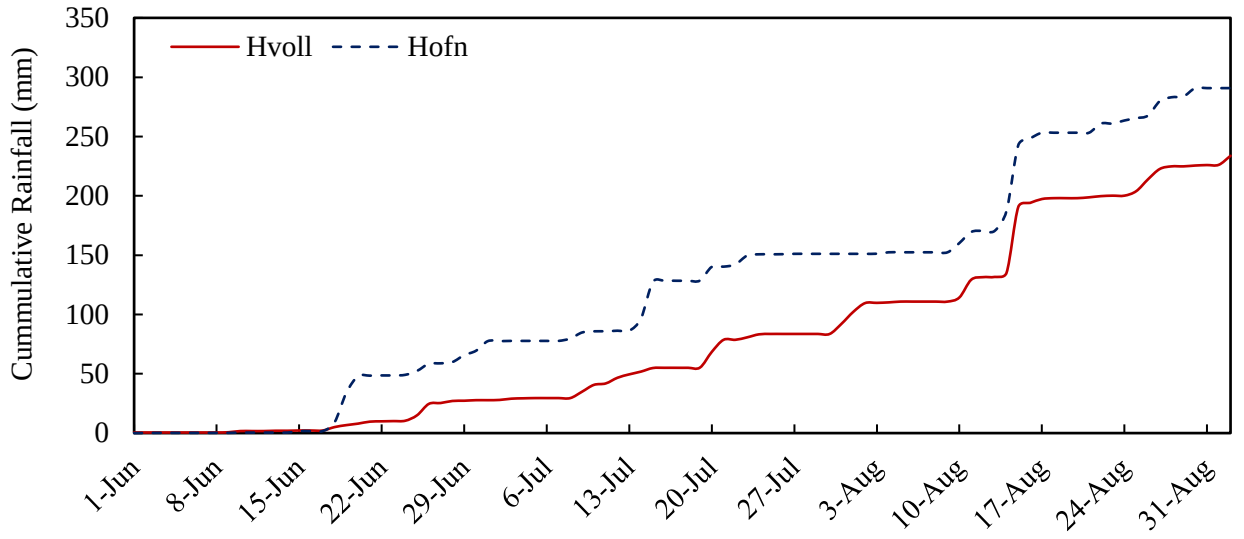

Figure 5.3 Comparison of cummulative precipiation records from the Hvoll farm and Höfn weather station located 128 km away from May 31st to September 2nd 2016.

5.1.4 Wind Speed

Wind speed information from the Höfn weather station provided valuable details on wind direction, duration and intensity. Longer time series information on wind direction and frequency in South Iceland was obtained from Einnarson (1984). During the study period (September 2015-September 2016), wind speeds at Höfn were highest during the winter and fall seasons with average wind speeds frequently over 15 m/s. Wind gusts often reached speeds > 20 m/s. The most intensive wind event occurred on December 30th 2015 with gusts reaching 26 m/s (IMO, 2016). Typically, about half of all dust events in South Iceland occur in the winter (Arnalds, 2016).

During June, July and August (JJA) 2016, two severe wind events occurred in southeastern Iceland. The first occurred on June 19 – 20 after a long drought, 14 days with little rain. Spot wind gusts (n = 4) reached over 22 m/s at Hvoll and dust devils were observed over Skeidararsandur. Similarly, wind gusts at Höfn reached 15 m/s and alerts by the IMO were sent out warning motorists of the strong winds. Visibility was poor and a thick cloud of fine dust particles rising as high as ca. 250 m blew north towards the Sidhujökull and Vatnajökull glaciers (Figure 5.4).

Another severe wind event occurred on August 7th 2016 with wind gusts reaching 25 m/s at Hvoll and 19 m/s at Höfn. Yet previously wet conditions over the sandur prevented fine materials becoming suspended.

Figure 5.4 Photograph taken on the wetland side at Hvoll on June 19th 2016 around 1500h looking east towards Vatnajökull. A layer of dust can be observed rising 150 m from the ground. Dust is being blown north towards the glaciers, ca. 36 km away. Arrow indicates wind direction.

5.1.5 Net Radiation

Net radiation is an important component of the surface energy budget and helps modify evapotranspiration losses, a critical component of the hydrology budget. Daily averages of net radiation (Q^*) are plotted in Figure 5.5. From June 6 to September 1st, 2016, net radiation of the sandur averaged 80 W/m^2 in comparison to the wetland (73 W/m^2). Overall, net radiation of the wetland correlated with the sandur (R^2 = 0.92), receiving slightly less Q^* (8%). Net radiation at the field site was highest in June, with an average of 87 W/m^2, though July (July 3rd to 9th) had several sunny days, averaging 120 W/m^2. Radiation levels dropped off at the end of the summer and remained low during periods of extensive cloud cover.

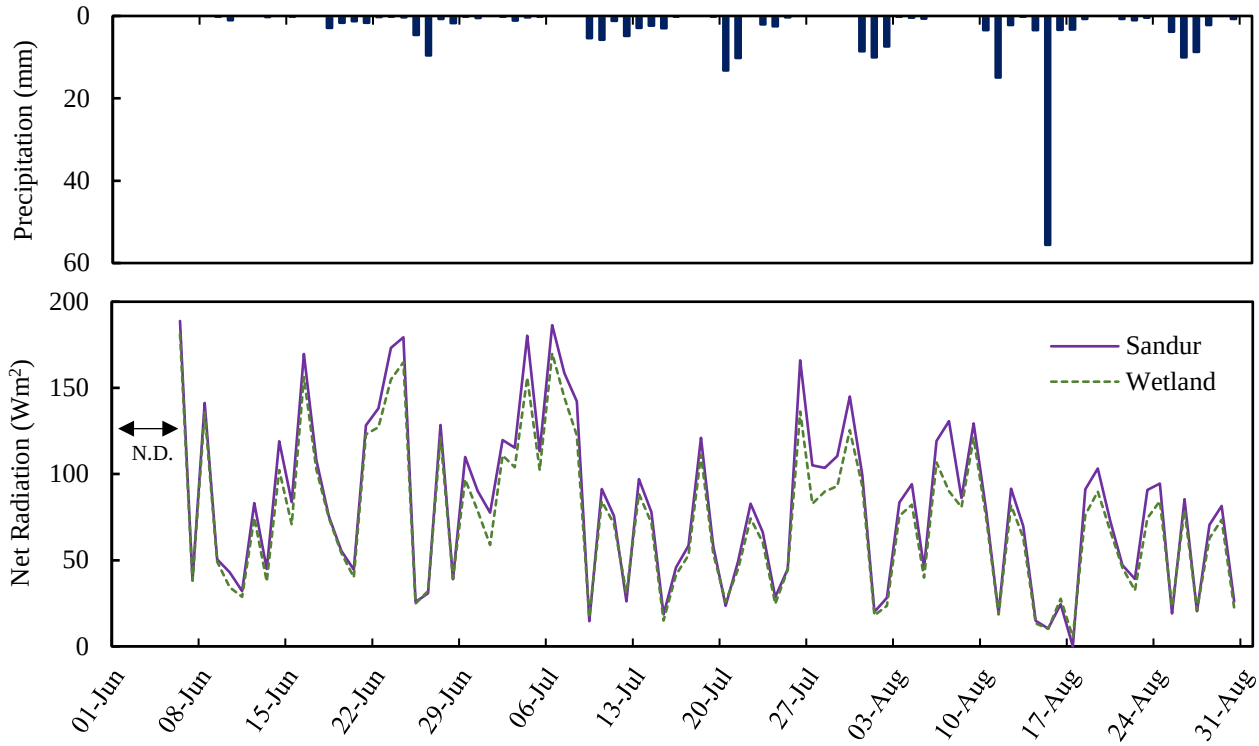

Figure 5.5 Seasonal pattern of net radiation over the sandur and adjacent wetland. Precipitation (mm) is included in the top diagram. N.D. indicates no data available.

Albedo (α) measurements, for which an average of four samples were taken per surface type, yielded α values of 0.04 for the sandur, 0.25 for the berm and 0.18 for the wetland. Diurnal variations in surface energy fluxes together with air and near surface ground temperatures are plotted in Figure 5.1.6. Positive values of Q^* and Q_H are gains to the surface, but losses for Q_E and Q_G. On a cloudless day, net radiation (Q^*) peaks at about 530 W/m^2, and owing to the low albedos of both surfaces (wetland and sandur) the difference in absorption is minimal. As expected, most of the energy being consumed is going into the latent heat flux (evaporation). This suggests that in addition to energy requirements being met, the moisture supply in both terrain types is sufficient for Q_E losses. Sensible heat contributions are generally positive during the day whenever the air temperature (T_{air}) is greater than the surface temperature (T_s), with losses occurring when the $T_s > T_{air}$, or at night when the atmosphere cools off faster than the ground surface. Typical of other wetland terrain, the ground heat flux (Q_G) is small, generally consuming < 10% of net radiation. This is typical of other arctic wetlands (Young and Woo, 2004).

On a cloudy day $Q^* > Q_E > Q_H > Q_G$, the magnitude of the fluxes are reduced, and the peaks and troughs of energy receipt are being controlled by atmospheric conditions, likely cloud cover. Dampened Q^* results in lower latent heat fluxes (evaporation) and cooler air and surface temperatures with smaller gradients. The distribution of energy into both surface types over the JJA 2016 study period is listed in Table 5.3 below.

Table 5.3 Proportion of Q^* being consumed for sensible (Q_H), latent (Q_E) and ground heat exchanges (Q_G) over a sandur and wetland surface type.

	QH	QE	QG
Sandur	25.88%	70.75%	3.37%
Wetland	21.12%	71.02%	7.85%

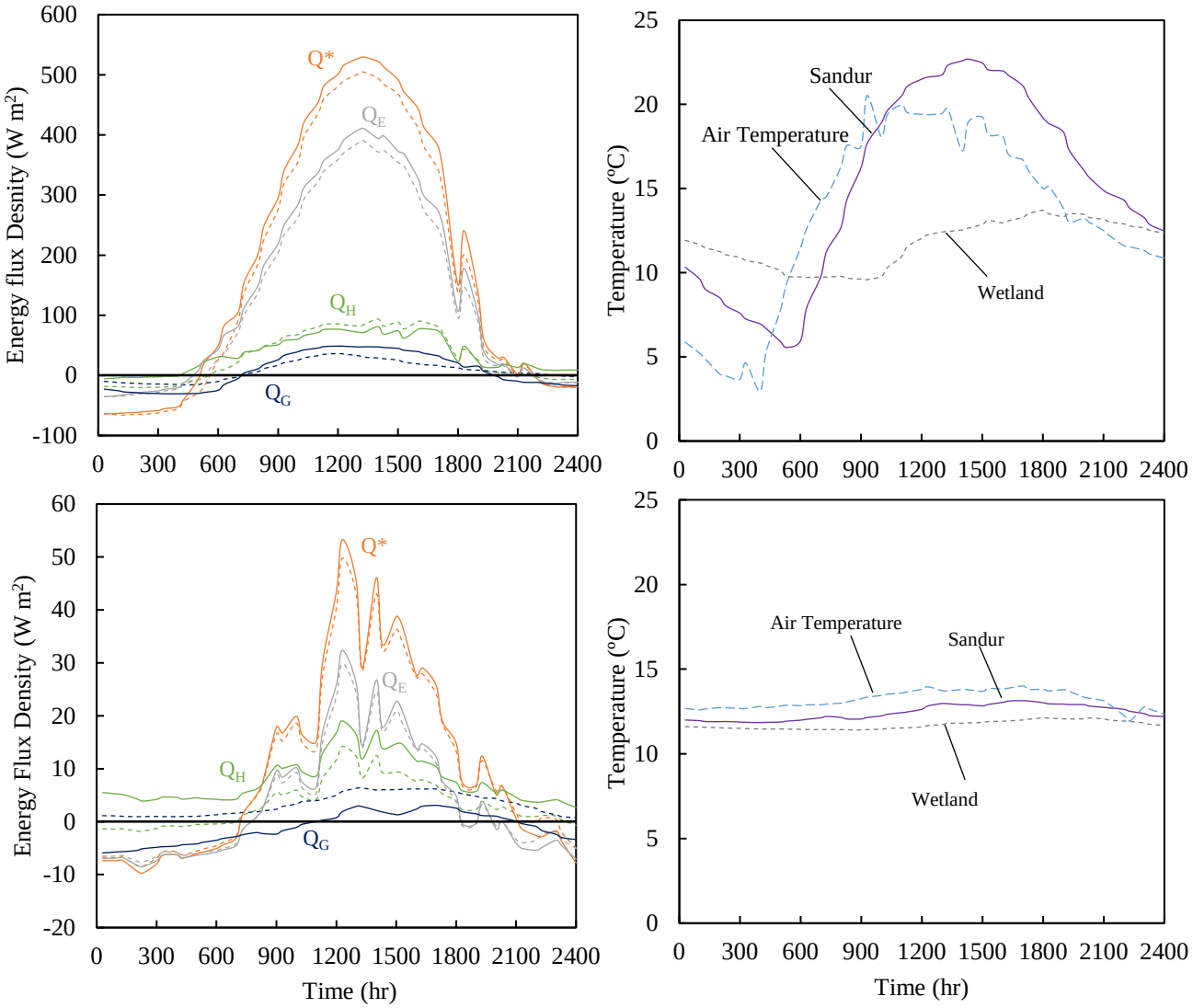

Figure 5.6 Surface energy exchanges at the wetland and sandur on a cloudless day (July 7th 2016- Top graphs) and on a cloudy, rainy day (August 15th 2016 – bottom graphs). Wetland is represented with a dashed line and sandur with a bold line. Graphs on the right are soil surface temperatures for the two surfaces (Sandur, Wetland). Positive Q* is gain to surface, + Q_E is loss from surface, + Q_H is gain to surface and + Q_G is loss from surface.

5.2 Hydrology

This section describes the various hydrologic characteristics of the Sandur-Wetland zone, and, presents temporal and spatial patterns observed within the study areas from September 1st 2015 to September 1st 2016, and more specifically, from the June 1st – September 1st 2016. Precipitation results have previously been presented in Section 5.1.

5.2.1 Fluctuations in Water Table and Water Levels

Changes in water levels and groundwater tables reflect a response to inputs, losses and storage of water. An examination of daily water tables in water wells across several transects provides an indication of the response of the sandur and adjacent wetland to inputs of rainfall, glacial melt and drying periods. Water table measurements on the shores of the Brunná River began on August 30th 2015 at a series of wells along Transect 2: T2W2, T2W3, T2W4 (South-east site), and Transect 5: T5W1, T5W4, T5W5 (South-west site) (see Figure 4.1).

During the September 2015 – September 2016 year, the Brunná River water levels were highest in the summer and fall (Figure 5.7). Glacial rivers in southern Iceland are typically highest during fall, however a jökulhlaup originating from the Western Skaftá cauldrons (see IMO, October 1st 2015) further raised sandur water levels along the Brunna River on October 1st 2015. The increasing rate of discharge at the Skaftá von Sveinstindur station (sensor v299 on Figure 3.1) turned out to be the highest recorded ever since the station was established in 1971. This jökulhlaup eventually reached the sensor at Kirkjubaejarklustur (v183 on Map 3.2.1) located 22 km from Hvoll during the early hours of October 3rd 2015. Water levels at the Hvoll farm, at the nearby Hverfisfljót and Brunná Rivers which are the next rivers east of the Skafta River, reached their highest levels on the night of October 4th and early morning of the 5th.

Precipitation events strongly affected groundwater tables in both the sandur and wetland at the South-east and South-west sites (Fig. 5.7). However, occasionally, increases in water tables were substantially greater than associated precipitation totals. For example barely any rainfall fell in the region from early April to mid-June, yet pond water levels and groundwater tables would experience small peaks during that same drought period. On June 20th 2016, a small jökulhlaup developed and discharged considerable amounts of water down the Brunná River, which raised water levels/tables in the sandur. Water levels of the Skaftá River at Sveinstindur (sensor v299 on Figure 3.1) rose slowly as did electrical conductivity readings from the same location, indicating the advancement of a jökulhlaup (IMO, 2016). This process resulted in a rapid water level rise of ca. 13 cm at the water wells closet to the Brunná River (T2W2). Further details on this jökulhlaup event will be discussed later (see Section 6.2).

A severe rainfall event (PPT= 55 mm) occurred on August 15th 2016 rising water levels and flooding most wells in sandur sites. Water tables rose 21 cm in wells highest in elevation in relation to the Brunná River (T5W4, T5W3). Moreover, this large rain event caused a rapid rise of 36 cm at T2W4 located in the South-west site; the well farthest and highest in elevation in the sandur, relative to the Brunná River.

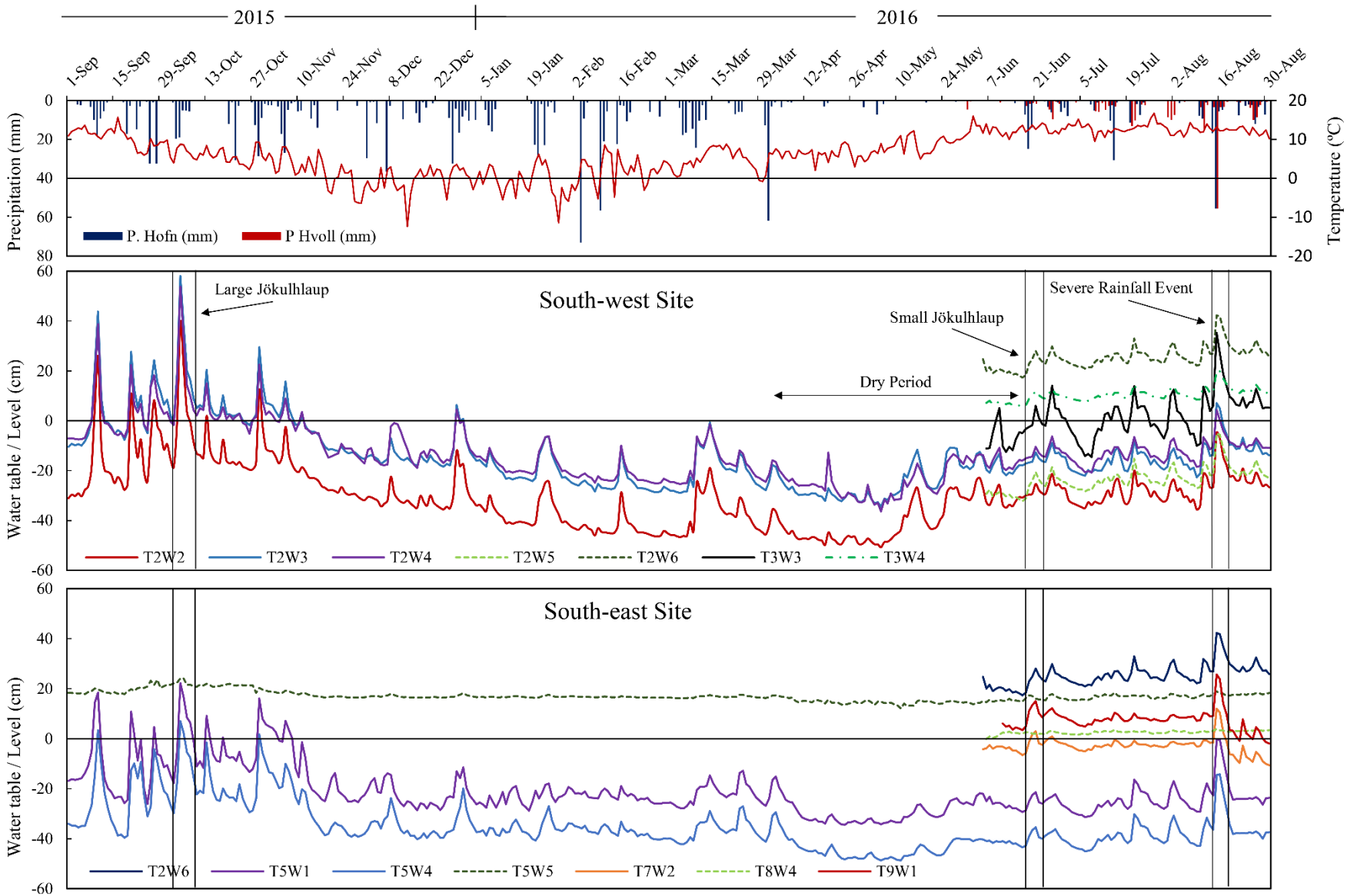

Figure: 5.7 Yearly pattern of mean daily water tables/levels, at wells installed on Transect 2 at the South-west site (Middle diagram) and Transect 5 at the South-east site (Bottom diagram) from September 1st 2015 to September 1st 2016. The wells shown here collected continuous water level data (every 30 minutes) in comparison to the rest of the wells which provided intermittent measurements.

Water levels at the South-west and South-east sites during the October 4th 2015 jökulhlaup, June 20th 2016 jökulhlaup and August 15th 2016 rainfall event are plotted against rainfall in Figure 5.8. Fluctuations in water tables/levels in the sandur and wetland varied depending on the site.

At the South-west site, water levels in the sandur and wetland would respond synergistically to seasonal and episodic events such as the June 20th jökulhlaup and August 15th 2016 rainfall event. Groundwater levels at wells T2W5, T2W6 and T3W4 located in the wetland side of the South-west study site respond to these events in similar fashion to water levels in the sandur though water table amplitudes are less (see Figure 5.8). However, at the South-east site, on the wetland side, water levels were rather steady and did not respond the same as the sandur water wells.

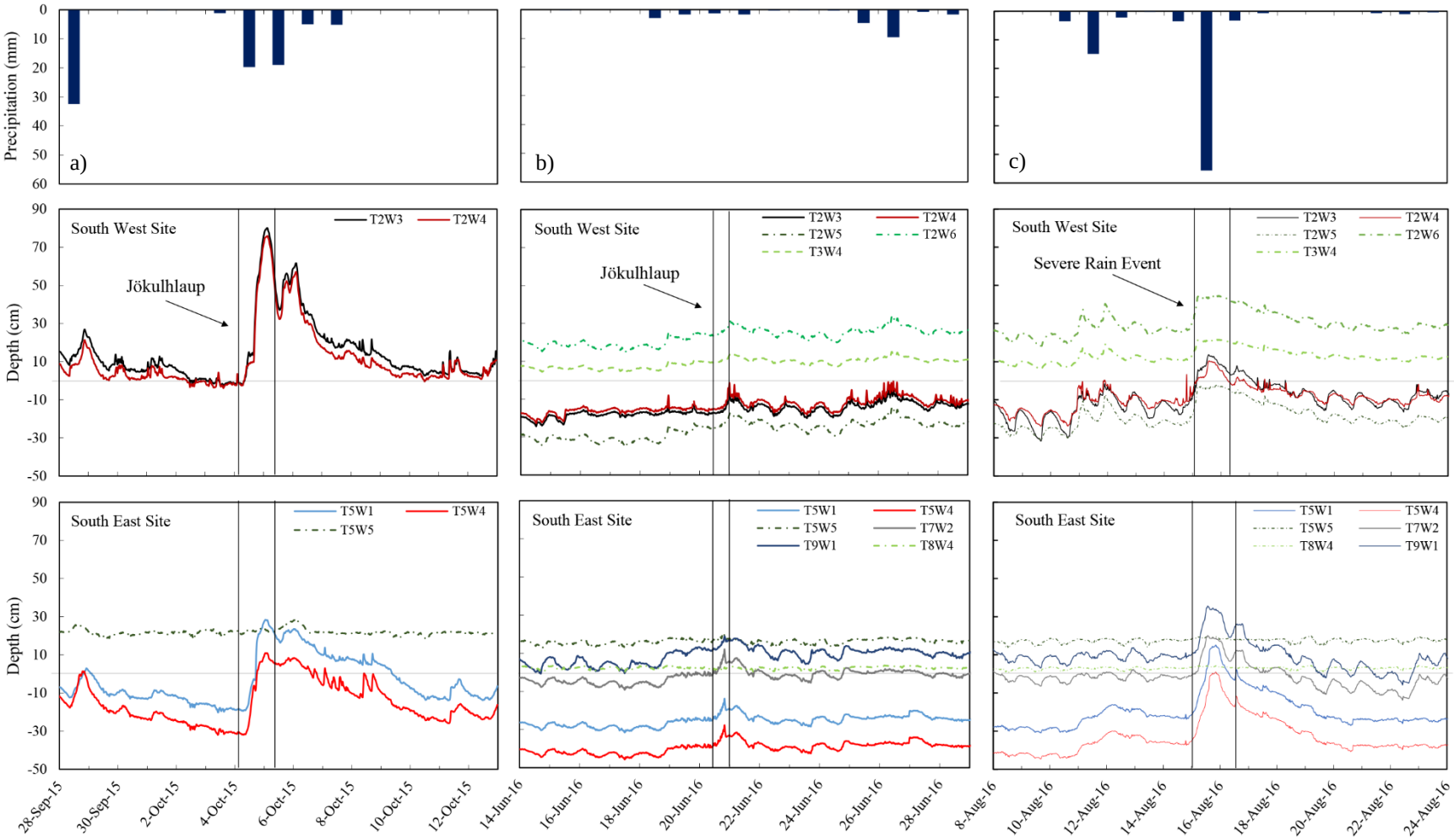

Figure 5.8 Water table response to: a) jökulhlaup event that occurred over in the Brunná River on October 4th 2015; b) a jokulhlaup following a sandstorm event on June 20th 2016 and c) the water table response to an intense rainfall event that occurred here on August 15th 2016. Precipitation is plotted at the top of the diagram.

5.2.2 Hydraulic Conductivity

Hydraulic conductivity (*k*) values measured at water wells found throughout the study site are listed in Table 5.4. As expected, hydraulic conductivity values were much higher in the sandur than in the wetland, owing to the sandy-gravelly soils. These *k* (sandur) values are an order of magnitude lower to those reported by Robinson et al. (2008), who measured the hydraulic conductivity of a nearby ice-marginal zone.

Table 5.4 Average rates of hydraulic conductivity (mm/s, m/d). Measurements were made on June 26th and August 23rd 2016.

Transect & Well #	Measurements (*n*)	*k* (mm/s)	*k* (m/d)	Site - Well Location
T2 W4	3	0.0419	3.620	South-west - Sandur
T2 W5	3	0.0039	0.337	South-west - Wetland
T5 W4	4	0.0084	0.726	South-east - Berm
T9 W2	3	0.0481	4.152	South-east - Berm
T6 W3	1	0.0213	1.840	South-east - Sandur

The *k* value used in groundwater calculations from the sandur to the wetland along Transects 5, 6 and 7 was 0.726 m/d (South-east site). For the South-west site, an average *k* = 1.939 m/d was employed (a *k* estimate averaged from T2W4 and T2W5 values) (Table 5.4).

5.2.3 Groundwater

Subsurface flows are influenced by the hydraulic gradient, the size of the aquifer and characteristics of its hydraulic conductivity (*k*) – the ability of sediments or substrate to transfer water. Seasonal groundwater fluxes at the South-west (Transect 2 and 3) and South-east sites (Transect 5 to 7) are plotted in Figure 5.9. Subsurface flows from the sandur to the wetland

occurred on a continuous basis throughout the study period at the South-west and South-east sites. During the JJA 2016 study period, barely any subsurface flows occurred along Transect 2. Some groundwater did flow along Transect 2 in early June (sandur to wetland), in response to a steep hydraulic gradient, arising from a period of warm, dry conditions. However, a severe rainfall event (August 15, 2016) caused a flow reversal and 0.054 m^3 of groundwater, instead moved from the wetland to the sandur. Here, the flow path was assumed to be 65 m in width.

Along Transect 3, groundwater flowed from the sandur into the wetland on a continuous basis and with higher discharge rates during both seasonal and episodic events. For instance, during the June 20th 2016 jökulhlaup, or August 15th 2016 severe rainfall event, groundwater flow was ca. 1 m^3/d and 1.6 m^3/d respectively, again, assuming a 65 m wide flow path.

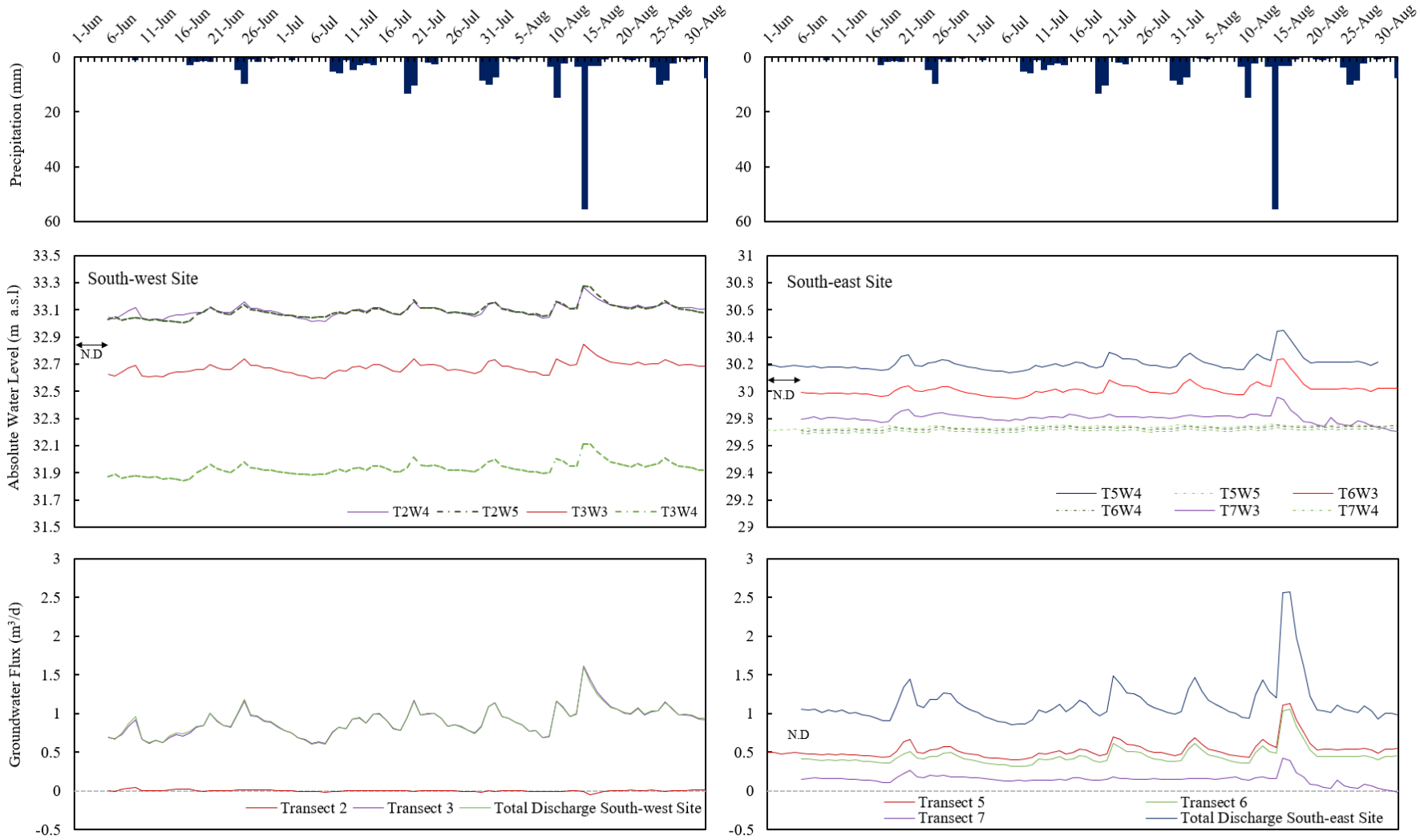

Figure 5.9 Transfer of groundwater (m^3/d) from the sandur to the wetland at the south-west site (bottom left plot) and at south-east site (bottom right). One hydraulic conductivity measurement (k = 0.726 m/d, n = 4) was used to calculate groundwater flux across the three transect. The k value was determined at a well installed in the berm near T5W4 and likely represent the hydraulic conductivity of the berm, as the berm here is made of the same material with vegetation cover until Transect 8. Water levels (m a.s.l.) at wells at the South-east site and south-west site were used to calculate groundwater flow are shown (middle plots). Precipitation is also shown to illustrate response of groundwater fluxes to rainfall events.

5.2.4 Soil Moisture

Near surface soil moisture readings (60 mm depth) for all wells on the West, South-west and South-east sites are plotted in Figure 5.10. As expected, wetland vegetated areas had higher soil moisture values in relation to the barren sandur. Sandur surficial soils tended to dry up after rainfall events (ca. 1-2 days). The sandur which is predominantly made of black sand and gravels cannot easily retain moisture due to its rapid drainage, high surface temperatures and elevated evaporation losses (Table 5.4 and Figure 5.6).

Continuous patterns of soil moisture (15 and 30 cm depths) before and after the June 20th 2016 jökulhlaup and August 15th 2016 rainfall event are shown in Figure 5.11. The June 20th jökuhlaup caused an initial 10% rise in soil moisture in the sandur, but after 48 hours, soil moisture levels returned slightly above pre-event levels. The August 15th severe rainfall event raised moisture levels by 20% but soils were a slower to dry out, taking 72 hours to reach pre event levels. As expected, soil moisture changes throughout the 2016 season were most pronounced in the top 15 cm soil profile than further in the soil profile (30 cm). Moisture levels in the wetland were more stable than the sandur over the season, only rising by 2% in response to the August 15th 2016 rainfall event (Figure 5.11).

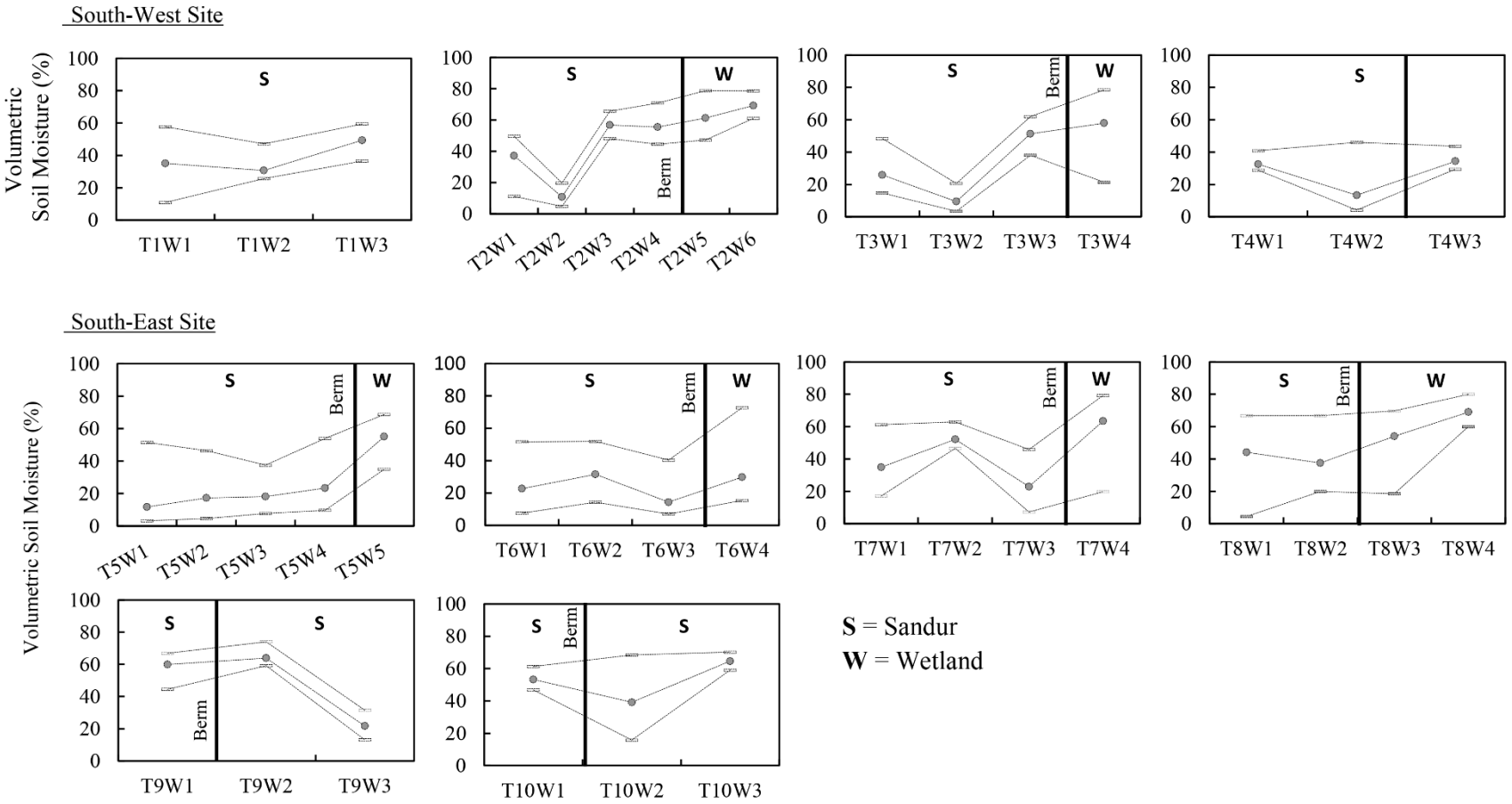

Figure 5.10 Spring and summer 2016 min, max and average soil moisture values across transects with x-axis plotting Transect and Well number (T#W#) and y-axis being volumetric soil moisture (%). Samples were taken daily from June 5th to September 1st 2016.

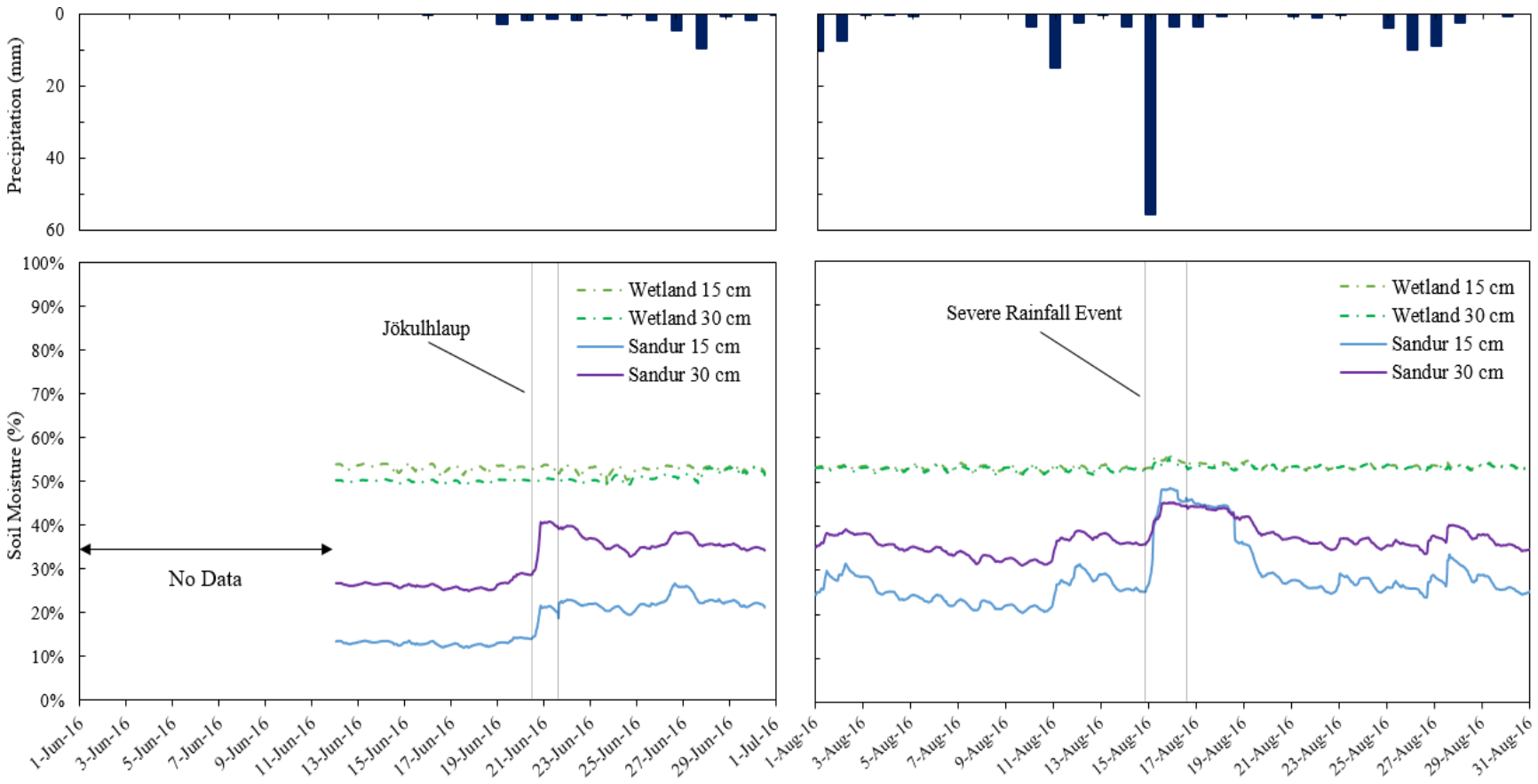

Figure 5.11 Soil moisture pattern and response to a jökulhlaup event that started in the Brunná River on June 20th 2016 (left graph), and to a severe rainfall event that occurred here on August 15th 2016 (right graph)

5.2.5 Soil Infiltration Rates

Infiltration experiments were useful in evaluating the vertical drainage properties of the sandur and wetland soils. Experiments indicated some spatial variations across the sandur. Steady-state infiltration rates for the sandur over a sand and gravel surface revealed an average rate of 40 cm/hr. Areas where layers of fine ash were located at or just below the surface exhibited much lower infiltration rates. For instance, at one site, infiltration dropped to 3.4 cm/hr owing to a fine ash layer 13 cm below the ground surface. The vegetated berm, a consolidated ridge of volcanic sediments had an infiltration rate of 21.6 cm/hr. As mentioned previously, the berm is man-made and is used to prevent water inundation from the sandur to the wetland.

5.2.6 Evaporation

Based on large latent heat fluxes (Q_E) (see Figure 5.6), daily evaporation rates were similarly high for the two terrain types ($R^2 = 0.88$) (Figure 5.12). Dynamic recharge of the sandur through rainfall, glacial meltwater, together with sufficient energy likely contributed to this pattern. Over the JJA period, the daily average evaporation rate was 2.1 mm/d for the sandur and 2.3 mm/d for the wetland, while totals equalled 177 mm – sandur and 191 mm – wetland. Peak evaporation rates were 5.6 mm/d for the sandur (June 22, 2016) and 6.4 mm/d, wetland on July 5th, 2016. Daily evaporation rates here were comparable to those measured in wet fens in the subarctic Hudson Bay lowland regions (2.6 mm/d over the Summer 1990) (Lafleur, 1990), patchy wetlands near Resolute on Cornwallis Island during a warm and dry summer in 1998 (2.6 mm/d) (Young and Woo, 2003), and evaporation from ponds at Polar Bear Pass, Bathurst Island in July 2012 (2.6 mm/d) (Young, Submitted).

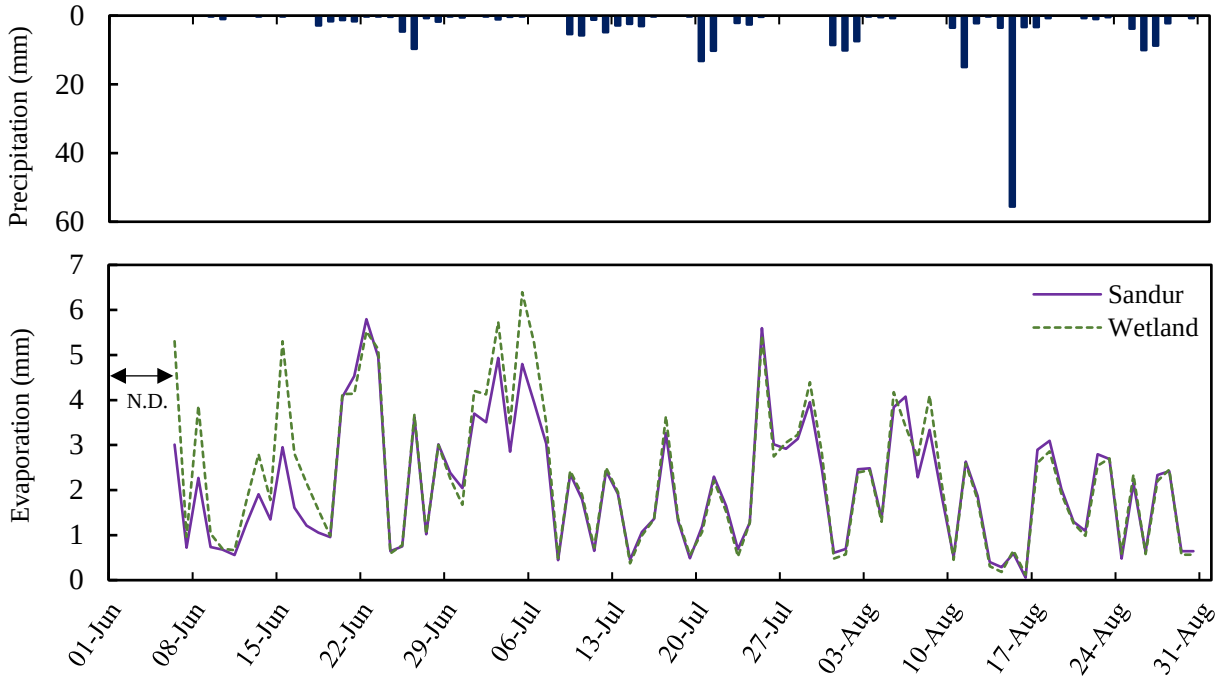

Figure 5.12 Daily evaporation rates of the Sandur and Wetland between June 6th and September 1st 2016 plotted against precipitation. N.D. indicates no data available.

5.2.7 Water Conductivity

Water conductivity is useful in defining water sources. For example, snowmelt water will have a lower conductivity than groundwater. Water conductivity monitored in the Brunná River and at Hverfisfljót demonstrated similar patterns (R^2 = 0.602 Figure 5.13). The two rivers carry meltwater from the Síðujökull glacier (658 m. a.s.l.) located about 38 km up the Brunná and have a similar hydrological regime. An initial drop in readings occurred between the 18th and 21st of June 2016 at both rivers, during the passage of the jökulhlaup followed by a rise which lasted for 3 more days This translated to a change in conductivity readings of 25 μS/cm for the Brunná River and 10 µS/cm for the Hverfisfljót over 4 days.

Fluctuations in conductivity readings throughout the study period were observed in response to rain events. Peak conductivity levels occurred on the 18th of August 2016 at the Hverfisfljót River (44.6 μS/cm) and one day later on the Brunná (57.7 μS/cm). Heavy rainfall here (August 15th, 2016) raised conductivity levels for a period of 4-5 days.

The water conductivity regime of the Skafta River at Svevindur (v299) located 8 km away from the snout is plotted in Figure 5.13. Here, the typical rise/fall pattern in conductivity during a jökulhlaup is observed across all three glacial rivers. Such a pattern in water conductivity is typical of jökulhlaups (IMO, 2016).

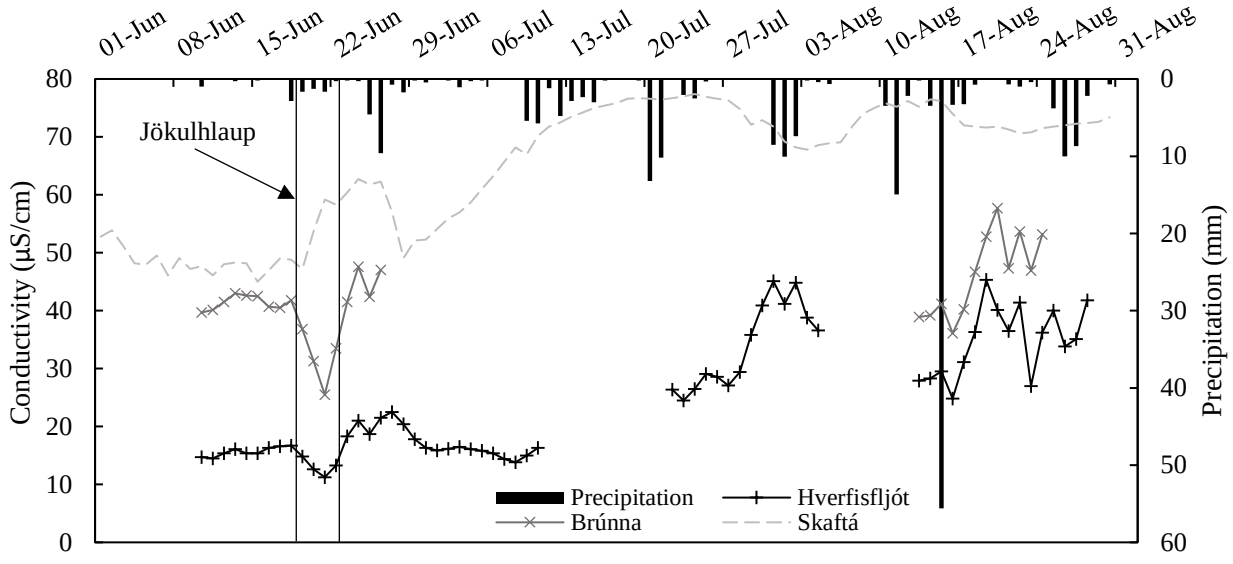

Figure 5.13 Water electrical conductivity values during Spring and Summer 2016 at Hverfisfljót (v71), Skaftá (v299) and Brunná River (Hvoll) plotted against precipitation.

5.3 Fluvial Processes and Flooding Patterns

This section describes the changes in surface types and the erosional, depositional and flooding patterns around the Hvoll property that have resulted from seasonal weather and episodic events since 1979, and more specifically between September 1st 2015 – September 1st 2016.

5.3.1 Erosion and Revegetation

An unsupervised classification helped to define areas and the direction of change between sandur and wetland surface types. Much research has already demonstrated the value of multi-temporal imagery for the classification of land types (Lillesand et al. 1998; Lunetta; Wolter et al. 1995, and Yuan et al. 2005).

The two pairs of cloud-free Landsat images selected to classify the study area revealed areas of change in surface types between 1985 and 2016 (Table 5.5 and Figure 5.14). Overall, around the Hvoll farm, the sandur expanded ca. 0.35 km^2. This expansion has been linked to several large floods occurring in 1994, 1995, 2006 and 2011 (Einarsson, 2009; per. comm. Haness, 2016). The sandur at the South-west site is now only about 100 m away from the nearest farm building. However, the analysis also revealed ca. 0.15 km^2 of revegetation around the property during that same period. Berms have been installed here in the recent years to prevent additional flooding into the wet meadows/farm land and have allowed plants to revegetate over previously inundated areas. The nature and extent of these floods will be discussed later (see Section 6.4).

The far south-eastern part of the property has been the most affected, losing an area of 0.26 km^2 to the sandur between 1985 and 2016. Within the boundaries of the South-east site, ca. 0.014 km^2 was lost to the sandur. During that same time interval, only about 0.002 km^2 was reclaimed

by vegetation here. In the South-west site, on the eastern shores on the Brunná River, an area of ca. 0.048 km^2 was lost to erosion. On the western bank, about 0.007 km^2 was eroded. Other zones within the South-west site behind the berm have managed to revegetate an area of ca. 0.016 km^2. In the West site, ca. 0.02 km^2 of vegetated land was lost to the sandur, however other areas which are now away from the river and sheltered from erosion have revegetated here an area ca. 0.454 km^2. Throughout the length of the Brunná River, erosion has occurred on the vegetated banks of the river but most significantly on the eastern banks close to the Hvoll farm.

Additionally, outside the boundary of the change detection analysis, the Landsat images revealed an expansion of grasslands (ca. 0.9 km^2) eastwards along the south-western shores of the Djúpá River (1985-2016). The installation of berms and ditches built by a neighbouring farmer suggest that that water inundation by the Djúpá River has been stalled and re-directed. An area of 0.15 km^2 was reclaimed by grassland (Purple in Figure 5.14) around the farm. Other notable changes in land type were found along the south-western shores of the Hverfisfljót River, near its outlet into the sandur. Here the sandur increased in size by 0.11 km^2, expanding into an adjacent lavafield.

Table 5.5 Mean area gains and losses in m^2 around the Hvoll farm at the West, South-west, South-east site and property Totals for each class (Erosion, Revegetation are listed). These values represent averages between the 1985-2015 and 1986-2016 analyses.

Erosion		West Bank (m^2)	East Bank (m^2)	Total (m^2)
	West Site	6750	13950	20700
	South-west Site	7200	48600	55800
	South-east Site		14400	14400
	Total property			355950
Revegetation		West Bank (m^2)	East Bank (m^2)	Total (m^2)
	West Site	12150	33300	45450
	South-west Site	13050	16650	29700
	South-east Site		2700	2700
	Total property			156600

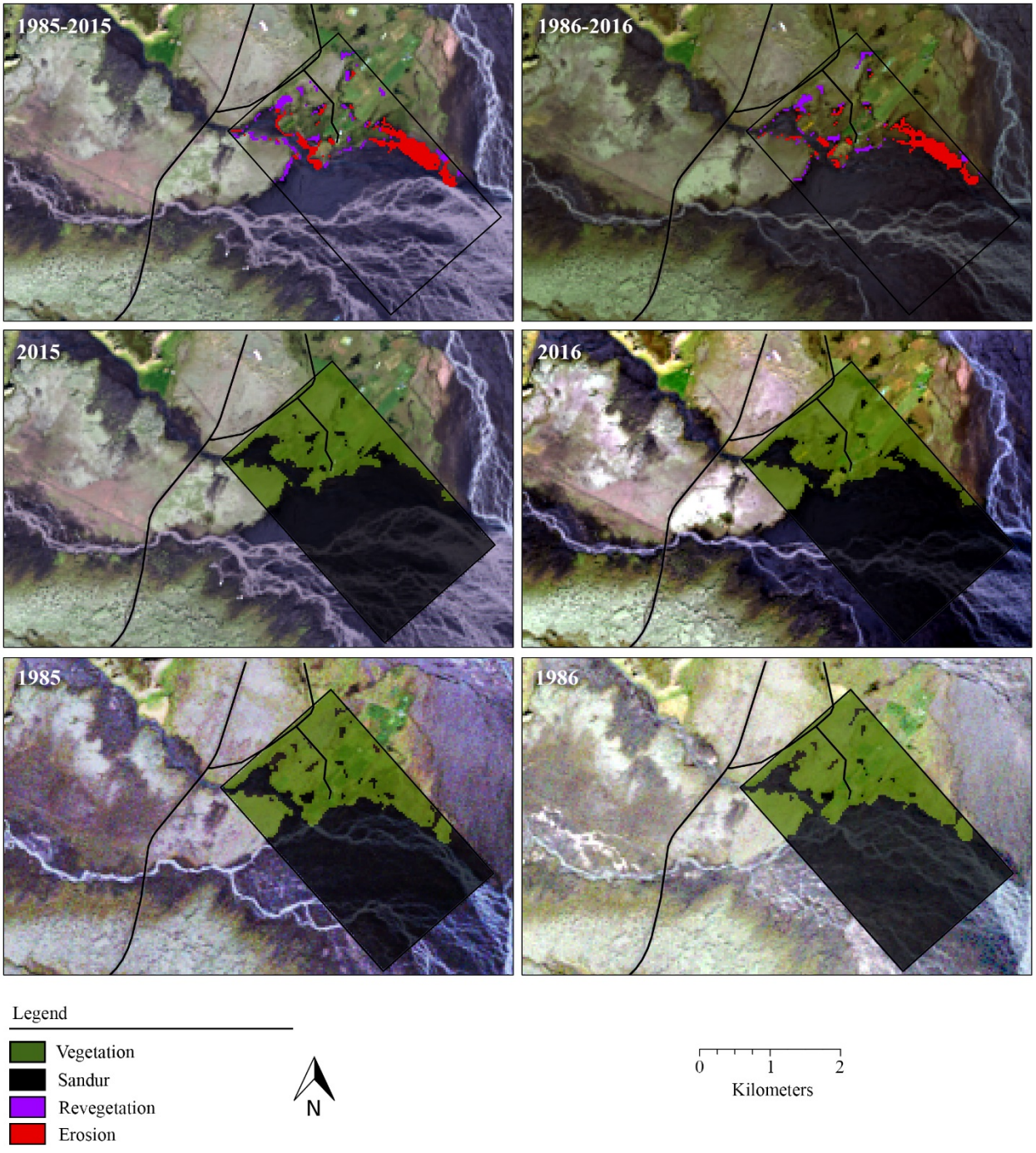

Figure 5.14 Pair of Landsat images comparing land cover (Vegetation, Sandur) shifts between 1985-2015 (left panes) and 1986-2016 (right panes). Areas that have changed from Vegetation to Sandur are shown in red, while gains in Vegetation are shown in purple.

5.3.2 Topography and Elevation

Elevation data of the region provided valuable information on the local topography and outlined flood prone areas. The digital elevation model produced by the NLSI with a spatial resolution of 5 m, showed that the area gently slopes ($\theta = 0.06$) in a south-easterly direction, until reaching the Djúpá River. Incised channels are found near the smaller springs in the wetland and next to the inhabited areas, to the south of the farm property (see Figure 3.4). The NLSI DEM details the berms on the South-west and South-east sites. As mentioned previously, farmers use them to minimize overland flow from the Brunná River.

In order to assess depositional or erosional patterns over the course of the study (JJA 2016), the DEM of the south side, scanned June 23rd 2016 was compared to the September 2nd 2016 DEM (Figure 5.15). It is important to note that DoDs analyses are only accurate within the network of ground control points and that results generated outside GCPs are not as reliable (Photoscan, 2014).

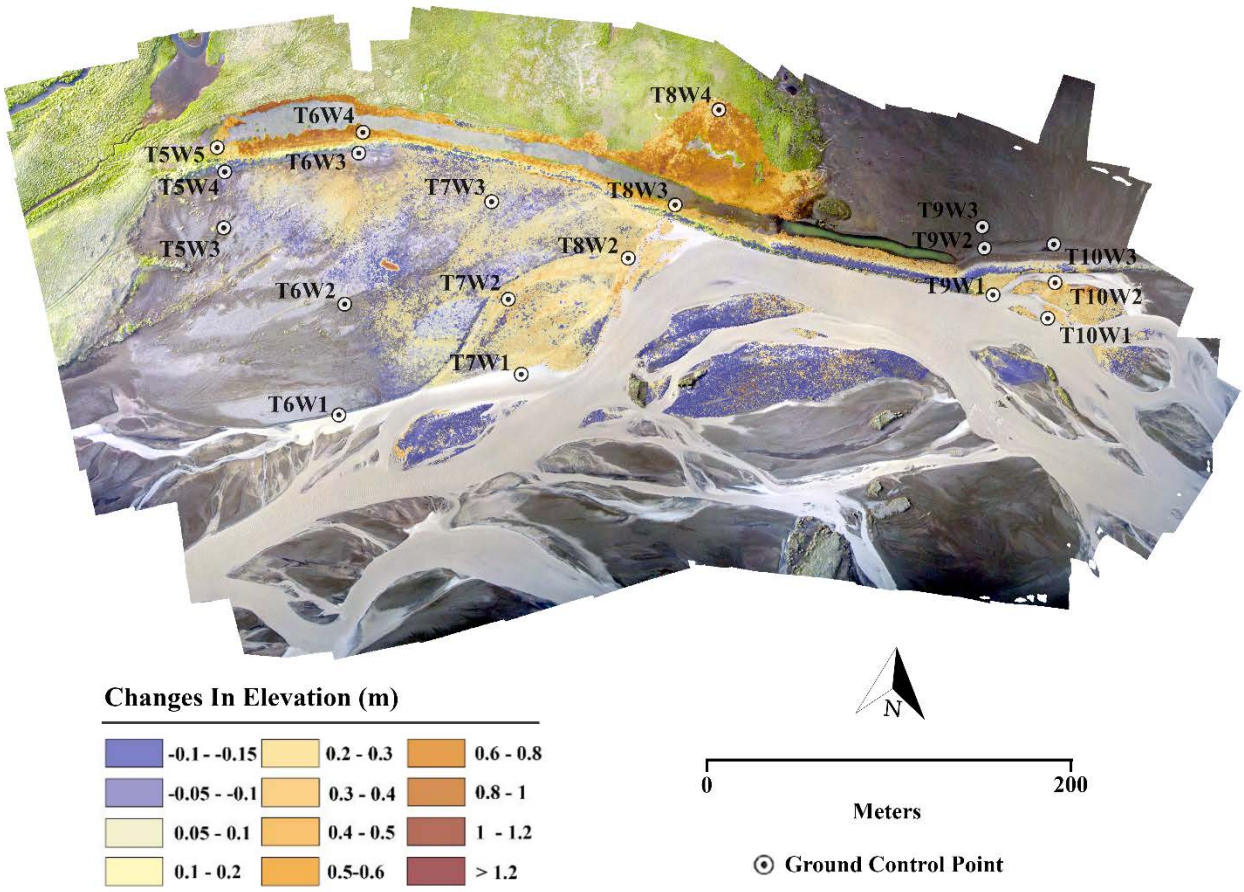

Figure 5.15 DoD analysis between DEMs of the South-east site taken on June 22nd 2016 and September 2nd 2016. Change in elevation is expressed in m. Note DoD analyses yield most accurate results in between the network of Ground Control Points (GCPs).

A number geomorphological changes across the sandur were detected over this 71 day interval. At wells T7W1, T7W2 and T8W2, a small sand bar developed on the shores of the Brunná River. Here gains of 0.05 - 0.3 m were detected. Another bar developed where wells T9W1, T10W1 and T10W2 were found. At this juncture, gains of ca. 0.15 m were found. Elevation increases were also detected around T7W3 on the sandur side near the berm. A hay bale of approximately 1.6 m high was placed on the sandur by the farmer sometime during the last week of August. On the DoD map it is the highest change in elevation between the two DEMs. Around the hay bale, slight losses (ca. 0.05 m) in elevation were also documented. Increases in elevation

(ca. 0.35 m) were also identified in the wetland, where grasses and shrubs grew, elevating the height of the DEM. Areas which saw the greatest loss in height between the two dates were predominantly between T7W1 and T9W1, in central sandur bars exposed to frequent river floods. Areas which saw significant erosion were adjacent to the Brunná River. Here vegetation mounds were continuously undercut and eroded by the river causing the berm to sink ca. 10 cm. A comparison between two images dating from 1989 and 2016 shows this phenomenon of river bank erosion (Figure 5.16). A closer view of these eroded vegetation mounds can be seen in Figure 5.17.

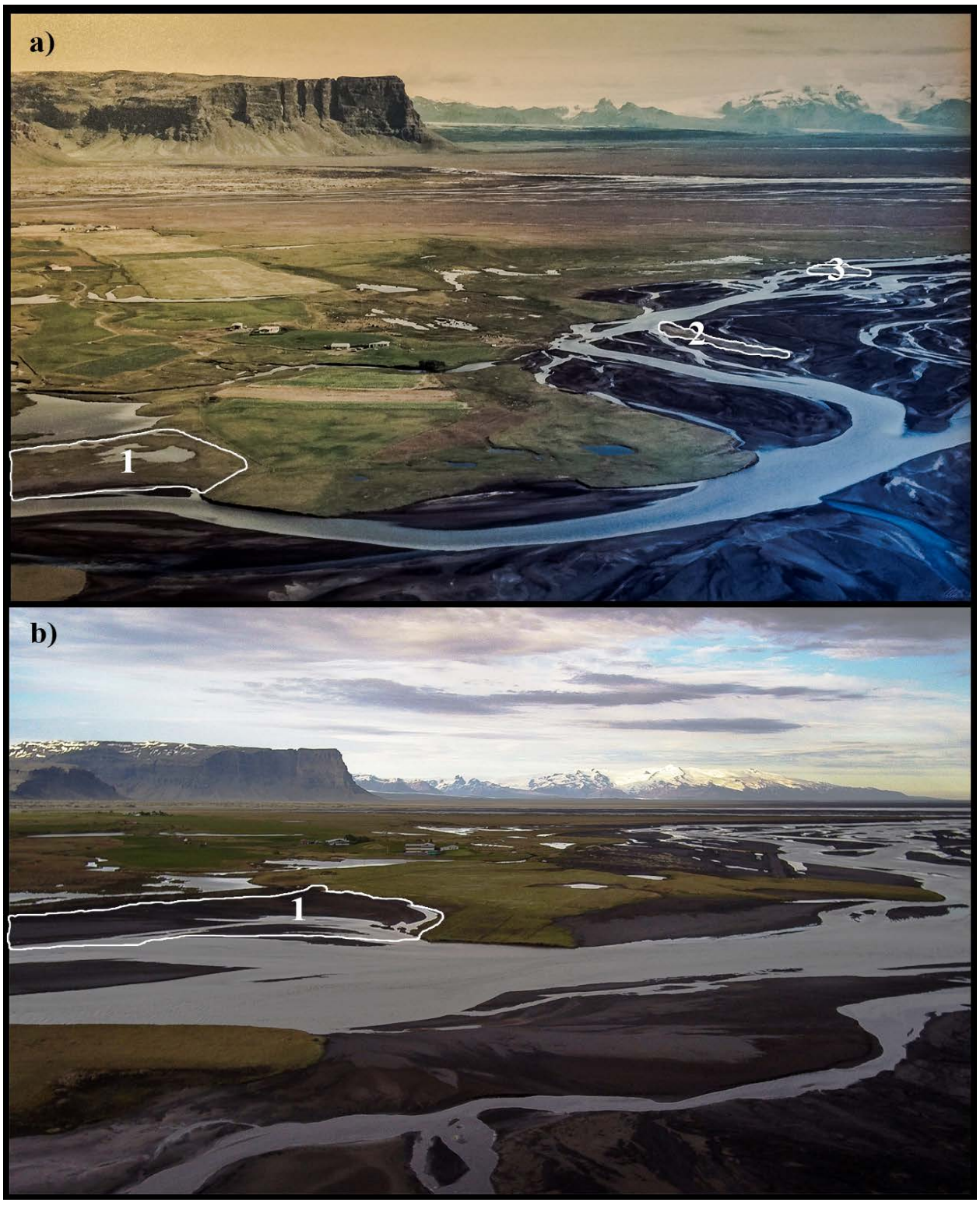

Figure 5.16 Aerial photograph taken by reconnaissance aircraft in summer 1983 (a) and summer 2016 by UAV (b). (1) Illustrates an area where sandur eroded a vegetated section c. 52.000 m^2. (2) and (3) illustrate previously eroded vegetated mounds which, nearly fully disappeared in the 2016 photograph.

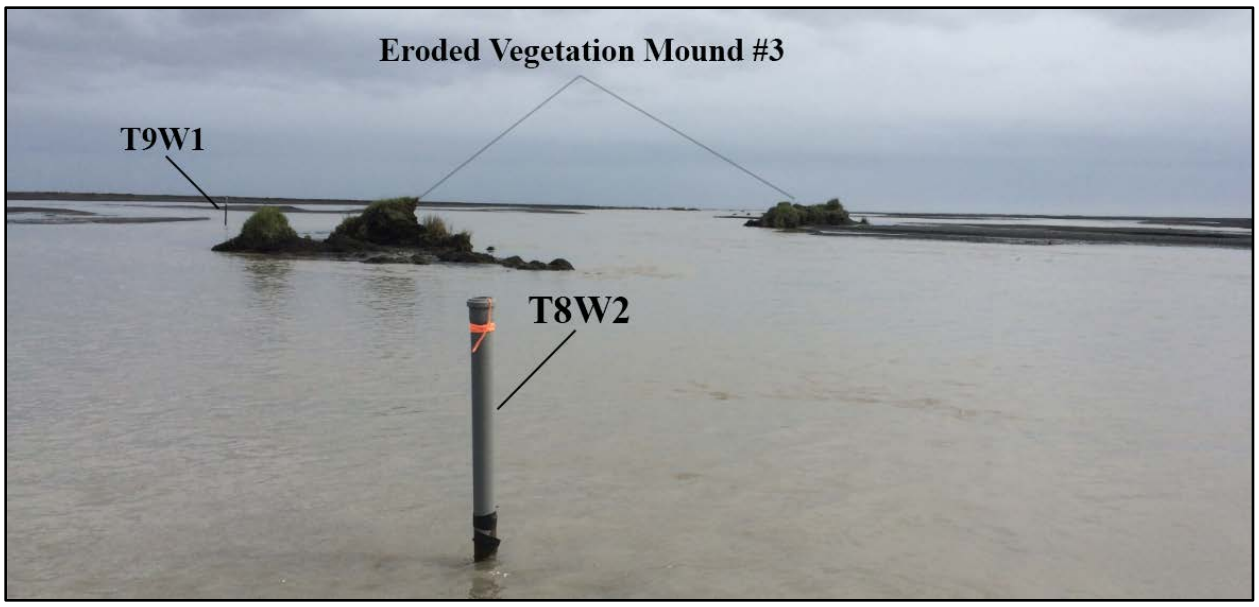

Figure 5.17 Photograph taken at South-west site near well T8W2 with well T9W1 seen in the background. Here we can see the last remnants of vegetation mounds which are continuously eroded. In 1989, approximate area of this mound (#3 on Figure 3.3.3) was ca. 1540 m^2**.** Today only three smaller patches of this mound remain, for a total area of 60 m^2.

The high spatial resolution DEM of the NLSI was mosaicked with the ultra-high resolution DEMs originating from the UAV. The data was compared to see elevation differences between the two data sets and to verify the degree of agreement between the DEM originating from the NLSI and the DEMS generated through photogrammetric processes. To assess the vertical accuracy of the high resolution DEMs, they were first georeferenced and fitted to GCPs surveyed on site by a total survey station. They were then compared against the heights of the DEM of the NLSI at the same coordinates. The DEM heights from the UAV follows the heights of the NSLI DEM, although there is a slight positive bias due to the finer vertical and horizontal resolution. A profile of the NLSI DEM is plotted against the DEMs generated from stereo-photogrammetry in Figure 5.18.

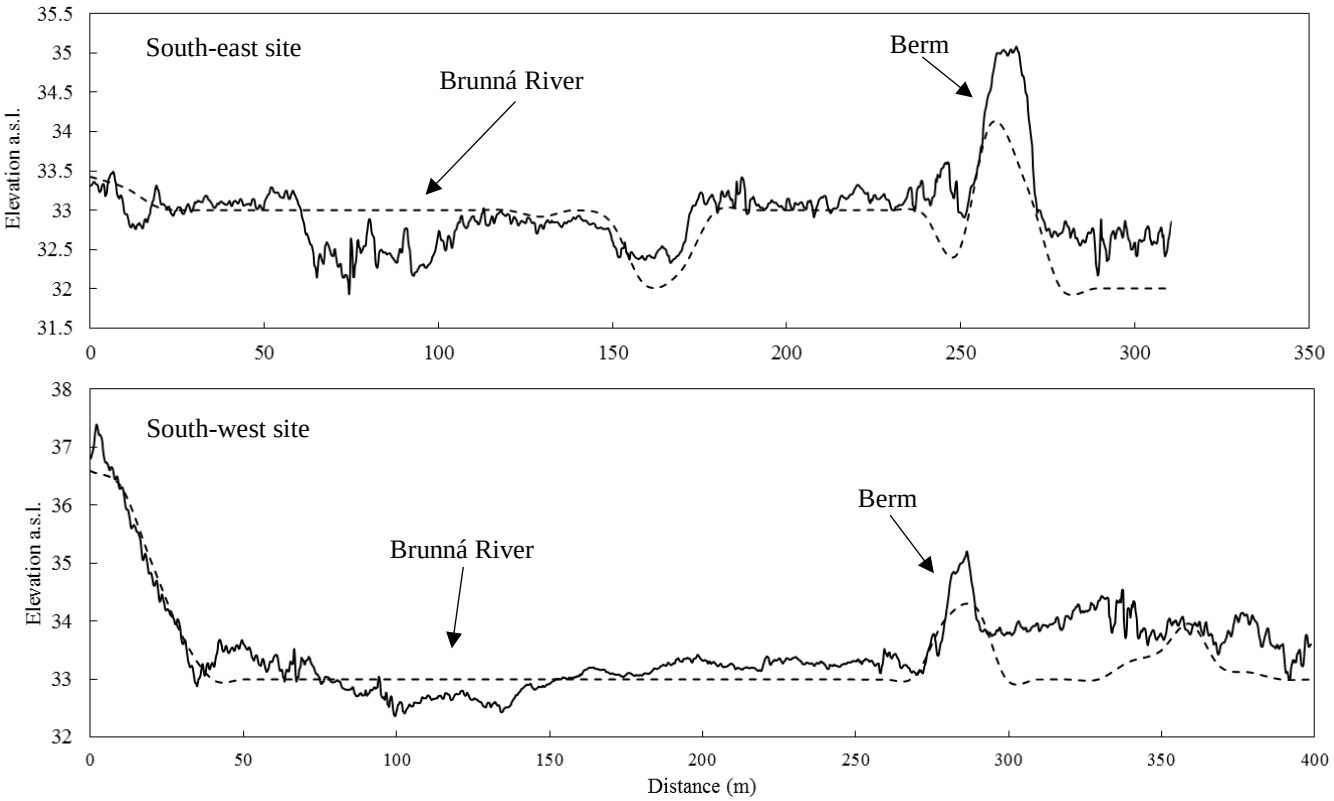

Figure 5.18 Two profiles of the DEM from the NLSI and the DEM generated from stereo-photogrammetry at the South-west site (top graph) and South-east site (bottom graph). Dashed line is DEM from the NLSI. Bold is DEM acquired from the UAV. Elevation differences beyond the ca. 275 m mark are likely caused by vegetation height differences between the two datasets.

5.3.3 Flood Maps

Water levels during floods that occurred during the September 1st 2015 – September 1st 2016 period were simulated in Arc Map 10.4 employing high resolution DEMs of the South-east site, derived from images acquired by the UAV (Figure 5.19). Here, the topography of the sandur at the south site decreases in elevation (ca. $\theta = 0.25$) from T5W4 down to T10W1. The modeled flooding extent of the South-east site is shown in Figure 5.20.

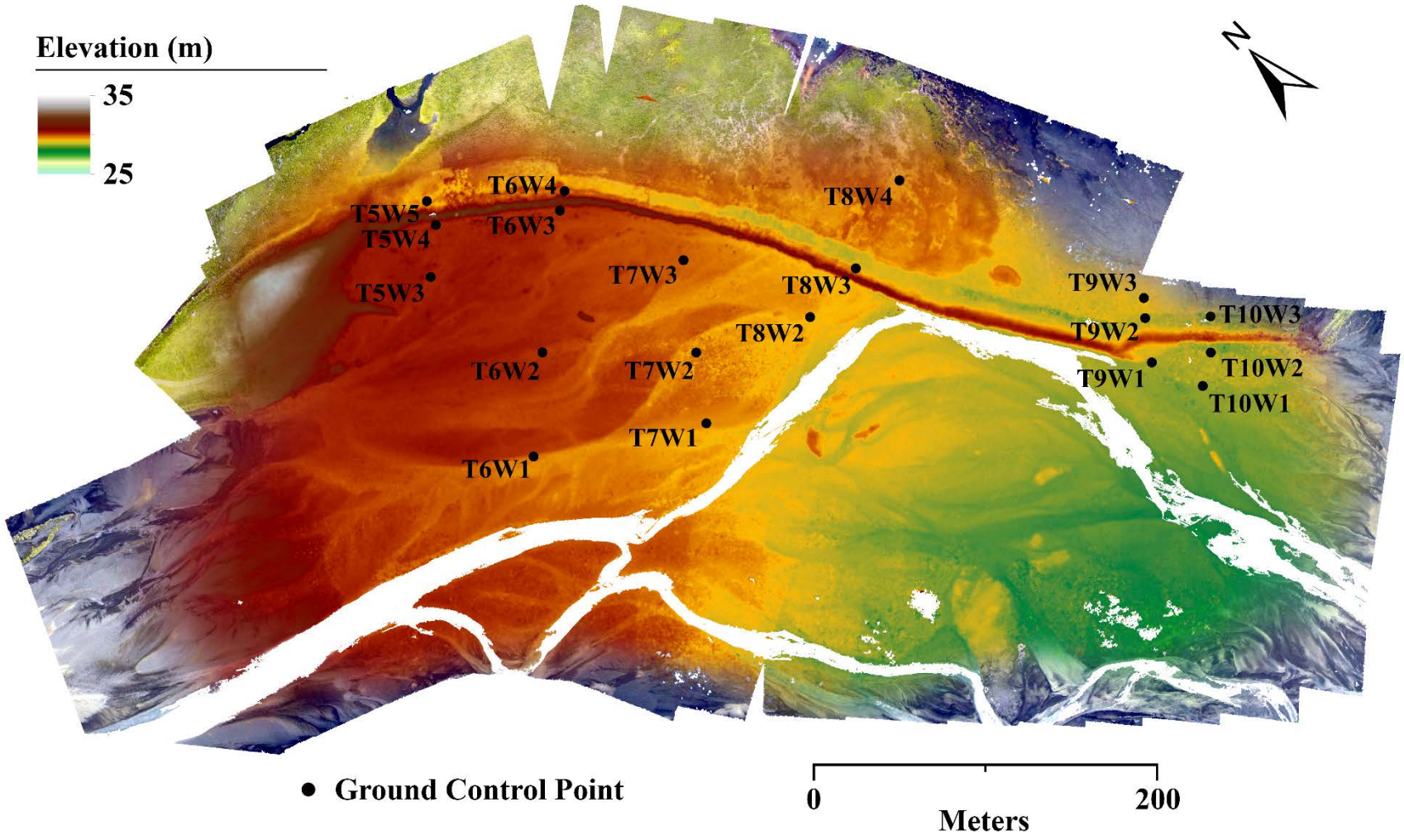

Figure 5.19 Structure from motion DEM of the South-east site acquired on September 2nd 2016 with a pixel resolution of ca. 0.05m.

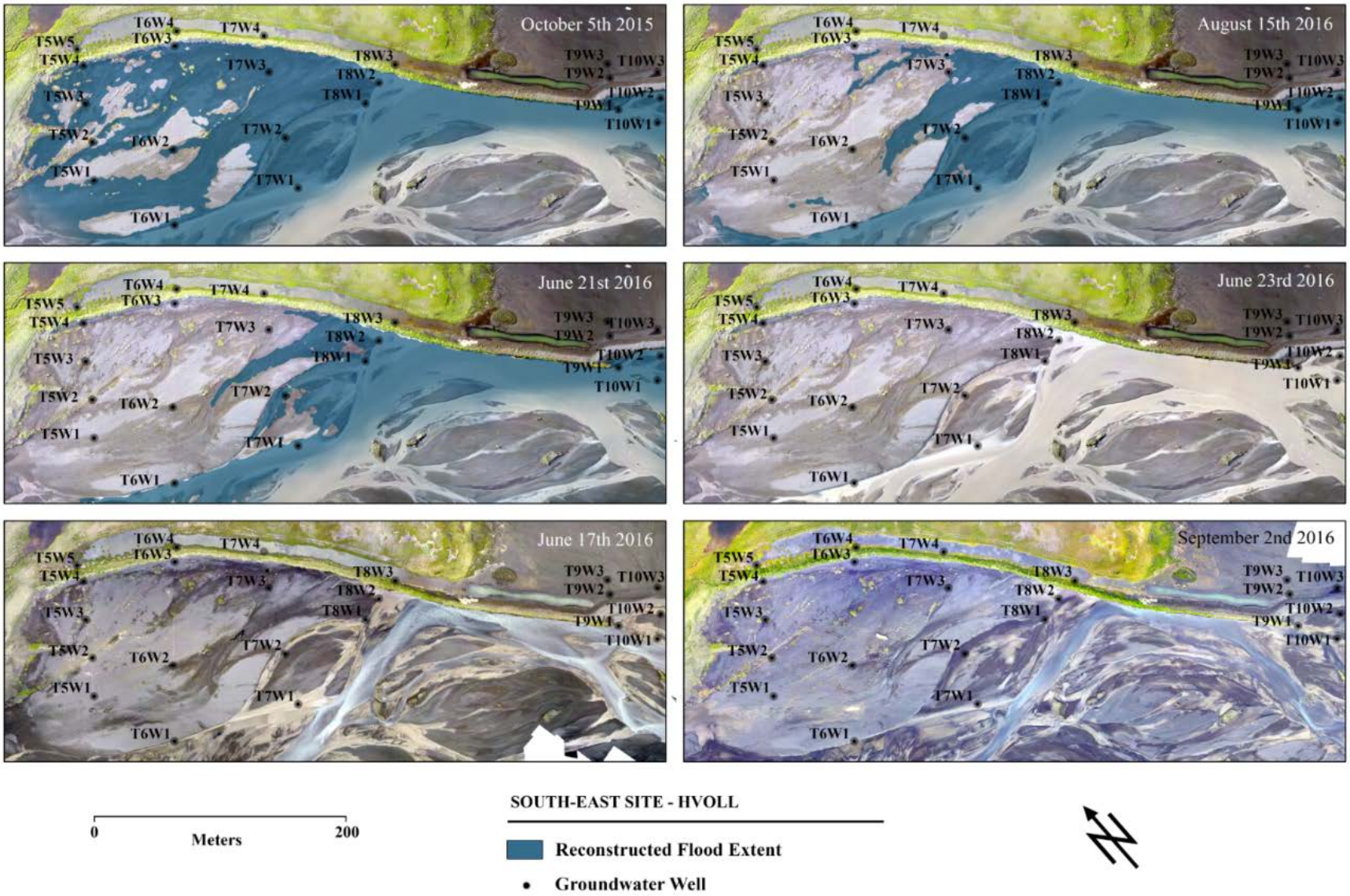

Figure 5.20 Flooding pattern during events which occurred over the September 2015 – September 2016 study period including: the jökulhlaup of October 5th 2015 at 01h00 when water levels were highest, the severe rainfall event of August 15th 2016, the jökuhlaup after the dust storm that occurred on June 21st 2016 including receding water levels on the 23rd; dry and low water levels conditions on June 17th and September 2nd 2016.

As previously mentioned, the South-west site berm is composed of crushed basalt versus the berm in the South-east site which is predominantly made of sand, hay and vegetation. The total height of the berm between wells T2W4 and T2W5 is ca. 2.4 m and only ca. 0.8 m at T5W4 on the sandur side or 1.5 m at T5W5 on the wetland site.

The simulation based on water level sensor data indicated that no overland flow into the adjacent wetland had occurred at the South-east site. Furthermore, the flood model demonstrated periods of high water levels but levels never reached a tipping point where overflow above the berm occurred. Water table data from the pressure transducers installed in the wells recorded a maximum water level peak of 10 cm of water above the surface on September 10th 2015 at well T5W4, a location which is the farthest from the river and is higher in elevation than other wells located in the sandur. During the October 4th 2015 jökulhlaup event, an additional 67 cm of water at well T5W4 would have been needed to over flow into the wetland on the South-east site. Photographs captured from the UAV on June 17th and 23rd 2016, before and after the June 20th 2016 jökulhlaup event, demonstrate little change in flow direction in the south.

At the South-west site, the highest well in elevation on this side of the sandur is well T2W4. On September 10th 2015, there was about 66 cm of water above the ground at this well. On October 4th 2015 water levels were even higher with 72.5 cm of water above the ground surface at T2W4 by the adjacent ca. 2.4 m high berm (See water tables/levels in Figure 5.8). Therefore no flooding had occurred.

However, UAV imagery taken from the West site where Transect 1 is located, detected upwelling from macropores (previously plugged with sediment), spilling spring water from the lava field back into the Brunná River (Figure 5.21).

Figure 5.21 Photograph of two macropores located on the West site near the lavafield, at the border of the sandur-wetland. They contributed spring water to the Brunná River on June 20th 2016.

Large vegetated sections of the farm have been eroded since 1979 as can be seen in Figure 5.22 which shows photographs of the area surrounding Hvoll and the various flow paths that the Brunná River has adopted in 1979, 1986 and 2011 as well as the decreasing coverage of vegetation in comparison to the sandur.

Figure 5.22 Aerial photographs from 1979, 1986 and 2011 showing changes in flow of the Brunná River in nearly all three sites (site outlines are shown). Notice expansion of the sandur and flood path at the South-west and South-east sites.

CHAPTER SIX: DISCUSSION

6.1 Introduction

The major aim of this thesis was to better understand the hydrology of a sandur-wetland landscape in South-east Iceland. The study highlighted the behaviour of the sandur and the nearby-wetland in response to seasonal inputs of water (meltwater, rainfall), and identified their response during extreme events, such as heavy rainfall or jökulhlaups (glacial floods). Additionally, this study evaluated the hydrologic dynamics of the sandur-wetland boundary, primarily through groundwater exchange. Satellite, aerial and UAV derived imagery was useful in tracking elevation changes in the sandur, documenting sediment erosion/deposition and flooding extent. In the final part of the discussion, impact of climate warming on this unique landscape is also discussed. Furthermore, this study seeks to augment our current understanding of the paraglacial therory by highlighting Iceland's unique environmental conditions and sediment availability, therefore distinguishing it from the traditional sediment exhaustion scheme of paraglacial landscapes initially coined by Church and Ryder (1972).

6.2 Hydrological Regime of Sandur

6.2.1 Response to Seasonal Climate

The seasonal response of the sandur's water table along the Brunná River at the South-west and South-east study sites, identifies it as being impacted by a proglacial regime (Woo, 2012), with the bulk of the water coming from the nearby Síðujökull glacier (Figure 5.7) Additionally, inputs of seasonal rainfall over the site and catchment areas often provided a quick response in sandur water tables.

Since the Brunná River is a glacial river, it is typical for water levels to be highest in the summer and fall, corresponding to peak melt periods. The seasonal occurrence of frequent rainfall in the fall further increases water levels, often generating peak discharges which translate into flooding of the sandur. These events are feared by the local farmers, as they can have a destructive effect on adjacent inhabited wetlands (per. comm. Haness, 2016)

Sustained glacial melt mixed with frequent and prolonged rainfall in the fall regularly triggers a rise in sandur water tables and causes surface flooding. For instance, water levels in sandur water wells rose between 29-60 cm (see Figure 5.7) in response to rainy, windy weather in early September, 2015 (>30 mm over 72 hours; winds were 20-25 m/s) (IMO, 2015). As water tables were retreating, another rainfall event started on the 18th of September and brought over 20 mm of rain in 3 days, rising water levels in some wells again (42-77 cm). A few days later, 20 mm of rain fell. By the end of September, another low pressure system deposited 33 mm of rainfall (IMO, 2016), generating an even larger flood, larger than the previous ones at the South-east and South-west study sites. Here water levels rose between 49 and 77 cm at several wells.

This reoccurring seasonal regime of high water levels in the Fall over the sandur triggered by glacial discharge and frequent rainfalls have generated some of the largest floods recorded here at the Hvoll farm (e.g. September 30th 2011 flood event) (IMO,2011).

6.2.2 Response to Extreme Events

As previously mentioned, southern Iceland is geographically predisposed to severe wind, dust-storms and frequent heavy rainfall events. These climatic events in synergy with glacial outburst floods (jökulhlaups) are significant contributors to the hydrology of the sandur, terrain changes here and impact on the Hvoll farm (wetland).

Frequent extreme climatic and hydrological events affecting the streamflow regime of the Brunná River and flooding pattern of the sandur occurred here throughout the September 2015 – September 2016 study period. Water levels in the sandur at all three study sites increased sharply in response to high precipitation inputs (e.g. September 2015, August 15th 2016), leading to rapid inundation of the sandur (Figure 5.8, Figure 5.20). The water table of the study sandur is usually found less than 1 m from the surface; hence any heavy rainfall can lead to exceptionally large floods here. Flooding in response to rainfall is a common occurrence for other sandur locations such as in floodplain deposits within braided sandur systems in upper Erdalen (Nordfjord, western Norway (Beylich et al. 2010).

Water level rise in response to a dust storm (June 19-20, 2016), in the absence of much precipitation is perhaps one of the more interesting features of this thesis, demonstrating the unique linkage between atmospheric conditions and hydrology. Specifically, water tables in the sandur rose June 20, 2016 (1900h) triggered by a rapid melt event, which followed a large dust storm

(>22 m/s) and warm air temperatures (>24ºC). Glacial meltwater increased along the Brunná River (small jökulhlaup), as the dust would have lowered the Sidhujlkull glacier's albedo, enhancing Q^* receipt, while warm air temperatures and windy conditions would have enhanced sensible heat exchange. A search of the glacial and hydrology literature indicated that this process has previously been documented by Prospero et al., (2012) which associated Icelandic dust storms with glacial outwash deposits and to sub-glacial floods occurring by the Mýrdalsjökull and Vatnajökull glaciers.

Glacial outburst floods (jökulhlaups) are typical in southeast Iceland and are said to occur 5–10 times annually (Sigurðsson and Einarsson, 2005) with the biggest triggered by volcanic activity. These extreme floods carry large quantities of meltwater and eroded material to the lower sandur with the most frequent ones originating from the nearby Grímsvötn and the Skaftá cauldrons. The 1996 jökulhlaup from Grímsvötn down the Skeidara River (located 16 km due east from Hvoll) is one of the best known jökulhlaups of this type and has been heavily documented by Magilligan et al. (2002). During these jökulhlaups, great quantities of ash and sediment are transported downstream, ending up being assimilated into the river channel for months subsequent to the next event (Hardardottir and Snorrason, 2013). The sudden release of this meltwater from glaciers and ice sheets can be attributed to a variety of factors, such as spring melting events (Anderson et al., 1999), intense rainfall (Russell et al., Collins, 1997) or snowmelt (Lawson, 1993; Röthlisberger and Lang, 1987), the sudden drainage of stored meltwater (Thorarinsson, 1939; Björnsson, 1992; Tweed and Russell, 1999, Magilligan et al, 2002), the breaching of moraine dams (Costa and Schuster, 1988; Clague and Evans, 2000) and volcanic activity (Tómasson, 1996).

During the September 2015 – September 2016 field period, the jökuhlaups along the Brunná River (October 4th 2015, June 20th 2016) caused water levels and turbidity to increase (see

Figure 6.1). The Skaftá jökulhlaup which started on October 1st 2015 caused by the drainage of subglacial lakes at the Skaftá cauldrons near Grímsvötn; ones which had not drained since June 2015, (IMO, 2015) led to elevated discharge rates along the Skaftá River, which spilled over into the Brunná River. On average, the Skaftá cauldrons drain every two years, often producing floods reaching 1,500 m^3/s (IMO, 2015). If the interval between floods is short, the flood tends to be smaller (IMO, 2015).

This jökulhaup was especially large in comparison to the June 20th 2016 jökulhlaup due in part to the prolonged and intense rainfall period, the previous week leaving the ground saturated and river levels high. Flood maps generated from water level data at the South-east site (October 4, 2015) illustrate a large proportion of the sandur being flooded (see Figure 5.20).

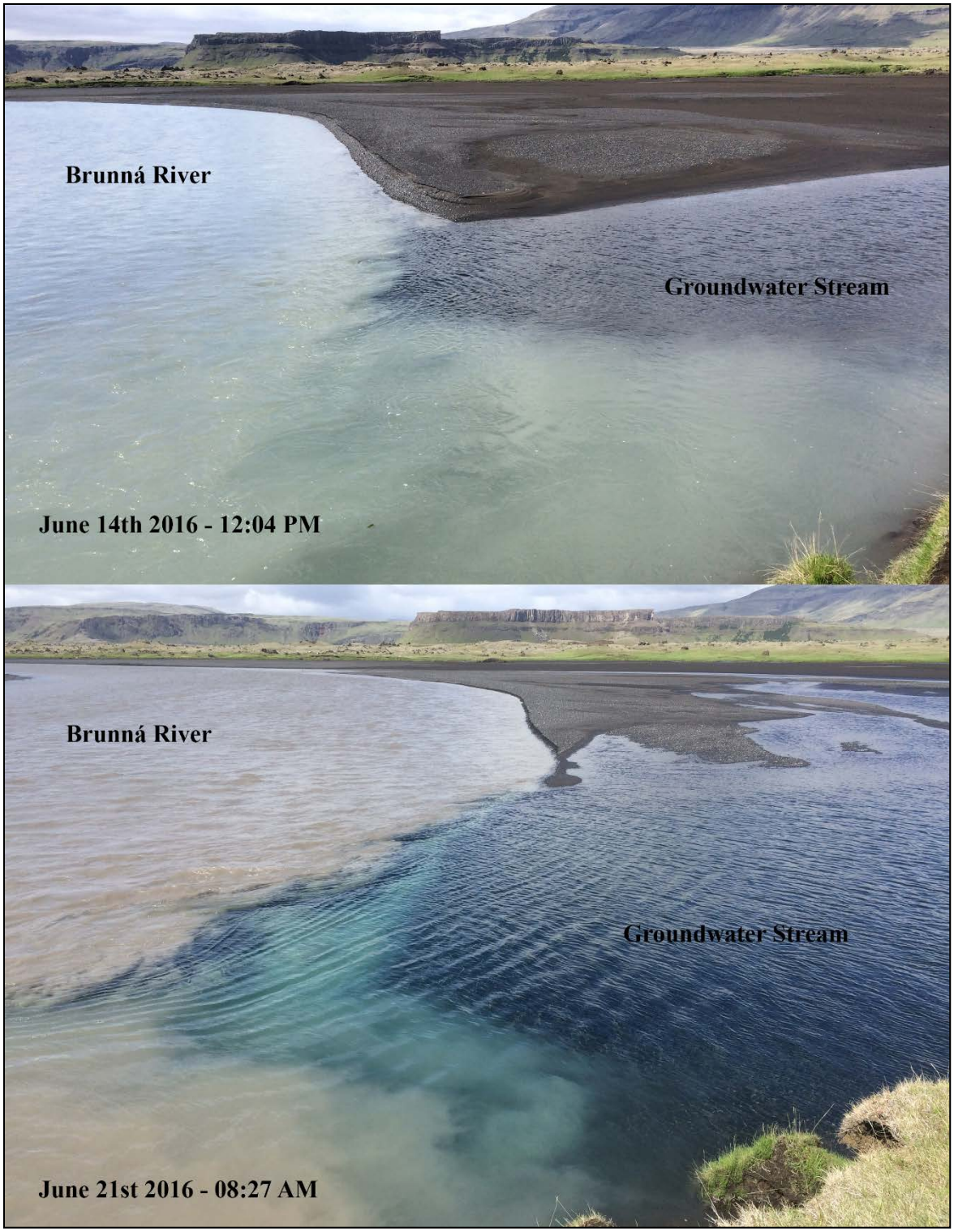

Figure 6.1 Two photographs taken at the West study area illustrating change in turbidity of the Brunná River after the June 19th 2016 sandstorm event. Water level in the Brunná River started to rise around 2000h on the 20th of June and tubidity changed around then, lasting until the 22nd of June 2016. (Note change in water levels and more turbid water in the bottom photograph in comparison to the June 14th 2016 photo).

6.3 Hydrological Regime of Wetland

6.3.1 Response to Seasonal Climate

Wetland water levels at the study site were more stable than the surrounding sandur but spatial differences did exist. For instance, the hydrological regime of the wetland (South-east side) responded little to seasonal climatic conditions (see Figure 5.24). However, throughout the JJA period, water levels on the South-west site fluctuated similarly to the neighbouring sandur but with smaller amplitudes. Despite differences in water table response, flood mapping showed no overland flow from the sandur to wetland from September 2015 – September 2016. Undoubtedly, the man-made berms were a successful barrier in preventing severe autumn floods (2015) from penetrating the wetland. Whether they would be able to handle much larger flood events, for example, future jökulhlaups triggered by volcanic eruptions remains unclear.

The dynamic water table and pond levels in the wetland along Transect 2 and 3 (South-west site) can be partially attributed to water seepage from the Brunná River, as water levels in the wetland rose in a similar manner to the river. Spring water from macropores contributed additional water to the wetland but it is not clear whether the river controlled this water input or the water came from the surrounding Laki lava field (See Figure 3.3). Additional information on these macropores and springs will be discussed in Section 6.4.1.

Wetlands typically require an ample and persistent water supply for their existence (Winter and Woo, 1990). Here, the wetland received adequate amounts of water in the form of precipitation, subsurface flows and direct water inputs from smaller streams draining into it. During the JJA period (2016), water storage remained positive as evaporation losses did not exceed precipitation inputs: 191 mm (evaporation) to 225 mm (rainfall). Similarly, the sandur water

storage remained positive, as gains from precipitation (225 mm) were greater than evaporative losses (177 mm). Furthermore, groundwater seeping through the berm continuously added inputs of water. For most arctic wetlands, seasonal snowmelt contributions and summer rainfall are critical for their sustainability (Woo and Young, 2006). The wetland in this study depends on both; summer rainfall to exceed evaporation losses, and groundwater/spring water inflow.

6.3.2 Response to Extreme Events

The wetlands response to extreme events differed from the sandur. For instance, during the October 4th 2015 jökulhlaup, water levels in the wetland (South-east side) barely responded to the flooding in the adjacent sandur. During this flood, water wells in the sandur closest to the berm (T5W4) rose over 60 cm in 24 hours, while water levels in the wetland barely fluctuated (ca. 1 cm). Only on the next day did water levels increase by ca. 5 cm (T5W5), the highest for the entire study period (September 2015 – September 2016). A similar pattern occurred on the 28th of September 2015 after the passage of a heavy rainfall event. During and after the October 4th jökulhlaup, groundwater inputs into the wetland were estimated to be ca. 12 m^3. These inputs of groundwater from the sandur into the wetland, albeit small, likely helped raise wetland water levels, the following day.

At the South-west site, water levels in the wetland responded to the June 20th 2016 jökulhlaup in a similar fashion but with damped amplitudes (see Figure 5.8). Between June 20 – 23, 2016 ca. 3 m^3 of water discharged into the wetland along Transect 2 and 3. It is important to note that discharge rates are likely much larger here, since the thickness of aquifer (d_s) at both sites was only measured to the bottom of wells (ca. 40 cm below the ground surface). Skeiðarársandur

contains an extensive unconfined aquifer whose thickness typically varies between 100-250 m (Levy et al., 2012). However, difficulty in assessing the size of the aquifer here at this site only permitted calculations to the bottom of the groundwater wells. Several of the springs emerging from the macropores responded in the same pattern as the Brunná River (suggesting a linkage to it), though again, water table amplitudes were dampened. More on groundwater rates will be examined in the section 6.4.1: Groundwater Sandur-Wetland interaction.

During the intense precipitation event of August 15th 2016, water levels in the wetland (South-east side) responded little in comparison to the adjacent sandur. Field site observations by K. Young in August 2014 (rainstorm = ca. 65 mm/24 hours) revealed high water levels right up to the berm with some inundation into the wetland. However, extensive overland flow has not occurred here (both South-west and South-east sites) since late September 2011. Aerial photographs of the farm then, confirmed the occurrence of a destructive flood, which breached through the sandy-ash berm between Transect 8 and 10. This flood carried large quantities of water and sediment, eventually leaving a black ground surface devoid of vegetation as water levels retreated.

In summary, the wetland's hydrological regime was generally stable, providing a suitable habitat for migratory birds. Soil moisture was similarly constant throughout periods of drought and severe events, again ensuring a stable and viable environment for vegetation growth.

6.4 Sandur – Wetland interactions

6.4.1 Groundwater

The hydraulic conductivity and infiltration rates measured in the transition zone (berm) between the sandur and wetland (see section 5.2.2 and 5.2.5) suggested high permeability permitting groundwater to percolate into adjacent wetland ponds and meadows, mostly on the South-west side). However, numerous stream channels were found throughout the sandur-wetland interface making reliable estimation of discharge from the sandur to the wetland rather difficult.

Elevated water levels in the sandur relative to the wetland in the summer and during extreme events tended to direct more groundwater into the lower-lying wetland, in contrast to the winter period due to greater hydraulic gradients.

Hydraulic conductivity rates in the sandur were higher in the South-west site (3.620 m/d) versus the South-east (0.762 m/d). The high hydraulic conductivity of the berm in the South-west site permitted water to seep laterally into the wetland, though water table gradients did not differ much between the wetland and the sandur along Transect 2 (see Figure 5.7 and Figure 5.8). However, at the South-east site, even though water seepage (*k*) was lower than the South-west side, the hydraulic gradient (change of water table over distance) during events was enhancing groundwater inflow from the sandur to the wetland.

Small artesian springs emerging from macropores formed small rivulets in the wetland, and appeared to be another source of water to wetland ponds. They tended to cluster about 800 m upstream from the study area at the edge of the Laki lava field (Figure 3.4 and Figure 6.2). Water levels in one of these spring rivulets during the jökulhlaup event of June 21st 2016 (Figure 6.3), suggested a strong linkage between it and water levels in the Brunná River.

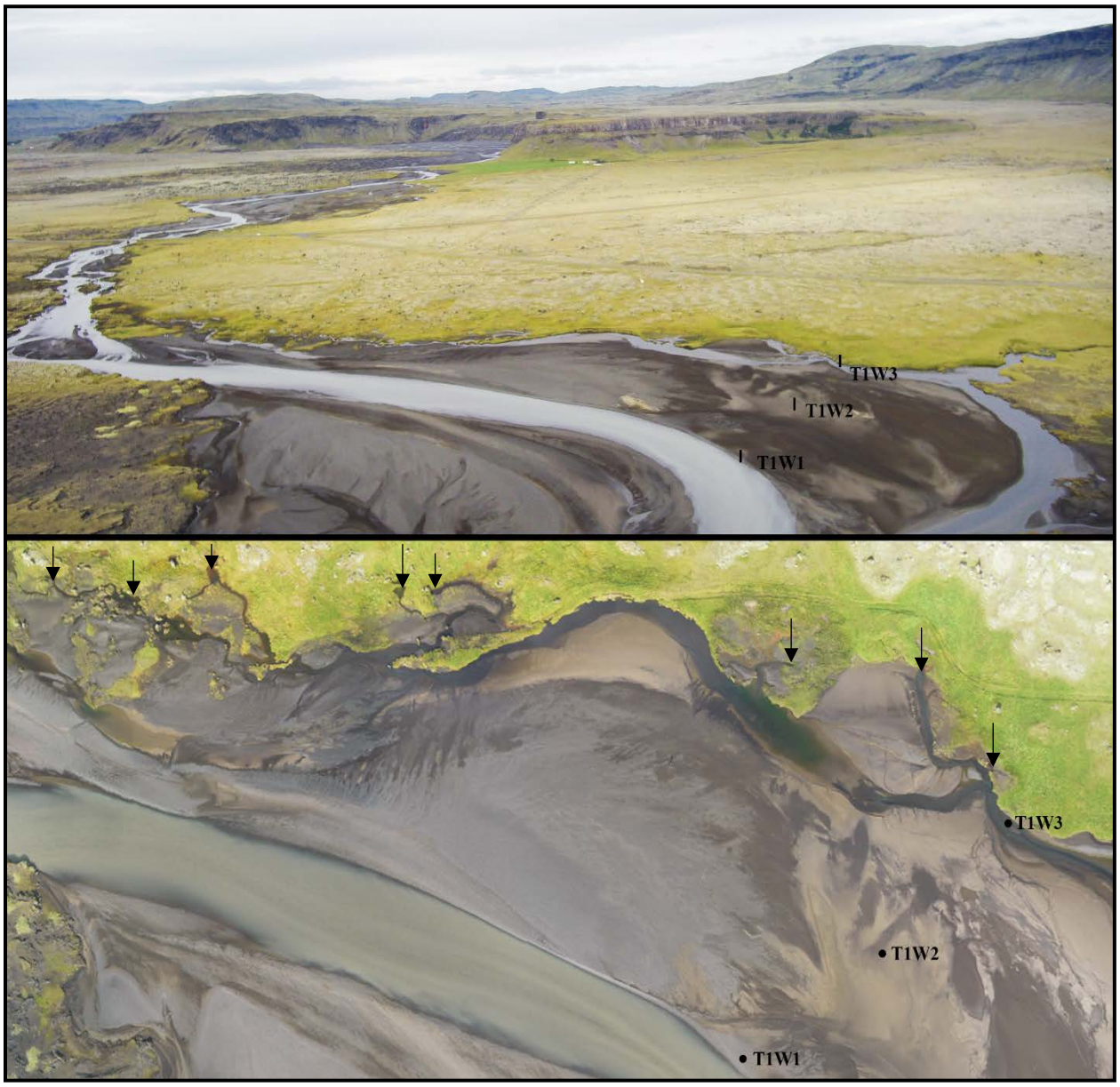

Figure 6.2 Photographs of the West site with Transect 1 reaching from the Brunná River (T1W1) to a small stream (T1W3) entirely nourished from groundwater originating from the border of the ancient Laki lava field. Temperature records showed that water originating in those streams never fluctuate below or higher than 4ºC versus the Brunná River which ranged from 5 to 9ºC. Emergence of groundwater through macropores along the ancient lavafield are indicated with arrows.

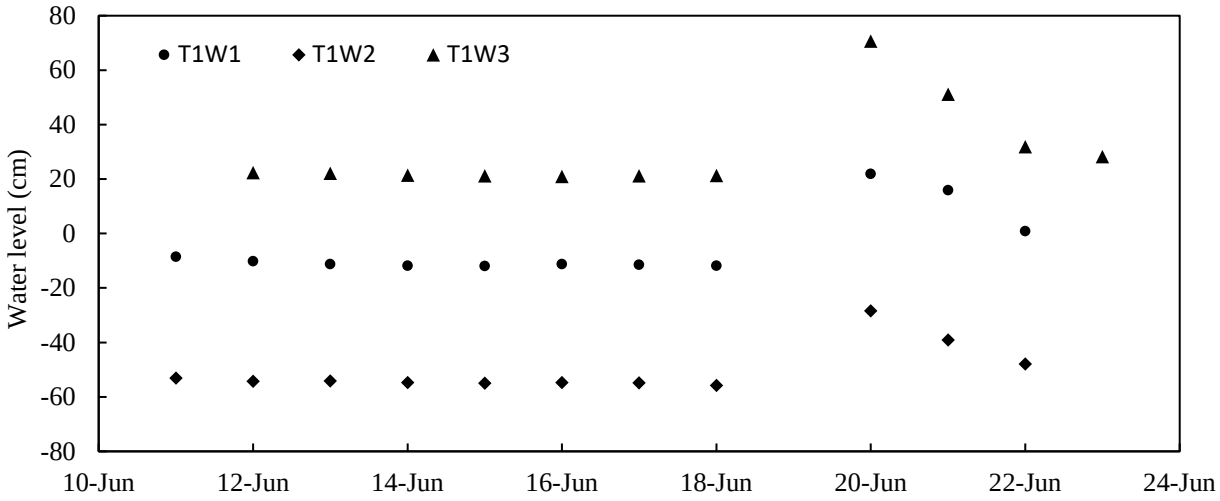

Figure 6.3 Spot measurements of the water table at wells along Transect 1 between June 10th and 24th 2016. Water levels at all wells including the groundwater stream (T3W3) responded to rising water level of the Brunná River during the June 20th jökulhlaup.

This notion was further reinforced by the presence of small artesian wells spewing water and very fine ash into the wetland (T3W4). The bedrock here is porous, mainly comprised of tertiary plateau basalts and large macropores sometimes over 1 m in diameter can be found (Johannesson, 2007). In such areas precipitation infiltrates through the porous surface to the groundwater aquifers (Jónsdóttir, 2008). The network of macropores and springs in this area is not well understood and thus further research is required.

Finally, the water levels and groundwater transfers described in this study illustrated quite different groundwater flux regimes between: (i) a sandur and a wetland; and (ii) between different locations along a sandur-berm-wetland landscape. Even though a berm is present as a line of defense against flooding, the varying responses to jökulhlaup events at water wells in the wetland (South-east versus. South-west) illustrates a complex hydrological system, and cautions against sampling in just one location.

6.4.2 Floods and Overland Flow

Most floods in Iceland, mainly involve snow and ice (Snorrason et al., 2000). They include ice-jam floods, release of sub-glacial or glacier-margin lakes and floods caused by the inter-play of rain and melting snow and ice (Johannesson et al., 2007).

At Hvoll, seasonal flooding of the sandur and floods from severe events (heavy rainfall, jökuhlaups) were documented over the study period. Although water levels got high next to the berm (0.75 m and 0.1 m at T2W4 and T5W4 during the October 4-5th jökuhlaup), they never reached the threshold level to spill over into the wetland (2.4 m and 0.8 m at T2W4 and T5W4). The most significant flooding events across the sandur occurred during the fall season, and were a combination of glacial melt and rainfall. Overall, there were four events where water levels rose over 40 cm at sandur water wells, and they all occurred between September 10th and October 10th 2015. Most of the large floods occurring here, aside from ones triggered from subglacial geothermal activity generally occur in the fall.

Together with changes in water levels, sandur flooding can alter the landscape through erosion and re-deposition. At the South-east site (past Transect 8, see Figure 4.1), the berm lacks vegetation and is unstable, and along Transects 8 and 9 some under-cutting is now occurring. A breach also occurred here during an earlier flood in September 30th 2011 (See Figure 6.4). Moreover, DoD analysis documented a drop of elevation (13 cm) along this section of the berm during the JJA study period. Similarly, vegetated patches here and at the South-west site are being undercut by the river, leading to collapse (Figure 6.5).

The loss in elevation along the South-east site is disturbing as continued undercutting of river flood waters will make the adjacent wetland vulnerable to future floods. Efforts by the farmer to protect this area, through the placement of hay (sand dunes) are showing some promise, but this

area was the site of a large breach in 2011. Expansion of the sandur into the wetland area will lead to altered surface conditions, one which will have quite different hydrologic (soil moisture, drainage) and surface-atmospheric (albedo, temperature) characteristics than now.

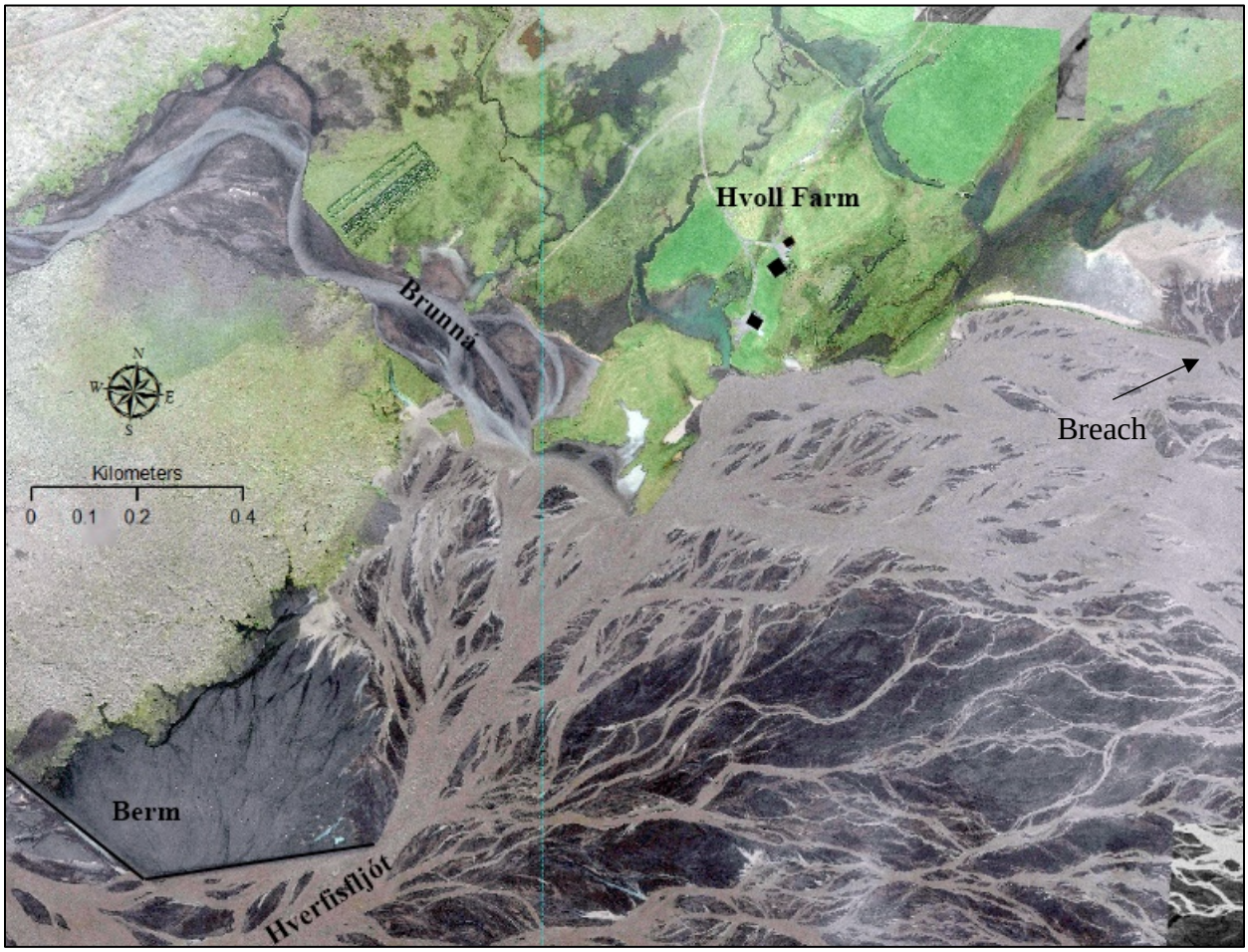

Figure 6.4 Satellite imagery obtained on Microsoft Bing map portal sourcing DigitalGlobe imagery of a flood event which occurred at the Hvoll farm around September 30th 2011 after a series of precipitation event. Notice inflow of the Hverfisfljót River from the south mixing with waters of the Brunná River.

Figure 6.5 A photograph from the West site looking south towards the South-west site. Notice collapse of the vegetated bank along the Brunná River.

6.5 Climate Change

Although severe wind, dust and rain events were recorded during the study period, it would be desirable to further understand their trends for the foreseeable future. Research carried out in the area has already pointed towards an increase in precipitation and flooding during the fall and winter seasons (Jónsdóttir, 2012). There has been a slight warming of 0.1°C in the region and an increase in annual precipitation by about 26 mm in the last decade. Annual reports by the IMO (2016, 2017) describe 2015 and 2016 temperatures and annual precipitation totals to be above the 1967 to 2017 normals at most stations including Höfn. Therefore, it is suggested that the additional precipitation and inputs of glacial melt will bring even higher water levels in the early fall (September) when glacial meltwater, rainfall and runoff is considerable. Change in mean annual and seasonal runoff from 1961-1991 to 2071-2100 is expected to exceed 100 mm in this region of southern Iceland (Arctic-HYDRA, 2010). Meltwater and runoff will then eventually decrease due to significant losses in glacier ice (Aðalgeirsdóttir, 2006).

These changing discharge patterns are likely to shift the sediment regime into and through Skeiðarársandur. Increasing discharge rates in glacial streams during certain seasons could potentially threaten the inhabited wetland with increasing water levels and additional inputs of sediment. Additionally, the occurrence of large unpredictable jökulhaups, originating from Síðujökull flowing down the Brunná river, an occurrence which has not occurred here since 2006 presents a real threat for the wetland at the Hvoll farm. The local farmer expressed his concern in managing such floods as they are unpredictable, and can lead to quickly rising water levels leaving little time to manage them adequately.

6.6 Expansion of the Paraglacial Theory

Although Church and Ryder (1972) developed the paraglacial theory for landscapes undergoing deglaciation, such as in this study area, where the ancient ice sheets have now retreated up to the current extent of Vatnajökull, little information exists about the role of frequent tephra fallouts on sediment replenishment here.

When looking at the sediment exhaustion model of paraglacial landscapes by Church and Ryder (1972), sediment depletion continually occurs until nominal glacial material cannot be transported downstream to lower elevations, essentially a point is reached where the glacial ice mass has shrunk so much that its influence on discharge and sediment transport is minimized. Ballantyne (2002) augmented this model by including rockwalls, drift-mantled slopes, valley floor glacigenic deposits or coastal glacigenic deposits as inputs into the paraglacial sediment exhaustion scheme.

However, in Iceland, reoccurring large scale eruptions and jökulhlaups have the potential to continually deposit significant amounts of ash and material in short periods of time within these paraglacial landscapes. For instance, in June 2011, the study site (Hvoll), which is located 39 km South-west from Grímsvötn volcano received about 4-6 cm of ash in a few hours (per. comm. Haness). Wind storms, similar to the one described earlier have the potential to erode and re-deposit the ash too. In fact, the local farmer shared photos in 2015 showing sediment accumulations of up to 7 cm over top of wetland vegetation (per. comm. K. Young). Even now, some of this ash exists throughout the landscape (within the sandur soils, wetland, and in depressions). Wind storms, stream discharge and jökuhlaups likely remobilize these materials, moving them downstream to lower reaches of the catchment.

Therefore, if one follows Church and Ryder's (1972) theory on deglaciation, sediment deposition patterns and surface morphology should have adjusted to new conditions here by now. Yet this dynamic landscape continues to be in a state of flux, where new additions of sediment, much of it derived from volcanic activity continues to add material to the system, and the drainage system continually tries to adapt to it (Figure 6.6).

Finally, being at an active plate boundary, new volcanic systems will continue to emerge and erupt in this region of southern Iceland for centuries to come. This will prolong the paraglacial transitioning phase here, the sediment yield, and hence its hydrology, until long after the cessation of volcanic activity.

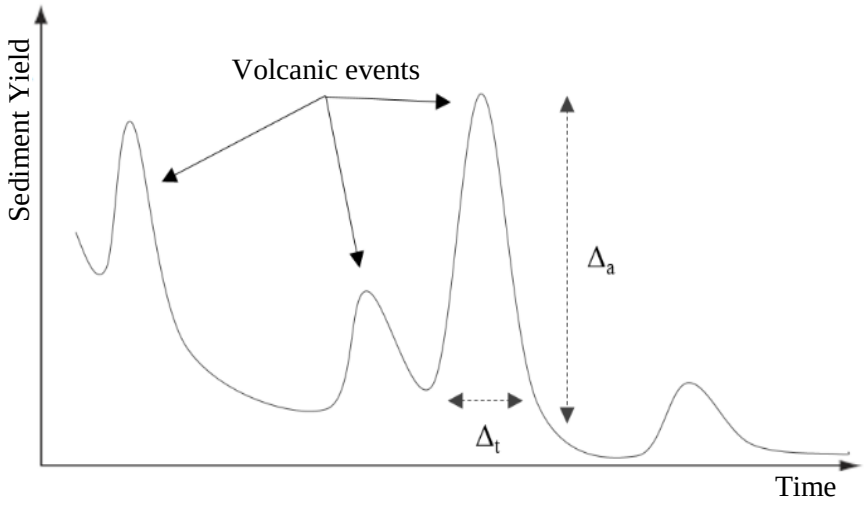

Figure 6.6 Conceptual graph showing a decline in sediment yield over time during a period of paraglacial readjustment and the role of volcanic activities in refilling sediment yield (after Church and Ryder 1972; Ballantyne 2002; Knight & Harrison 2014). Δ_t is the period of volcanic eruption and ensuing tephra dispersal and ends when the deposits are trapped within the environment and tephra deposit mobility through fluvial or aeolian processes are small. Δ_a is amplitude, where the quantity of sediment available in this paraglacial environment is related to the quantity of volcanic ash and materials dispersed following the eruption. The duration of sediment yield depletion of ash and tephra fallouts during the paraglacial period is higher with larger volcanic eruptions which generate more ash deposits, and therefore longer potential inputs of sediment.

CHAPTER SEVEN: CONCLUSIONS

The aim of this study was to further understand the hydrology of a sandur-wetland setting near an inhabited farm in South Iceland and understand the hydrological interactions between the two landscapes. The hydrological and fluvial regimes which occurred here are associated with the local climate and episodic events which are characteristic of the region. The streamflow regime is representative of glacial rivers with water levels being highest during early fall. Additional rainfall can yield large floods over the sandur as baseline fall water levels are already elevated. However intense localized and steady rainfall in the summer was similarly shown in being effective in enhancing the occurrence of floods here. In the winter, runoff rates in the nearby catchments are usually high in this region due to little vegetation found and frozen grounds impeding infiltration and therefore permitting sandur water levels to respond quickly to precipitation events during this time of year.

Furthermore, the passage of a severe unique sandstorm event enhanced glacial melt and likely triggered a small glacial outburst flood (June 20, 2016). Rainfall records show that little precipitation had fallen over the region during this time span but abnormally high air temperatures (>15°C) and winds (>16 m/s) occurred. Much of this warm, dry, and dusty air likely travelled away from Skeidararsandur into the Iceland interior accelerating melt on the nearby Vatnajökull glacier, by raising net radiation inputs ($\downarrow\alpha$) and advection of sensible heat (Qh).

The dynamic hydrological regime of the sandur contrasts to the wetland for which the wetland, sheltered by manmade berms, provides a stable ecosystem for vegetation and bird populations to sustain. Groundwater exchanges from the sandur into the wetland are uninterrupted

throughout the year, however rates significantly increase when sandur water tables are high during the passage of heavy rainfall or jökulhlaup events.

Photogrammetric tools here assisted in developing ultra-high resolution digital elevation models which helped establish a yearly flooding pattern at this sandur-wetland site. The erosional and depositional pattern of sediment here was supervised by monitoring a 2.5 km stretch of the Brunná River with the UAV from June to September 2016. Additionally, satellite and archival imagery since 1979 provided information of the shrinkage of the inhabited wetland. The images demonstrated a highly dynamic environment in which sediments and fluvial processes have eroded significant valuable agricultural land. Now, berms made of ash and hay act as a line of defense to prevent reoccurring sandur floods from spilling over into an adjacent wetland. However, the unpredictability of severe events such as jökulhlaups and high rainfall events during the fall is a real threat to the local farmer who has already lost 0.33 km^2 of vegetated fields in the wetland from the expansion of the sandur since 1985.

Furthermore, this study examined characteristics of this paraglacial environment. Its sediment exhaustion scheme is unique due to the proximity to volcanoes which have previously generated significant quantities of ash to precipitate in nearby catchments and eventually flow down to outwash plains of Skeidararsandur. This augments our current understanding on paraglacial landscapes, encompassing features which builds on Church and Ryder's (1972) initial theory of sediment exhaustion in these environments.

Through a combination of hydrological and remote sensing measurements, this study provided spatial and temporal information of the hydrology, morphology and flooding levels in response to rainfall and episodic floods at this inhabited Sandur-Wetland site. Further work should focus on groundwater contributions coming from macropores and small streams draining from the

postglacial Laki lavafield. These natural springs together with landscape changes made by the farmer (drainage channels and berms) make for a complicated wetland within a broader sandur fluvial landscape. Additional work should be focused on the stability and reinforcement of the berms which now act as the sole line of defense between the Hvoll farm built in the wetland and the dynamic hydrological regime of the sandur, which with a changing climate is expected to see an amplification of the regimes already examined in this study.

REFERENCES

Abnizova, A. and Young, K.L., 2010. Sustainability of High Arctic ponds in a polar desert environment. *Arctic*, pp.67-84.

Aðalgeirsdóttir, G., Jóhannesson, T., Björnsson, H., Pálsson, F. and Sigurðsson, O., 2006. Response of Hofsjökull and southern Vatnajökull, Iceland, to climate change. *Journal of Geophysical Research: Earth Surface*, *111*(F3).

Arnalds, O., 2000. The Icelandic 'rofabard'soil erosion features. *Earth Surface Processes and Landforms*, *25*(1), pp.17-28.

Arnalds, Ó., 2008. Soils of Iceland. *Jökull*, *58*, pp.409-421.

Arnalds, Ó., 2010. Dust sources and deposition of aeolian materials in Iceland. *Icelandic Agricultural Sciences. 23*, pp. 3-21.

Arnalds, O., 2013. The influence of volcanic tephra (ash) on ecosystems. *Advances in. Agronomy*, *121*, pp.331-380.

Arnalds, O., Dagsson-Waldhauserova, P. and Olafsson, H., 2016. The Icelandic volcanic aeolian environment: Processes and impacts—A review. *Aeolian Research*, *20*, pp.176-195.

Arnalds, O., Gudmundsson, J., Oskarsson, H., Brink, S.H. and Gisladottir, F.O., 2016. Icelandic inland wetlands: characteristics and extent of draining. *Wetlands*, *36*(4), pp.759-769.

Arnalds, O. and Kimble, J., 2001. Andisols of deserts in Iceland. *Soil Science Society of America Journal*, *65*(6), pp.1778-1786.

Arnalds, O., Ólafsson, H. and Dagsson-Waldhauserova, P., 2014. Quantification of iron-rich volcanogenic dust emissions and deposition over the ocean from Icelandic dust sources. *Biogeosciences*, *11*(23), pp.6623–6632.

Arnalds, O., Thorarinsdottir, E.F., Thorsson, J., Waldhauserova, P.D. and Agustsdottir, A.M., 2013. An extreme wind erosion event of the fresh Eyjafjallajökull 2010 volcanic ash. *Scientific reports*, 3, pp.1257.

Ballantyne, C.K., 2002. Paraglacial geomorphology. *Quaternary Science Reviews*, *21*(18), pp.1935-2017.

Beylich, A.A., Liermann, S. and Laute, K., 2010. Fluvial transport during thermally and pluvially induced peak runoff events in a glacier-fed mountain catchment in western norway. *Geografiska Annaler: Series A, Physical Geography*, *92*(2), pp.237-246.

Björnsson, H., 1992. Jökulhlaups in Iceland: prediction, characteristics and simulation. *Annals of Glaciology*, 16, pp.95-106.

Björnsson, H., 2003. Subglacial lakes and jökulhlaups in Iceland. *Global and Planetary Change*, *35*(3), pp.255-271.

Björnsson, H. and Pálsson, F., 2008. Icelandic glaciers. *Jökull*, 58, pp.365-386.

Björnsson, H., Pálsson, F., Gudmundsson, S., Magnússon, E., Adalgeirsdóttir, G., Jóhannesson, T., Berthier, E., Sigurdsson, O. and Thorsteinsson, T., 2013. Contribution of Icelandic ice caps to sea level rise: Trends and variability since the Little Ice Age. *Geophysical Research Letters*, *40*(8), pp.1546-1550.

Blake, G.R. and Hartge, K.H., 1986. Particle density. *Methods of soil analysis: Part 1—Physical and Mineralogical methods*, methodsofsoilan1, pp.377-382.

Box, J.E., Bromwich, D.H., Veenhuis, B.A., Bai, L.S., Stroeve, J.C., Rogers, J.C., Steffen, K., Haran, T. and Wang, S.H., 2006. Greenland ice sheet surface mass balance variability (1988–2004) from calibrated polar MM5 output. *Journal of Climate*, *19*(12), pp.2783-2800.

Black, G.R., 1965. Bulk density: method of soil analysis monograph No. 9, Part I. American Society of Agronomy Inc., Madison, WI.

Bullard, J.E., 2013. Contemporary glacigenic inputs to the dust cycle. *Earth Surface Processes and Landforms*, *38*(1), pp.71-89.

Burgy, R.H. and Luthin, J.N., 1956. A test of the single-and double-ring types of infiltrometers. *Eos, Transactions American Geophysical Union*, *37*(2), pp.189-192.

Cartier, K. M. S. (2017), Southern Greenland wildfire extinguished, *Eos*, 98, retrieved from https://eos.org/articles/southern-greenland-wildfire-extinguished

Church, M. and Ryder, J.M., 1972. Paraglacial sedimentation: a consideration of fluvial processes conditioned by glaciation. *Geological Society of America Bulletin*, *83*(10), pp.3059-3072.

Compton, K., Bennett, R.A. and Hreinsdóttir, S., 2015. Climate-driven vertical acceleration of Icelandic crust measured by continuous GPS geodesy. *Geophysical Research Letters*, *42*(3), pp.743-750.

Conway, H., Gades, A. and Raymond, C.F., 1996. Albedo of dirty snow during conditions of melt. *Water Resources Research*, *32*(6), pp.1713-1718.

Cossart, E. and Fort, M., 2008. Sediment release and storage in early deglaciated areas: Towards an application of the exhaustion model from the case of Massif des Écrins (French Alps) since the Little Ice Age. *Norsk Geografisk Tidsskrift-Norwegian Journal of Geography*, *62*(2), pp.115-131.

Crusius, J., Schroth, A.W., Gasso, S., Moy, C.M., Levy, R.C. and Gatica, M., 2011. Glacial flour dust storms in the Gulf of Alaska: Hydrologic and meteorological controls and their importance as a source of bioavailable iron. *Geophysical Research Letters*, *38*(6).

Dagsson-Waldhauserova, P., Arnalds, O., Olafsson, H., Skrabalova, L., Sigurdardottir, G. M., Branis, M., Hladil, J., Skala, R., Navratil, T., Chadimova, L., von Lowis of Menar, S.,

Thorsteinsson, T., Carlsen, H. K., and Jonsdottir, I, 2014. Physical properties of suspended dust during moist and low-wind conditions in Iceland. *Icelandic. Agricultural. Sciences*, *27*, pp.25-39.

Dagsson-Waldhauserova, P., Arnalds, O., Olafsson, H., Hladil, J., Skala, R., Navratil, T., Chadimova, L. and Meinander, O., 2015. Snow–dust storm: unique case study from Iceland, March 6–7, 2013. *Aeolian Research*, *16*, pp.69-74.

Dawson, J., Delbos, E., Hough, R., Lumsdon, D., Mayes, B. and Watson, H., 2010. Impacts of volcanic ash originating from the April 2010 eruption in Eyjafjallajökull (Iceland) on the natural resources of Scotland. *The Mcaulay Land Use Research Institute, Aberdeen*.

Dunne, T. and Leopold, L.B., 1978. *Water in environmental planning*. Macmillan.

Etienne, S., Mercier, D. and Voldoire, O., 2008. Temporal scales and deglaciation rhythms in a polar glacier margin, Baronbreen, Svalbard. *Norsk Geografisk Tidsskrift-Norwegian Journal of Geography*, *62*(2), pp.102-114.

Einarsson, M.A., 1984. Climate of Iceland. 000072851.

Einarsson, B., 2009. Jökulhlaups in Skaftá: A study of a jökulhlaup from the Western Skaftá cauldron in the Vatnajökull ice cap, Iceland. *Icelandic Meteorological Office.*

Eythorsson, J., Sigtryggsson, H. and Bertelsen, E., 1971. The climate and weather of Iceland. *Zoology of Iceland, 1, pp. 1-62*

Forbes, D.L. and Taylor, R.B., 1994. Ice in the shore zone and the geomorphology of cold coasts. *Progress in Physical Geography*, *18*(1), pp.59-89.

Fowler, A.C., 1999. Breaking the seal at Grímsvötn, Iceland. *Journal of Glaciology*, *45*(151), pp.506-516.

Fraser, C.S. and Cronk, S., 2009. A hybrid measurement approach for close-range photogrammetry. *ISPRS journal of photogrammetry and remote sensing*, *64*(3), pp.328-333.

Freeze, R.A. and Cherry, J.A., 1974. A. 1979. Groundwater. *Prentice—Hall, Inc Englewood cliffs, New Jersey*, *604*, pp.2l5-227.

Gardarsson, A., 1979. Vistfraedileg flokkun íslenskra vatna [An ecological classification on Icelandic freshwaters]. *Tyli*, *9*, pp.1-10.

Gassó, S., Stein, A., Marino, F., Castellano, E., Udisti, R. and Ceratto, J., 2010. A combined observational and modeling approach to study modern dust transport from the Patagonia desert to East Antarctica. *Atmospheric Chemistry and Physics*, *10*(17), pp.8287.

Gíslason, G.M., Ólafsson, J.S. and Adalsteinsson, H., 1998. Animal communities in Icelandic rivers in relation to catchment characteristics and water chemistry. *Hydrology Research*, *29*(2), pp.129-148.

Gunnarsson, T.G., Gill, J.A., Appleton, G.F., Gíslason, H., Gardarsson, A., Watkinson, A.R. and Sutherland, W.J., 2006. Large-scale habitat associations of birds in lowland Iceland: implications for conservation. *Biological Conservation*, *128*(2), pp.265-275.

Hadley, O.L. and Kirchstetter, T.W., 2012. Black-carbon reduction of snow albedo. *Nature Climate Change*, *2*(6), pp.437-440.

Haraldsson, H., 1997. Vatnajokull. Cos oghlaup 1996. Iceland Public Roads Administration, Reykjavik, Iceland.

Hayashi, M., 2004. Temperature-electrical conductivity relation of water for environmental monitoring and geophysical data inversion. *Environmental Monitoring and Assessment*, *96*(1), pp.119-128.

Héquette, A. and Ruz, M.H., 1990. Sédimentation littorale en bordure de plaines d'épandage fluvioglaciaire au Spitsberg nord-occidental. *Géographie physique et Quaternaire*, *44*(1), pp.77-88.

Hillel, D., 1980. Fundamentals of Soil Physics Academic. San Diego, CA.

Jóhannesson, H. and Saemundson, K., 1989. *[Geological map of Iceland 1: 500 000]; Jarðfræðikort af Íslandi: berggrunnur*. Icelandic Museum of Natural History and Iceland Geodetic Survey.

Jonsdottir, J.F., 2008. A runoff map based on numerically simulated precipitation and a projection of future runoff in Iceland. *Hydrological Sciences Journal*, *53*(1), pp.100-111.

Jónsdóttir, J.F. and Uvo, C.B., 2009. Long-term variability in precipitation and streamflow in Iceland and relations to atmospheric circulation. *International Journal of Climatology*, *29*(10), pp.1369-1380.

Jones, P.D. and Mann, M.E., 2004. Climate over past millennia. *Reviews of Geophysics*, *42*(2).

Jónsdóttir, J.F. and Uvo, C.B., 2009. Long-term variability in precipitation and streamflow in Iceland and relations to atmospheric circulation. *International Journal of Climatology*, *29*(10), pp.1369-1380.

Kane, D.L. and Hinzman, L.D., 1988, August. Permafrost hydrology of a small arctic watershed. In Proceedings: Fifth International Conference on Permafrost. Trondheim, Norway (pp. 590-595).

Kjartansson, G., 1945. *Íslenzkar vatnsfallategundir* [Icelandic river types]. *Náttúrufræðingurinn* 15, pp. 113–126.

Knight, J. and Harrison, S., 2009. Periglacial and paraglacial environments: a view from the past into the future. *Geological Society, London, Special Publications*, *320*(1), pp.1-4.

Knight, J. and Harrison, S., 2012. Evaluating the impacts of global warming on geomorphological systems. *Ambio*, *41*(2), pp.206-210.

Knight, J. and Harrison, S., 2014. Mountain glacial and paraglacial environments under global climate change: lessons from the past, future directions and policy implications. *Geografiska Annaler: Series A, Physical Geography*, *96*(3), pp.245-264.

Koster, R.D., Dirmeyer, P.A., Guo, Z., Bonan, G., Chan, E., Cox, P., Gordon, C.T., Kanae, S., Kowalczyk, E., Lawrence, D. and Liu, P., 2004. Regions of strong coupling between soil moisture and precipitation. *Science*, *305*(5687), pp.1138-1140.

Lillesand, T., Chipman, J., Nagel, D., Reese, H. and Bobo, M., 1998. *Upper Midwest gap analysis program, image processing protocol*. Wisconsin Univ-Madison.

Long, N., Millescamps, B., Guillot, B., Pouget, F. and Bertin, X., 2016. Monitoring the topography of a dynamic tidal inlet using UAV imagery. *Remote Sensing*, *8*(5), p.387.

Liu, E.J., Cashman, K.V., Beckett, F.M., Witham, C.S., Leadbetter, S.J., Hort, M.C. and Guðmundsson, S., 2014. Ash mists and brown snow: Remobilization of volcanic ash from recent Icelandic eruptions. *Journal of Geophysical Research: Atmospheres*, *119*(15), pp.9463-9480.

Marcus, W. A., & Fonstad, M. A. (2008). Optical remote mapping of rivers at sub-meter resolutions and watershed extents. *Earth Surface Processes and Landforms*, *33*(1), 4-24.

Magilligan, F.J., Gomez, B., Mertes, L.A.K., Smith, L.C., Smith, N.D., Finnegan, D. and Garvin, J.B., 2002. Geomorphic effectiveness, sandur development, and the pattern of landscape response during jökulhlaups: Skeiðarársandur, southeastern Iceland. *Geomorphology*, *44*(1), pp.95-113.

Maizels, J., 1997. Jökulhlaup deposits in proglacial areas. *Quaternary Science Reviews*, *16*(7), pp.793-819.

Magnússon, E., Gudmundsson, M.T., Roberts, M.J., Sigurðsson, G., Höskuldsson, F. and Oddsson, B., 2012. Ice-volcano interactions during the 2010 Eyjafjallajökull eruption, as revealed by airborne imaging radar. *Journal of Geophysical Research: Solid Earth*, *117*(B7).

Marsh, P., Rouse, W.R. and Woo, M.K., 1981. Evaporation at a High Arctic site. *Journal of Applied Meteorology*, *20*(6), pp.713-716.

Marcus, W.A. and Fonstad, M.A., 2008. Optical remote mapping of rivers at sub-meter resolutions and watershed extents. *Earth Surface Processes and Landforms*, *33*(1), pp.4-24.

Matthews, N.A., 2008. *Aerial and close-range photogrammetric technology: providing resource documentation, interpretation, and preservation*. US Department of the Interior, Bureau of Land Management.

Meinander, O., Kontu, A., Virkkula, A., Arola, A., Backman, L., Dagsson-Waldhauserová, P., Järvinen, O., Manninen, T., Svensson, J., de Leeuw, G. and Leppäranta, M., 2014. Brief communication: Light-absorbing impurities can reduce the density of melting snow. *The Cryosphere*, *8*(3), pp.991-995.

Mercier, D., 2008. Paraglacial and paraperiglacial landsystems: concepts, temporal scales and spatial distribution. *Géomorphologie: relief, processus, environnement*, *14*(4), pp.223-233.

Nummedal, D., Hine, A.C. and Boothroyd, J.C., 1987. Holocene evolution of the south-central coast of Iceland. *Glaciated Coasts*, pp.115-150.

Ólafsson, J.S., Gíslason, G.M. and Aðalsteinsson, H., 2002. Icelandic running waters; anthropological impact and their ecological status. *TemaNord*, *266*, pp.86-88.

Ólafsson, H., Furger, M. and Brummer, B., 2007. The weather and climate of Iceland. *Meteorologische Zeitschrift*, *16*(1), pp.5-8.

Old, G.H., Lawler, D.M. and Snorrason, Á., 2005. Discharge and suspended sediment dynamics during two jökulhlaups in the Skaftá River, Iceland. *Earth Surface Processes and Landforms*, *30*(11), pp.1441-1460.

Oskarsson Framræsla votlendis á Vesturlandi. (Wetland drainage in W-Iceland) J.S. Olafsson (Ed.), Íslensk votlendi-verndun og nyting, University of Iceland Press, Reykjavik (1998) (In Icelandic with an English summary)

Painter, T.H., Skiles, S.M., Deems, J.S., Bryant, A.C. and Landry, C.C., 2012. Dust radiative forcing in snow of the Upper Colorado River Basin: 1. A 6 year record of energy balance, radiation, and dust concentrations. *Water Resources Research*, *48*(7).

Pedersen, S.H., Liston, G.E., Tamstorf, M.P., Westergaard-Nielsen, A. and Schmidt, N.M., 2015. Quantifying episodic snowmelt events in Arctic ecosystems. *Ecosystems*, *18*(5), pp.839-856.

Peltoniemi, J.I., Gritsevich, M., Hakala, T., Dagsson-Waldhauserová, P., Arnalds, Ó., Anttila, K., Hannula, H.R., Kivekäs, N., Lihavainen, H., Meinander, O. and Svensson, J., 2015. Soot on snow experiment: bidirectional reflectance factor measurements of contaminated snow. *The Cryosphere*, *9*(6), pp.2323-2337.

Priestley, C.H.B. and Taylor, R.J., 1972. On the assessment of surface heat flux and evaporation using large-scale parameters. *Monthly Weather Review*, *100*(2), pp.81-92.

Prospero, J.M., Bullard, J.E. and Hodgkins, R., 2012. High-latitude dust over the North Atlantic: inputs from Icelandic proglacial dust storms. *Science*, *335*(6072), pp.1078-1082.

Raynolds, M., Magnússon, B., Metúsalemsson, S. and Magnússon, S.H., 2015. Warming, sheep and volcanoes: Land cover changes in Iceland evident in satellite NDVI trends. *Remote Sensing*, *7*(8), pp.9492-9506.

Remondino, F. and El-Hakim, S., 2006. Image-based 3D modelling: A review. *The Photogrammetric Record*, *21*(115), pp.269-291.

Rist, 1957 Skeiðararhlaup, 1954, *Jökull*, 2 (1957), pp. 30-36

Roberts, M.J., 2005. Jökulhlaups: a reassessment of floodwater flow through glaciers. *Reviews of Geophysics*, *43*(1).

Robinson, Z.P., Fairchild, I.J. and Russell, A.J., 2008. Hydrogeological implications of glacial landscape evolution at Skeiðarársandur, SE Iceland. *Geomorphology*, *97*(1), pp.218-236.

Roussel, E., Chenet, M., Grancher, D. and Jomelli, V., 2008. Processus et rythmes de l'incision des sandar proximaux postérieure au petit âge glaciaire (sud de l'Islande). *Géomorphologie: relief, processus, environnement*, *14*(4), pp.235-247.

Serreze, M.C., Walsh, J.E., Chapin, F.S., Osterkamp, T., Dyurgerov, M., Romanovsky, V., Oechel, W.C., Morison, J., Zhang, T. and Barry, R.G., 2000. Observational evidence of recent change in the northern high-latitude environment. *Climatic change*, *46*(1-2), pp.159-207.

Smith, L.C., Sheng, Y., Magilligan, F.J., Smith, N.D., Gomez, B., Mertes, L.A., Krabill, W.B. and Garvin, J.B., 2006. Geomorphic impact and rapid subsequent recovery from the 1996 Skeiðarársandur jökulhlaup, Iceland, measured with multi-year airborne lidar. *Geomorphology*, *75*(1), pp.65-75.

Steenburgh, W.J., Massey, J.D. and Painter, T.H., 2012. Episodic dust events of Utah's Wasatch Front and adjoining region. *Journal of Applied Meteorology and Climatology*, *51*(9), pp.1654-1669.

Stone, R.S., Dutton, E.G., Harris, J.M. and Longenecker, D., 2002. Earlier spring snowmelt in northern Alaska as an indicator of climate change. *Journal of Geophysical Research: Atmospheres*, *107*(D10).

Stroeve, J., Markus, T., Meier, W.N. and Miller, J., 2006. Recent changes in the Arctic melt season. *Annals of Glaciology*, *44*(1), pp.367-374.

Thorarinsson, S. (1939). Hoffellsjökull, its movement and drainage. *Geografiska Annaler*, 21, 189-215.

Thorhallsdottir, T.E., Thorsson, J., Sigurdardottir, S., Svavarsdottir, K. & Johansson, M.H. 1998. Röskun votlendis á Suðrurlandi. [Wetland drainage in S-Iceland]. In Olafsson, J.S. (ed.) Íslensk votlendi-verndun og nyting [Icelandic Wetlands, Conservation and Utilization]. Reykjavik: University of Iceland Press (in Icelandic with an English summary).

Thordarson, T. and Höskuldsson, Á., 2008. Postglacial volcanism in Iceland. *Jökull*, *58*(198), pp.228.

Thornthwaite, C.W., 1955. *The water balance* (No. 551.57 T515w). Drexel Institute of Technology, Centerton, NJ (EUA). Laboratory of Climatology.

Thorsteinsson, T., Jóhannsson, T., Stohl, A. and Kristiansen, N.I., 2012. High levels of particulate matter in Iceland due to direct ash emissions by the Eyjafjallajökull eruption and resuspension of deposited ash. *Journal of Geophysical Research: Solid Earth*, *117*(B9).

Tweed, F.S. and Russell, A.J., 1999. Controls on the formation and sudden drainage of glacier-impounded lakes: implications for jökulhlaup characteristics. *Progress in Physical Geography*, *23*(1), pp.79-110.

Vandenberghe, J. and Woo, M.K., 2002. Modern and ancient periglacial river types. *Progress in Physical Geography*, *26*(4), pp.479-506.

Van Vliet-Lanoë, B., Laurent, M., Bahain, J.L., Balescu, S., Falguères, C., Field, M., Hallégouët, B. and Keen, D.H., 2000. Middle Pleistocene raised beach anomalies in the English Channel: regional and global stratigraphic implications. *Journal of Geodynamics*, *29*(1), pp.15-41.

Westoby, M.J., Brasington, J., Glasser, N.F., Hambrey, M.J. and Reynolds, J.M., 2012. 'Structure-from-Motion'photogrammetry: A low-cost, effective tool for geoscience applications. *Geomorphology*, *179*, pp.300-314.

Wittmann, M., Zwaaftink, C.D.G., Schmidt, L.S., Guðmundsson, S., Pálsson, F., Arnalds, O., Björnsson, H., Thorsteinsson, T. and Stohl, A., 2017. Impact of dust deposition on the albedo of Vatnajökull ice cap, Iceland. *The Cryosphere*, *11*(2), p.741.

Wolter, P. T., Mladenoff, D. J., Host, G. E., & Crow, T. R. (1995). Improved forest classification in the Northern Lake States using multi-temporal Landsat imagery. *Photogrammetric engineering and remote sensing*, 61(9), 1129-1144.

Woo, M.K., 2012. *Permafrost hydrology*. Springer Science & Business Media.

Woo, M.K. and Guan, X.J., 2006. Hydrological connectivity and seasonal storage change of tundra ponds in a polar oasis environment, Canadian High Arctic. *Permafrost and Periglacial Processes*, *17*(4), pp.309-323.

Woo, M.K., Heron, R. and Marsh, P., 1982. Basal ice in high arctic snowpacks. *Arctic and Alpine Research*, pp.251-260.

Young, K.L., Scheffel, H.A., Abnizova, A. and Siferd, J.R., 2017. Spatial and temporal dynamics of groundwater flow across a wet meadow, Polar Bear Pass, Bathurst island, Nunavut. *Permafrost and Periglacial Processes*, *28*(2), pp.405-419.

Young, K.L. and Woo, M.K., 2004. Queen Elizabeth Islands: water balance investigations. *IAHS Publications-Series of Proceedings and Reports*, *290*, pp.152-163.

Yuan, F., Bauer, M.E., Heinert, N.J. and Holden, G.R., 2005. Multi-level land cover mapping of the Twin Cities (Minnesota) metropolitan area with multi-seasonal Landsat TM/ETM+ data. *Geocarto International*, *20*(2), pp.5-13.

Þorkelsson, B., Karlsdóttir, S., Gylfason, Á.G., Höskuldsson, Á., Brandsdóttir, B., Ilyinskaya, E., Guðmundsson, M.T. and Högnadóttir, Þ (2012). The 2010 Eyjafjallajökull eruption, Iceland: report to ICAO-June 2012.